Studies on Natural Adsorbents for the Treatment of Industrial Effluents

Thesis submitted by

R. GOPINATHAN

Doctor of Philosophy

(Engineering)

DEPARTMENT OF CHEMICAL ENGINEERING

FACULTY COUNCIL OF ENGINEERING AND TECHNOLOGY

JADAVPUR UNIVERSITY

KOLKATA – 700 032

2018

JADAVPUR UNIVERSITY

KOLKATTA – 700 032, INDIA

INDEX NO: 277 / 14 / E

Title of the Thesis: "Studies on Natural Adsorbents for the Treatment of Industrial Effluents"

Name, Designation and Institution of Supervisor(s):

Dr. Avijit Bhowal
Professor
Chemical Engineering Department
Jadavpur University, Kolkatta – 700 032, India.

&

Dr. G. Chandrasekhar
Professor
Department of Chemical Engineering
Pondicherry Engineering College
Puducherry – 605 014, India.

List of Publications:

1. R. Gopinathan, Avijit Bhowal, Chandrasekar Garlapati, Adsorption Characteristics of Activated Carbon for the Reclamation of Colored Effluents Containing Orange G and New Solid−Liquid Phase Equilibrium Model, J. Chem. Eng. Data 62, (2017) 558−567.
2. R. Gopinathan, Avijit Bhowal, Chandrasekar Garlapati, Thermodynamic study of some basic dyes adsorption from aqueous solutions on activated carbon and new correlations, J. Chem. Thermodyn. 107 (2017) 182–188.

3. R. Gopinathan, Avijit Bhowal, Chandrasekar Garlapati, Adsorption characteristics of activated Palmyra male inflorescence for the reclamation of colored effluents containing Malachite green oxalate, J. Appl. Sci. Eng. Methodol. 3(3) (2017) 502 – 510.

4. R. Gopinathan, Avijit Bhowal, Chandrasekar Garlapati, Removal of Indigo Carmine and Eosin Y Anionic Dyes from Aqueous Solution by Fixed Bed Chitosan. J. Appl. Sci. Eng. Methodol. 4(1) (2018) 558 – 566.

5. R. Gopinathan, Avijit Bhowal, and Chandrasekhar Garlapati, Adsorption Studies of Some Anionic Dyes Adsorbed by Chitosan and New Four Parameter Adsorption Isotherm Model. J. Chem. Eng. Data 64(6), (2019) 2320−2328.

CERTIFICATE FROM THE SUPERVISORS

This is to certify that the thesis entitled **"Studies on Natural Adsorbents for the Treatment of Industrial Effluents"** submitted by R. Gopinathan, who got the name registered on 28.02.2014 Ref. No. D-7/E/90/14 for the award of Ph.D. (Engineering) degree of Jadavpur University is absolutely based upon his own work under the supervision of **Dr. Avijit Bhowal** and **Dr. G. Chandrasekhar** and that neither the thesis nor any part of the thesis has been submitted for any Degree/ Diploma or any academic award anywhere before.

Dr. Avijit Bhowal
Professor
Chemical Engineering Department,
Jadavpur University
Kolkatta – 700 032
India.

Dr. G. Chandrasekhar
Professor
Chemical Engineering Department
Pondicherry Engineering College
Puducherry – 605 014
India.

Acknowledgement

I would like to express my sincere and heartfelt thanks to my research supervisors Dr. Avijit Bhowal, Professor, Department of Chemical Engineering, Jadavpur University Kolkata and Dr. G. Chandrasekhar, Professor, Department of Chemical Engineering, Pondicherry Engineering College, Puducherry. I take this opportunity to express my gratitude to my supervisors for their kind patience, constant support and timely guidance which made me to complete this dissertation, without their help nothing would have been possible.

I would like to thank the Head of the Department and the Faculty members of Chemical Engineering Department, Jadavpur University who were all present during the interview for admission into this Ph.D Programme. I am very much thankful to the Principal Secretary, Jadavpur University for permitting me to register for my Ph.D. degree.

My sincere thanks to the Principal, Pondicherry Engineering College, Puducherry for allowing me to register in Jadavpur University.

My special thanks to my wife Vinodha and my son G. Govardhan for their love and affection, constant encouragement and support.

R. Gopinathan

Department of Chemical Engineering

Pondicherry Engineering College

Puducherry

Notations

q_e	Solid phase adsorbate concentration at equilibrium (mg g^{-1})
K_F	Freundlich constant related to the adsorption capacity $\left((mg/g)/(mg/L)^{\frac{1}{n}}\right)$
n	Freundlich constant related to the intensity of the adsorbent
K_L	Langmuir adsorption constant (L mg^{-1})
q_m	Langmuir adsorption capacity (mg g^{-1})
C_e	liquid phase equilibrium concentration (mg L^{-1})
K_R	Redlich-Peterson model constant
a_R	Redlich-Peterson model constant
k_τ	Toth monolayer adsorptive uptake (mg g^{-1})
$a\tau$	constant (mg.L^{-1})
K_T	Temkin equilibrium binding constant (L mg^{-1})
B_1	Temkin constant related to heat of adsorption
ΔH^o	enthalpy change (J mol^{-1})
ΔS^o	entropy change (J mol^{-1} K^{-1})
ΔG^o	Gibbs energy change (J mol^{-1})
R	gas constant (8.314 J. mol^{-1} K^{-1})
q_t	solid phase adsorbate concentration at time t (mg g^{-1})
k_1	pseudo – first order rate constant (min^{-1})
k_2	pseudo – second order rate constant $\left(g\ mg^{-1}min^{-1}\right)$
k_p	intraparticle diffusion rate constant (mg g^{-1} $min^{-0.5}$)
C_o	initial adsorbate concentration (mg L^{-1})
C_t	outlet adsorbate concentration at time (mg L^{-1})

k_{TH} Thomas model kinetic coefficient (mL min $^{-1}$mg^{-1})

$q_{\max}$ maximum solid phase concentration (mg g^{-1})

Q volumetric flow rate (ml min^{-1})

m mass of the adsorbent (g)

k_{YN} Yoon-Nelson model rate constant (min^{-1})

k_{AB} Adam – Bohart kinetic constant (L mg^{-1}min^{-1})

N_o saturation concentration (mg.L^{-1})

Z column depth (cm)

U_o linear velocity of the bed (cm min^{-1})

A absorbance values (cm^{-1})

v volume of the solution (m^3)

w weight of the activated carbon (g)

$f_{\mathrm{i}}^{\mathrm{L}}$ fugacity of sorbate in liquid phase

$f_{\mathrm{i}}^{\mathrm{S}}$ fugacity of sorbate in solid phase

ΔH_{f} heat of fusion

T_{m} melting temperature (K)

z mole fraction of the solute in solid phase

x mole fraction of the solute in the liquid phase

Greek symbols

β_R constant in Redlich – Peterson equation which is less than unity

τ time required for 50% of adsorbate break through (min).

α constant

β constant

CONTENTS

List of Tables

List of Figures

CHAPTER 1
INTRODUCTION

Rapid industrialization over the past few decades is proving to be a big threat to the environment. Industries such as textile, cosmetics, leather, plastic, printing and paper utilize various types of dyes as a coloring agent for their products [1.1-1.4]. The effluent from the dyeing process sometimes contains upto 50% of the dye used because of low level of fixation of dye onto fibers [1.5]. The presence of even a very small amount of dye in the effluent is highly visible in solution. Most of the residual dyes present in the effluent are very stable and difficult to degrade. The disposal of the colored effluents into marine surface affects aquatic life as they reduce sunlight penetration through water [1.6]. The dyes present in the water affect the vital organs of human beings [1.7]. Hence it is essential to decolorize the effluent before discharging it to the environment.

1.1 Classification of Dyes

. The dye molecule consists of two important components, chromophores and auxochromes. The chromophore molecules are responsible for producing the colour whereas the auxochromes increase the affinity of the dye towards the fibers. Dyes may be classified according to their chemical structure and their application. The cationic dyes are basic dyes. It is water soluble and yield colored cations in solution. This class of dye is used in silk, nylon, acrylic, and wool dyeing. Cationic dyes are toxic and cause skin irritation, dermatitis, mutations and even cancer. The direct dyes, acid dyes, and reactive dyes are anionic dyes. They have good water solubility, but are very much harmful to humans since they are organo sulphonic acids [1.5, 1.8]. The properties and application of the various dyes used in textile industry is summarized in Table – 1.1.

Table 1.1 Various types of dyes, properties and application.

Class	Properties	Application (e.g.)
Basic dyes	Cationic dyes, water soluble, brighter shades, positively charged	Coloring wool, silk, paper and acrylic fibers
Acid dyes	Anionic, highly water soluble	Dyeing for wool, silk, poly amide and modified acrylics
Disperse dyes	Insoluble in water	Dyeing synthetic fiber, polyester yarn
Reactive dyes	Water soluble	Dyeing protein and cellulose fibers
Mordant dyes	Water soluble	Color wool products, leather
Direct dyes	Water soluble, anionic	Dyeing protein and cellulose fibers
Vat dyes	Natural coloring dyes, insoluble in water	Coloring cellulosic fiber and cotton
Sulphur dyes	Insoluble in water	Used for coloring rayon and cellulosic fiber

1.2 Treatment methods

Different techniques have been studied for the removal of dye from aqueous solution. The methods used to remove these pollutants from effluent are broadly classified into chemical, biological and physical process. Some of the processes generally employed in chemical treatment are chemical oxidation, oxidation with Fenton reagent, ozonation, photochemical oxidation, chemical precipitation and coagulation/ flocculation. The physical treatment methods include membrane filtration, ion exchange and adsorption. The biological treatment methods use various microorganisms to degrade the dyes [1.9-1.10]. A brief review of these methods is presented below.

1.2.1 Chemical treatment methods

1.2.1 (a) Chemical oxidation

Oxidation is commonly a adopted method for de-colorization. The oxidizing agents such as hydrogen peroxide (H_2O_2) and ozone (O_3) are used for the treatment of various dye effluents. These substances decompose to give OH^- radicals and water in presence of catalyst. The hydroxyl radical generated can readily undergo reaction with the chromophore of the dye molecule. The oxidizing agents transform the complex molecules into simple molecule like CO_2, H_2O and inorganic salts. Chemical oxidation produces colorless effluents [1.11]. The chemical reactions involved in the oxidation process are as follows.

O_3/H_2O_2 + Dye molecule -------› Product (1.1)

OH* + RH -------› H2O + R* (1.2)

R* + OH^- -------› ROH (1.3)

R* +H_2O_2 -------› ROH+ OH (1.4)

Ozone is a more powerful oxidizing agent than H_2O_2, and Cl_2. At pH 5 -6 ozone readily reacts with the double bond of the dye molecules selectively. At higher pH (above 8.0) it undergoes decomposition reaction resulting in formation of hydroxyl radicals [1.11].

In Fenton oxidation process, the Fenton reagent (a combination of H_2O_2 and ferrous ions) is used for decolorization. This is one of the advanced method of

the oxidation process. The hydroxyl radicals generated from H_2O_2 with the catalyst Fe^{2+}, degrade the dye compounds and convert them into simple harmless products like CO_2, H_2O and inorganic salts.

$$Fe_2^{+} + H_2O_2 \text{ ---------}\rightarrow OH^* + OH \qquad (1.5)$$

In the photochemical oxidation method, the dye molecules are degraded to CO_2 and H_2O in the presence of UV. The hydroxyl radicals generated in the process degrade the dyes in the effluent [1.12].

1.2.1 (b) Chemical precipitation

Precipitation is the method of creating a solid mass in the liquid effluent. In this method of treating effluent, certain chemicals which are termed as precipitants are added to precipitate dye in the effluents. The precipitated solids are removed by settling or clarification process. The process can handle large feed volume and has low capital cost.

1.2.1 (c) Coagulation / Flocculation

Coagulation is the process wherein the colloidal particles are destabilized by neutralizing the forces [1.13]. The coagulants added for the treatment should possess electric charge opposite to that of the particles in suspension in the liquid phase. The small suspended particles are flocked together once the charge is neutralized. Flocculation is the process where the particle size increases from the microscopic level to visible level on addition of chemicals under the influence of gentle mixing. The collision of the particles leads to the formation big flocks.

Once the flocks reached the optimum size, it can be removed by filtration or by sedimentation method.

1.2.2 Biological treatment method

Biological treatment methods like fungal decolorization, microbial decolorization, are commonly applied to degrade dyes. Biological treatment methods are classified as aerobic and anaerobic process based on the oxygen demand. The conventional and extended activated sludge processes are based on aerobic digestion [1.14]. Bioremediation is a green technique adopted to remove dye from the effluent. Living or dead microbial biomass are also used to adsorb the dyes.

1.2.3 Physical treatment method

The physical method adopted for the treating dye effluent is the membrane technology, ion exchange and adsorption technique. The membrane technology is based on the separation factor. Based on micropore diameter, the membrane process can be categorized as ultrafiltration, microfiltration, reverse osmosis and nano-filtration [1.15]. The main difference between reverse osmosis, nano filtration and ultrafiltration is configuration of the membrane and the operation pressure. Ultra filtration can be used for the solute having the molecular size ranging from 0.001μm and0.1 μm. Nano filtration membranes have properties between ultrafiltration and reverse osmosis membranes [1.13, 1.5]. The solute having molecular weight > 300 can be retained by the ultrafiltration membrane. The operating pressure for the ultrafiltration system ranges from 0.069 Mpa and

0.69 Mpa. Reverse osmosis system operates at high pressure range of 0.69 to 6.9 Mpa. The membranes are made up of variety of polymers like polyamide, polystyrene copolymer, styrene copolymer, polyacrylonitrile and polysulfones. The membrane modules could be spiral wound, tubular, hollow fiber and plate and frame.

Ion exchange process involves the exchange of ion in the liquid and the solid phase (i.e resin). The process of ion exchange is a reversible chemical reaction. The ion exchange resins are made from polymeric materials with electrically charged sites and capable of exchanging the ions in the solution. The resin lose it exchange capacity when all the resin exchange sites are filled with the contaminants. Cationic and anionic dyes can be removed by the process. The process is not widely used because it cannot be useful for wide varieties of dyes [1.12]

1.2.3 (a) Adsorption Process

Adsorption is the process in which the molecules in the gas or in liquid phase concentrate on the solid surface. Adsorption occurs due to unbalanced or residual forces at the surface of liquid or solid phase. These forces attract the molecules which comes in contact with the surface of the adsorbent. Because of the forces of attraction between adsorbate and adsorbent, heat energy is released and the process of adsorption is exothermic. The adsorption process may be either physisorption or chemisorption.

The physisorption is due to the weak Vanderwaal forces of attraction that exists between the adsorbate and the adsorbent. The heat of adsorption is in the order of 20 – 40 KJ mol^{-1}. The chemical adsorption or chemisorption is due to chemical forces of attraction between the adsorbate and the adsorbent. The heat of adsorption in the range of 40 – 400 KJ mol^{-1}. The commercially used adsorbent is activated carbon. It is characterized by high adsorption capacity, high surface area, good micro porous structure and high degree of surface reactivity.

References

[1.1] S. Azizian, M. Haerifar, H. Bashiri, Adsorption of methyl violet onto granular activated carbon: Equilibrium, kinetics and modeling. Chem. Eng. J. 146 (2009) 36-41.

[1.2] S. Chen, J. Zhang, C.Zhang, Q.Yue, Y.Li, C. Li, Equilibrium and kinetic studies of methyl orange and methyl violet adsorption on activated carbon derived from phargmites australis. Desalination 252(2010) 149-156.

[1.3] A. Rodriguez, J. Garcia, G. Ovejero, M. Mestanza, Adsorption of anionic and cationic dyes on activated carbon from aqueous solutions: Equilibrium and kinetics. J. Hazard. Mater. 172 (2009) 1311-1320.

[1.4] I.D. Mall, V.C. Srivastava, N.K. Agarwal, Adsorptive removal of auramine – O; Kinetic and equilibrium study. J. Hazard. Mater. 143(2007) 386-395.

[1.5] M.A.M. Salleh, D.K. Mahmoud, W.A.W. Karim, A. Idris, Cationic and anionic dye adsorption by agricultural solid waste. Desalination 280 (2011) 1-13.

[1.6] F. Deniz, S. Karaman, Removal of basic red 46 dye from aqueous solution by pine tree leaves. Chem. Eng. J. 170 (2011) 67-74.

[1.7] S. Chen, J. Zhang, C. Zhang, Q. Yue, Y. Li, C. Li. Equilibrium and kinetic studies of methyl orange and methyl violet adsorption on activated carbon derived from Phragmites australis. Desalination 252 (2010) 149 – 156.

[1.8] I.D. Mall, V.C. Srivastava, G.V.A. Kumar, I.M. Mishra, Characterization and utilization of mesoporous fertilizer waste carbon for adsorptive removal of dyes from aqueous solution.Colloids and Surfaces A: Physicochem. Eng. Aspects 278 (2006) 175 – 187.

[1.9] N. Hoda, E. Bayram, E. Ayranci, Kinetic and equilibrium studies on the removal of acid dyes from aqueous solutions by adsorption onto activated carbon cloth.J. Hazard. Mater. B 137 (2006) 344 – 351.

[1.10] M.J. Iqbal, M.N. Ashiq, Adsorption of dyes from aqueous solutions on activated charcoal. J. Hazard. Mater. B 139(2007) 57-66.

[1.11] S. Sharma, A. Kaur, Various methods for removal of dyes from industrial effluents - A review. I. J.Sci. Technol.11(12) (2018) 1 – 21.

[1.12] T. Robinson, G. McMullan, R. Marchant, P. Nigam, Remediation of dyes in textile effluent: a critical review on current treatment technologies with a proposed alternative. Bioresource Technol. 77 (2001) 247- 255.

[1.13] M. Joshi, R. Bansal, R. Purwar, Color removal from textile effluents. Indian J. of Fiber and Textile Research. 29 (2004) 239 – 259.

[1.14] T. Panswald, K. Lamsamer, J. Anotai, Decolorization of azo-reactive dye by polyphosphate and glycogen-accumulating organisms in an anaerobic-aerobic sequencing batch reactor. J Biotech 76(2001)151-159.

[1.15] S. Mondal, Methods of dye removal from dye house effluent – an overview. Environ. Eng. Sci. 25 (3) (2008) 383 – 396.

CHAPTER 2
LITRATURE SURVEY

Effluents discharged from dyeing industries are highly colored and are one of the major sources of environmental pollution [2.1-2.3]. The government legislation requires textile waste water to be treated. Therefore, there is a need to adopt an efficient process to treat the effluents. A brief introduction of the methods adopted for the treatments of dyes were stated Chapter 1. In this chapter, the results obtained with the techniques has been presented.

2.1. Treatment methods

2.1.1Biological methods

The biological processes of dye removal are fungal decolorization, decolorization using bacteria, adsorption using biomass (living and nonliving) and bioremediation systems. Ghasemi et al. [2.4] studied the decolorization of various azo dyes by Phanerochaetechrysosporium. Decolorization of the solution by the enzyme was achieved within 24 hours. Pakshirajan and Singh [2.5] studied the degradation of direct red-80 and mordant blue-9 individually and in a mixture by immobilized Phanerochaetechrysosporium in a rotating biological contactor reactor. Decolorization efficiency was in the range of 94–100% and 77–97% for individual dyes, and mixture of the dyes respectively.

Ozer et al. [2.6] studied the removal of acid dyes such as acid blue 324 (AB 324) and acid red (AR 337) using brown algae. The experimental data obtained was correlated with the Langmuir and Freundlich isotherms. The maximum Langmuir adsorption capacity for AB 324 and AR 337 was 224 mg g^{-1} and 323 mg g^{-1} respectively. Lee et al. [2.7] studied the removal of reactive blue 19 (RB 19) using anaerobic granular sludge under mesophilic condition. The experimental results revealed that removal of dye was

87 %. Brown and Hamburger [2.8] studied the removal of disperse red 159 using biological method and observed there was no reduction in the concentration of the dye. Malpei et al. [2.9] found that there was no change in concentration of the disperse blue 56 dye by biological treatment method under anaerobic condition.

The removal of reactive blue 21 dye was studied by Willetts and Ashbolt [2.10] using biological method. Removal was reported to be 80%. The degradation of safranin dye using biological treatment method by aeromonashydrophil bacteria has been reported by Ogugbue et al. [2.11]. Maximum degradation attained was 70%. Sharma and Kaur [2.12] performed experiments to determine the removal efficiency of safranin O dye by various adsorbents such as red mud, activated rice husk, treated mango seeds, bacteria and fugai. The removal percentage varied between 41 % and 76%.

Selvam et al. [2.13] used biological process for removal of congo red, methyl orangeand erichrome black-T. The fungal culture like white rot fungi schizophyllum commune and lenziteseximia were used for decolorization. The decolorization achieved by batch and continuous operationwas approximately76% and 56% respectively. The time taken for the decolorization was 5 days. Raghukumar et al. [2.14] noted that white-rot basidiomycetous fungi and their lignin-degrading enzymes were effective in the colour removal of dye effluents. Cetinet et al. [2.15] reported the effect of sulfate-reducing bacteria for the treatment of industrial wastewater containing Remazol Blue, Reactive Black B, and Reactive Red RB. The results indicated that nearly 25 to 30% dye reduction was obtained within 72 h.

2.1.2 Chemical treatment methods

The method commonly adopted in the chemical treatment method are coagulation /flocculation, precipitation and oxidation process like electrochemical oxidation, photo catalytic oxidation etc. Some of the literature related to dye removal by these methods are listed below.

García-Morales et al. [2.16] studied the removal of textile effluents from denim industries. The integrated process of ozone and electrocoagulation was capable of reducing the dye concentration up to 64.27%. The effluent subjected to ozone treatment and electrocoagulation process separately resulted in 63.63% and 21.73% removal respectively. Muhammad et al. [2.17] studied the decolourization of dyes from the textile industries by various advanced oxidation process at constant contact time of 25 min. Dye removal of 58% was reported for ozonation process. Irradiation with UV rays and combined UV/H_2O_2 treatment resulted in 26% and 32% degradation of dye. The color removal of 40% was reported for photo-Fenton process. Dye removal by biological treatment by upflow anaerobic sludge blanket bioreactor followed by advanced oxidation has also been reported by the author. The maximum dye removal reported was 95%, 79% and 86% for ozone treatment, UV irradiation and photo Fenton oxidation process respectively.

Hussein et al. [2.18] studied the removal of reactive blue 19 from the textile waste water by electrocoagulation method. The effect of various parameters such as pH, time for dye removal, initial dye concentration, and effect of temperature were investigated. Dye removal upto 99.60% was reported at optimum pH 11.5 within 20 min. Decolorization of 65% was achieved for indigo carmine dye by Trujillo et al. [2.19] when

treated by advanced oxidation process (ozone treatment and electrocoagulation). Ahmed [2.20] studied the electrochemical oxidation process for treatment of acid yellow and acid violet. The operating parameters such as pH, time, initial concentration were examined. It was noted that the dye was completely degraded.

Sun et al. [2.21] used ZnO photocatalyst to degrade crystal violet, methyl violet and methylene blue dyes. The degradation efficiency obtained by this method was 68.0%, 99.0%, and 98.5% for crystal violet, methyl violet and methylene blue dyes respectively. Yu and Shi [2.22] studied the removal of acid chrome black dye by catalytic oxidation method using chlorine dioxide as an oxidant. Maximum removal obtained was 87.8%. Cristovao et al. [2.23] investigated the treatment of reactive black 5 dye by catalytic oxidation process. Dye removal of 86% was obtained by using the laccase as a catalyst.

Martin et al. [2.24] reported the applicability of a tannin based coagulant - flocculant for the treatment of dye effluents in a pilot scale level. The study indicated that 95% dye removal was achieved in the process. Zidane et al. [2.25] studied the performance of CI reactive red 141 dye by using mineral coagulant. The process reveals that 100% dye removal was achieved within contact time of 60 min.

2.1.3 Physical treatment process

The commonly adopted methods are membrane technology, ion exchange and adsorption technique. Abid et al. [2.26] investigated the removal dyes concentration using RO membrane. The process was carried out at 400 kPa. The results indicated that the removal was 97.2%, 99.58% and 99.9% for acid red, reactive black and reactive blue

dyes respectively. Puasa et al. [2.27] studied the dye removal of C.I reactive black 5 and C.I reactive orange 16 by ultrafiltration method. The operating pressure was maintained at 400 kPa. The removal efficiency by this process was reported to be 78.0% and 79.2% of RB5 and RO16 respectively. Altenbaher and Turk [2.28] studied the applicability of the membranes for the treatment of waste water generated from the textile mills. Nano filtration and two reverse osmosis membranes were connected in series. The results suggested that the treated water can be reused for the dyeing process.

2.1.4 Combination of various methods

Investigations using various combinations of methods for dye removal have also been reported. Harrelkas [2.29] studied the decolorization of synthetic dyestuff effluent with the combined treatment consisting of photocatalytic oxidation and reverse osmosis membrane. The results revealed that a reduction in 90% of the organic content. Souza et al. [2.30] investigated the applicability of the combined treatment of ozonation followed by biological degradation. The results from the study indicates that the degradation of remazol black B was 96%. The effluent was further subjected to biological degradation to reduce the toxicity level in the effluent. Garcia et al. [2.31] studied the removal of cibacron red FN –R azo dye with the two stage anaerobic – aerobic treatment followed by photo Fenton or ozonation process. The degradation of dye by the biological treatment was found to be in the range of 92 %– 97% for these techniques. It was also noted that the colorless effluent from the biological process is toxic. It was further treated by photo Fenton or ozonation process.

2.1.5 Other treatment methods

Bulc and Ojstrsek [2.32] studied the performance of biodegradation of waste water containing acid orange 7 in up flow constructed wet land. The studies were conducted at various initial concentration ranging from 50 – 100 mg L^{-1}. The constructed wet land was packed with various materials like gravel sand and zeolite. The experimental results revealed that this method is capable of reducing the color by 70%. Sheth and Dave [2.33] investigated the applicability of down flow fixed film bioreactor for the biodegradation of reactive violet 5R compound in the waste water. Percentage removal of 95% was achieved by the method. Biodegradation was enhanced by the increasing the dose of peptone. Ting and Jamaludin [2.34] studied the decolorization of reactive and disperse dyes by electron beam technology. The color removal was in the range of 87 % - 96%. The color removal efficiency was noted to be a function of the initial concentration, and the dose of irradiation.

2.1.6 Adsorption

The literature batch adsorption studies for various adsorbent - dye systems are summarized in Table 2.1. The systems studied in the literature using fixed bed are reported in Table 2.2.

Table 2.1 Batch adsorption studies of various adsorbent – dye systems.

Sl. No	Types of adsorbents	Dye compound studied	Temp (K)	Concentration range studied (mg/L)	Time (min)	Langmuir adsorption capacity (mg/g)	Ref.
1	Lignite	Methylene blue	293 - 333	10 - 100	-	31.15 - 41.49	[2.35]
2	Pine cone	Acid black 26 (AB26) Acid green 25 (AG25) Acid blue 7 (AB7)	298 298 298	25 - 100	-	62.9 43.3 37.4	[2.3]
3	Phargmitesaustralis	Methyl orange Methyl violet	283-323	-	-	212 – 238.10 476.19 – 526.32	[2.36]
4	Bagasse fly ash	Auramine–O	303	-	-	31.77	[2.37]
5	Acid activated bentonite	Acid red 57(AR57) Acid blue294 (AB 294)	298 298	1000	90	641.9 117.8	[2.1]
6	Bottom ash – thermal power plants	Methyl orange	303	$1x10^{-5}$ – $10x10^{-5}$M	240	$13.35x10^{-4}$	[2.1]
7	De – oiled soya	Methyl orange	303	$1x10^{-5}$ – $10x10^{-5}$M	150	$13.46x10^{-4}$	[2.38]
8	Chitosan	C.I. reactive red (RR141)	293 - 333			67.93 - 155.93	[2.39]
9	Chitosan/ montmorilimite	Congo red	303			53.42	[2.40]
10	Chitosan / polyurethane	Acid violet 48	303			30.0	[2.41]
11	Chitosan /activated clay	Methylene Blue Reactive dye RR222	303 303			330.0 191.2	[2.42]

12	Chitosan /bentonite	Tartrazine Malachite green	320 310			294.1 435.0	[2.43]
13	Activated carbon cloth	Acid blue 45 (AB45) Acid blue 92 (AB92) Acid blue120 (AB120) Acid blue120 (AB120)	298	3.0 x 10^{-5}M	2880	1.38x10^{-4} (mol/g) 7.12x10^{-5} (mol/g) 4.03x10^{-5} (mol/g) 7.34x10^{-4} (mol/g)	[2.44]
14	Pine tree leaves	Basic red 46 BR (46)		20 -100	75	71.94	[2.45]
15	Chitosan	Malachite Green(MG) Reactive Red 198(RR) Direct yellow 31(DY)	301			166.60 1250.00 250.0	[2.46]
16	Chitosan	Acid red 87	303			80.84	[2.46]
17	Bentonite clay	Malachite green oxalate	298 308 318 328			7.716 5.585 5.631 5.071	[2.47]
18	Corncob activated carbon	Safranin	303	50 -5000	1440	1428.57	[2.48]
19	Activated clay Montmorilloni - te Activated	Basic Green (BG5) Basic violet (BV10) Basic Green (BG5) Basic violet (BV10) Basic		300 – 700	180	271.3 216.5 127.6 158.3 272.0	[2.49]

	carbon	Green (BG5) Basic violet (BV10)				149.0	
20	Chitosan	Reactive blue 29 (RB29)		50	90	169.6	[2.50]
21	Carbonaceous adsorbent	Chrysoidine -G Crystal Violet Meldola Blue	298 318 298 318 298 318	3 x 10^{-4} – 4 x 10^{-4} M	120	80.6 76.3 163.0 148.4 171.2 150.4	[2.51]
22	Activated carbon	Methylene blue Orange II	303 313 338 303 313 338	300- 500		469.6 581.5 708.8 384.3 468.6 568.5	[2.52]
23	Activated sludge bio mass	Basic blue 9 (BB9) Basic Red 18(BR18)	293 308 323 293 308 323	100	300	256.41 208.33 172.40 285.71 270.27 181.81	[2.53]
24	Mesoporous fertilizer plant waste carbon	Auramine O Congo red Orange G Methyl violet	298		2880	246.29 233.86 236.07 240.26	[2.54]
25	Rice husk Carbon	Safranine O Methylene blue	303 313 323 333 303 313 323 333	100 - 200	300	294.12 270.27 256.41 227.27 333.33 303.03 277.77 238.09	[2.55]
26	Graphene	Methylene blue	293 313 333	1000		153.85 185.19 204.08	[2.56]
27	Raw kaolin Pure kaolin	Methylene blue		15	180	14.85 16.39	[2.57]

	Calcined raw ckaolin Calcined pure kaolin NaoH treated raw kaolin NaoH treated pure kaolin					6.57 9.01 17.04 23.05	
28	Activated carbon	Eosin Y	303	50-400	200	571.40	[2.58]
29	Coal fly ash Zeolite	Indigo carmine	298	2.8 – 23.8	240	1.48 1.23	[2.59]
30	Boran industry waste		298	50 -300	60-.90	74.73	[2.60]
31	Moroccan clay		298	20	60	54.0	[2.61]
32	Bagasse fly ash	Malachite green	303	5 - 250	240	170.33	[2.62]
33	Activated carbon commercial grade	Malachite green	303	5 - 250	240	8.27	[2.62]
34	Bagasse fly ash	Congo red	303	5 - 30	240	11.89	[2.63]
35	Activated carbon commercial grade	Congo red	303	5 - 30	240	0.635	[2.63]
36	Bagasse fly ash	Orange G	303	5-30	240	18.77	[2.64]
37	Bagasse fly ash	Methyl violet	303	5- 30	240	26.25	[2.64]
38	Commercial activated carbon	Methylene blue	303	100- 200	35	980.3	[2.65]
39	Bamboo dust carbon	Methylene blue	303	100 - 200	35	143.2	[2.65]
40	Coconut shell carbon	Methylene blue	303	200 - 400	35	277.9	[2.65]
41	Rice husk carbon	Methylene blue	303	200-400	35	342.5	[2.65]
42	Commercial activated carbon	Congo red	303	200 - 400	35	493.8	[2.66]
43	Activated carbon	Safranin	313	---	2880	564	[2.67]

44	Canola hull	Cationic dye	293	25	10	49.0	[2.68]
45	Princess tree leaf	Basic red 46	298	20 - 100	90	43.10	[2.69]
46	Gypsum	Basic red 46	323	20 - 60	60	39.17	[2.70]

Table 2.2 Fixed bed adsorption studies of various adsorbent – dye systems

Sl. No	Types of adsorbents	Dye compound studied	Flow rate (ml/min)	Concentration (mg/L)	Ref.
1	Tamarind seed powder	Acid yellow 17	5 - 20	50 - 400	[2.71]
2	Phoenix tree leaf powder	Methylene blue	5 -12	30 - 100	[2.72]
3	Chitosan Scale fish	Indigo carmine	4 -8	10-20	[2.73]
4	Polymer bound adsorbent	Rhodamine–B	5 - 15	25 – 75	[2.74]
5	Chitosan glutaraldehydebiosorbent	Azo dye – DB71	1 - 3	15-30	[2.75]
6	Granular activated carbon – from waste	Azo dye – (C.I. Reactive black)	10 - 30	50 -200	[2.76]
7	Biosorbent	Crystal violet	10 – 20	10 – 25	[2.77]
8	Kenaf core fibre	Anionic dyes	10	20- 60	[2.78]
9	Granular Activated carbon and Natural Zeolite	Basic dyes	40 - 100	40 – 100 2- 50	[2.79]
10	Chitosan Impregnated with a Cationic Surfactant	Azo dye	0.8 – 1.5	20- 100	[2.80]
11	Oil palm empty fruit bunch fibers	Cationic and anionic dyes	1.5 - 10	200 – 400	[2.81]
12	Oil palm fruit mesocarpfiber	Metanil–yellow	8 - 26	25 – 100	[2.82]

It is clearly evident from table 2.1 and table 2.2 that the adsorption has been extensively studied in batch process. Fixed bed operations are relatively less. These focus of these were on various factors affecting the adsorption phenomenon such as pH, temperature, initial concentration and adsorbent dosage. The tables also suggest that new adsorbents are continuously being developed for treatment of dye effluents.

2.2 Existing batch adsorption isotherm models

2.2.1 Freundlich isotherm

The empirical equation which describes multilayer intake of the solute onto a heterogeneous surface is written as [2.83 -2.84]

$$q_e = K_F C_e^{\frac{1}{n}} \qquad (2.1)$$

The linear form of the above equation is

$$\ln q_e = \ln K_F + \frac{1}{n} \ln C_e \qquad (2.2)$$

Where, ,K_F and n are the Freundlich constants related to the adsorption capacity, and the intensity of the adsorbent respectively. The heterogeneity factor $\frac{1}{n}$ and n is a measure of deviation from linearity. The value of n is usually greater than 1.

2.2.2 Langmuir isotherm

The Langmuir isotherm is derived based on the assumption that adsorption occurs at particular localized sites on the surface, and only one molecule of the solute binds to each site. The energy of adsorption is same for all the sites, and there is no force of

interaction between adjacently adsorbed molecules [2.85- 2.86]. The Langmuir equation can be written in the following form

$$q_e = \frac{q_m K_L C_e}{1 + K_L C_e} \tag{2.3}$$

The above equation can be linearized in the form

$$\frac{C_e}{q_e} = \frac{C_e}{q_m} + \frac{1}{K_L q_m} \tag{2.4}$$

Where q_e is the solid phase equilibrium concentration, C_e is liquid phase equilibrium concentration of dye, K_L is Langmuir adsorption constant, q_m signifies the adsorption capacity.

2.2.3 Redlich – Peterson (R-P) isotherm

It is a modified form of Radke and Prausnitz[2.87 – 2.88] three-parameter empirical equation. It is applicable to both homogeneous or heterogeneous system and is more versatile than Freundlich and Langmuir isotherm. The R-P Isotherm can be written in the following form.

$$q_e = \frac{K_R C_e}{1 + a_R C_e^{\beta_R}} \tag{2.5}$$

The linear form of the above equation is

$$\ln\left(K_R \frac{C_e}{q_e} - 1 \right) = \ln a_R + \beta_R \ln C_e \tag{2.6}$$

Where K_R and a_R is constant. The term β_R is exponent constrained to be less than unity.

2.2.4 Toth isotherm

It is applicable for adsorption on heterogeneous surface and was derived from the potential theory. It can be written in the following form [2.89]

$$q_e = \frac{k_\tau C_e}{\left[\frac{1}{a\tau} + C_e^{\tau}\right]^{\frac{1}{\tau}}} \qquad (2.7)$$

The linear form of the above equation is

$$\left[\frac{C_e}{q_e}\right] = \frac{1}{(k\tau)^{\tau} a\tau} + \frac{C_e}{(k_\tau)^{\tau}} \qquad (2.8)$$

Where K_τ is Toth constant and a_τ is a constant . Toth equation reduces to Langmuir equation when $\tau = 1$.

2.2.5 Temkin isotherm

The Temkin isotherm is based on the assumption that the adsorption is characterized by a uniform distribution of the forces attraction and the heat of adsorption of molecules in the layer decreases linearly with coverage due to adsorbent – adsorbate interactions. The equation is given as

$$q_e = \frac{RT}{b}\ln(k_T C_e) \qquad (2.9)$$

The linear form of the above equation is

$$q_e = B_1 \ln K_T + B_1 \ln C_e \qquad (2.10)$$

$$B_1 = \frac{RT}{b} \qquad (2.11)$$

Where, K_T is the equilibrium binding constant corresponding to maximum binding energy and B_1 is related to heat of adsorption [2.90].

2.2.6 Khan et al. [2.91] phase equilibrium model

Khan et al. [2.91] developed an expression for modeling liquid isotherms based on the phase equilibrium criteria. The model relates mole fraction of sorbate in solution at equilibrium (x) with the mole fraction of sorbent on adsorbent (z).

The equation is

$$x = z\exp\left[(1-z)^2\left(a + bz + cz^{0.5}\right)\right] \qquad (2.12)$$

Where *a*, *b* and *c* are temperature dependent model parameters.

2.3 Thermodynamic parameters

The thermodynamic parameters such as enthalpy change ΔH^o, entropy change ΔS^o and Gibbs energy change ΔG^o are estimated with the help of Langmuir isotherm parameters. The appropriate equations were listed below. More details related to these equations are reported elsewhere [2.38, 2.92]

$$\Delta G^o = -RT\ln b \qquad (2.13)$$

$$\Delta H^o = -R\left(\frac{T_2T_1}{T_2 - T_1}\right)\ln\left(\frac{b_2}{b_1}\right) \qquad (2.14)$$

$$\Delta S^o = \frac{\Delta H^o - \Delta G^o}{T} \qquad (2.15)$$

The terms *b*, b_1 and b_2 are the Langmuir constants at temperatures T , T_1 and T_2 respectively.

2.4 Adsorption Kinetics

The mechanism of adsorption of molecules from the liquid phase to the selected solid phase is considered as an reversible phenomenon, and that equilibrium exist at the interface between the solid phase and the liquid phase. The effect of parameters such as contact time, initial concentration of dye were reported. The following kinetic models are available in the literature [50].

2.4.1 Pseudo first order model.

The pseudo – first order kinetic is the simplest and oldest model. It can be represented by

$$\frac{dq}{dt} = k_1(q_e - q_t) \qquad (2.16)$$

Where k_1 is the pseudo – first order rate constant, q_e is the dye uptake at equilibrium.

By integration, the above equation becomes [2.93]

$$\ln(q_e - q_t) = \ln q_e - k_1 t \qquad (2.17)$$

2.4.2 Pseudo – second order kinetic model

The model equation is given by

$$\frac{dq}{dt} = k_2(q_e - q_t)^2 \qquad (2.18)$$

Where k_2 is the pseudo- second order rate constant. The linear form of the above equation [2.94]

$$\frac{t}{q_t} = \frac{1}{k_2\, q_e^2} + \frac{t}{q_e} \qquad (2.19)$$

2.4.3 Intraparticle diffusion model

The mathematical expression for the intraparticle diffusion model is [2.94]

$$q_t = k_p t^{0.5} + C \qquad (2.20)$$

Where k_p is the intraparticle diffusion rate constant (mg.g^{-1} min $^{-0.5}$)

2.5 Fixed bed break through models

2.5.1 Breakthrough curves

The performance of a fixed-bed column is described with the help of the breakthrough curve. The breakthrough curve is a plot of the concentration of solute exiting the adsorbent bed with time. There are several models in the literature to predict break through curve. Some of important models from the literature are briefly presented in the following section.

2.5.2 Thomas model

The breakthrough of a fixed bed column and the parameters influencing the column performance can be well described by Thomas model. The Thomas model assumes plug flow in fixed bed and uses Langmuir isotherm for equilibrium, and second order reversible kinetics. It is suitable for the adsorption process where both external and internal diffusion limitations are absent. The linear form of this model is used for the modeling. It is expressed as [2.71, 2.72, 2.95 – 2.97].

$$\ln\left[\frac{C_o}{C_t} - 1\right] = \frac{k_{Th} q_{\max} m}{Q} - k_{Th} C_o t \qquad (2.21)$$

Where C_t and m are the packed bed outlet adsorbate concentration at time t, and mass of adsorbent in the column. The term k_{Th} and q_{max} represent the Thomas model kinetic coefficient and maximum solid phase concentration respectively. The value of k_{Th} and q_{max} can be obtained from the plot of $\ln\left(\frac{C_o}{C_t}-1\right)$ versus t.

2.5.3 Yoon – Nelson model

It is based on the assumption that the rate of decrease in the probability of adsorption for each adsorbate molecule is proportional to the probability of adsorbate adsorption as well as the probability of adsorbate breakthrough on the adsorbent. This model is less complicated compared to other models, and does not requires any information such as characteristics of adsorbate, type of adsorbent, and the physical properties of the adsorption bed [2.71, 2.72, 2.97]. The linear form is

$$\ln\left(\frac{C_t}{C_o - C_t}\right) = k_{YN}\ t - \tau\ k_{YN} \qquad (2.22)$$

Where, k_{YN} and τ represent the Yoon-Nelson model rate constant and time required for 50% of adsorbate break through. The value of k_{YN} and τ can be obtained from the plot of $\ln\left(\frac{C_t}{C_o - C_t}\right)$ versus t.

2.5.4 Adam-Bohart model

The model assumes that the rate of adsorption is based on the concentration of the adsorbing species and residual capacity of the adsorbent. It is based on surface reaction and assumes that the surface reaction is not spontaneous. The model is quite frequently used for the delineation of fixed bed breakthrough for the initial state of the operation. The Adams–Bohart model is generally used to describe the initial part of the breakthrough curve [2.71, 2.72, 2.97]. The linear form of this equation is represented by Eq.2.23.

$$\ln\left[\frac{C_t}{C_o}\right] = k_{AB}C_o t - \frac{k_{AB}N_o Z}{U_o} \qquad (2.23)$$

Where k_{AB} is the Adam – Bohart kinetic constant, U_o is the linear velocity of the bed, Z and N_o are the column depth and saturation concentration respectively. The value of k_{AB} and N_o can be obtained from the plot of $\ln\left(\frac{C_t}{C_o}\right)$ versus *t*.

References

[2.1] A.S. Özcan, A. Özcan, Adsorption of acid dyes from aqueous solutions onto acid – activated bentonite. J. Colloid. Interface Sci. 276 (2004) 39 - 46.

[2.2] R. Ansari, Z. Mosayebzadeh, Removal of eosin Y, an anionic dye, from aqueous solutions using conducting electroactive polymers. Iranian polymer Journal 19 (2010) 541- 551.

[2.3] N.M. Mahmoodi, B. Hayati, M. Arami, C. Lan, Adsorption of textile dyes on pine cone from colored wastewater: Kinetic, equilibrium and thermodynamic studies. Desalination 268 (2011) 117-125.

[2.4] F. Ghasemi, F. Tabandeh, B. Bambai, Decolorization of different azo dyes by phanerochaetechrrysosporum RP78 under optimal condition. Int. J. Environ. Sci. Technol.7 (2010) 457 – 464.

[2.5] K. Pakshirajan, S.Singh, Decolorization of synthetic waste water containing azo dyes in a batch operated rotating biological contactor reactor with the immobilized fungus phanerochetechrysoporium. Ind. Eng. Chem. Res.49 (2010) 7484 – 7487.

[2.6] A. Ozer, M. Turabik, G. Akkaya, Biosorption of acid dyes by brown algadictyotadichotoma: equilibrium kinetic and thermodynamic studies. Fresenius Environ. Bull. 18 (2009) 1798 – 1808.

[2.7] Y.H. Lee, R.D. Matthews, S.G. Pavlostathis, Biological decolorization of reactive anthraquinone and phthalocyanine dyes under various oxidation – reduction conditions. Water Environ. Res. 78 (2006) 156 – 169.

[2.8] D. Brown, B. Hamburger, The degradation of dyestuffs: Part III – investigations of their ultimate degradability. Chemosphere 16 (1987) 1539 – 1553.

[2.9] F. Malpei, V. Andreoni, D. Daffonchio, A. Rozzi, Anaerobic digestion of print pastes: a preliminary screening of inhibition by dyes and biodegradability of thickeners. Biores. Technol. 63 (1998) 49 – 56.

[2.10] J.R.M. Willets, N.J. Ashbolt, Understanding anaerobic decolorization of textile dyes wastewater : mechanism and kinetics. Water Sci. Technol. 42 (2000) 409 – 416

[2.11] C.J. Ogugbue, T. Sawidis, N.A. Oranusi, Bioremoval of chemically different synthetic dyes by aeromonashydrophilla in simulated waste water containing dyeing auxillaries. 62 (2012)1141 – 1146.

[2.12] S. Sharma, A. Kaur, Various methods for removal of dyes from industrial effluents – A review. Ind. J. Sci. Technol. 11 (12) (2018)1 – 21.

[2.13] K. Selvam, M.S. Priya, Biological treatment of Azo dyes & textile industry effluent by newly isolated White rot fungi Schizophyllum commune and Lenziteseximia. Int. J. Environ. Sci. 2(4) (2012) 1926-1935.

[2.14] C. Raghukumar, C, D. D'Souza Ticlo, A.K. Verma, Treatment of colored effluents with lignin-degrading enzymes: An emerging role of marine-derived fungi. Crit. Rev. Microbiol. 34 (2008) 189-206

[2.15] D. Cetin, S. Donmez, G. Donmez, The treatment of textile wastewater including chromium(VI) and reactive dye by sulfate-reducing bacterial enrichment. J. Environ. Manage. 88 (2008) 76-82.

[2.16] M. A. García-Morales, G. Roa-Morales, C. Barrera-Díaz, V. Martínez Miranda, P. Balderas Hernández, T. B. PavónSilva, Integrated Advanced Oxidation Process (Ozonation) and Electrocoagulation Treatments for Dye Removal in Denim Effluents. Int. J. Electrochem. Sci. 8 (2013) 8752 – 8763

[2.17] A. Muhammad, A. Shafeeq, M. A. Butt, Z. H. Rizvi, M. A. Chughtai and S. Rehman, Decolorization and removal of COD and BOD from raw and bio treated textile dye bath effluent through advanced oxidation processes (AOPS). Brazilian J. of Chem. Eng. 25(03) (2008) 453 – 459.

[2.18] Hs. Hussein, R. Sabry, N. Hassan, M.S. Morsi, H.H. Sharrawy, Removal of Reactive Blue 19 from Textile Wastewater Using Iron Electrodes. Res. J. of Pharma. Bio.Che. Sci. 5(3) (2014) 2091 - 2105.

[2.19] O.A. Trujillo, S.A.M. Delgadillo, V.X. Mendoza, Escamilla, M.M. ZoZano, C.D. Barrera, Modelling the removal of indigo dye from the aqueous media in a sonoelectrochemical flow reactor. Int. J. Electrochemical Sci. 8 (2013) 3876-3887.

[2.20] M.M. Ahmed, Electrochemical Treatment of acid yellow and acid violet dyes assisted by transition metal modified kaolin. Portugaliae Electrochimia Acta. 26(6) (2008) 547-557.

[2.21] J.H. Sun, S.Y. Dong, Y.K. Wang, S.P. Sun, Preparation and photocatalytic property of a novel dumbbell shapeZnO microcrystal photocatalyst. J. Hazard. Mater. 172 (2009) 1520-1526.

[2.22] F. Yu, L. Shi, Catalytic oxidation and spectroscopic analysis of stimulated wastewater containing Acid Chrome Blue K by using chlorine dioxide as oxidant. Water Sci. Technol. 61 (2010) 1931-1940.

[2.23] R.O. Cristovao, A.P.M. Tavares, J.M. Loureiro, R.A.R. Boaventura, E.A.Macedo, Treatment of kinetic modeling of a simulated dye house effluent by enzymatic catalysis. Bioresource Technol. 100 (2009) 6236-6242.

[2.24] J.S. Martin, J. B. Heredia, C. S. Hernandez, Surface water and wastewater treatment using a new tannin-based coagulant. Pilot plant trials. J. Environ. Manage. 91 (2010) 2051-2058.

[2.25] F. Zidane, P.Drogui, B.Lekhlif, J. Bensaid, J.F. Blais, S. Belcadi, K.E. Kacemi, Decolorization of dye-containing effluent using mineral coagulants produced by electrocoagualtion. J. Hazard. Mater. 155 (2008) 153-163.

[2.26] M.F. Abid, M.A. Zablouk, A.M.B. Alameer, Experimental study of dye removal from industrial waste water by membrane technologies of reverse osmosis and nano filtration. Iranian J. of Environ. Health Sci. Eng. 9 (17) (2012) 1- 9.

[2.27] S.W. Puasa, M.S. Ruzitah, A.S.A.K. Sharifah, Competitive removal of Reactive Black 5/Reactive orange 16 from aqueous solution via micellar – enhanced ultrafiltration. Int. J. of Che. Eng. Appl. 3(5) (2012) 1567-1581.

[2.28] B. Altenbaher, S.S. Turk, Treatment of textile processing wastewater with membrane filtrations. Tekstil 58 (2009) 367-383.

[2.29] F. Harrelkas, A. Paulo, M.M. Alves, L.E. Khadir, O. Zahraa, M.N. Pons, F.P. van der Zee, Photocatalytic and combined anaerobic-photocatalytic treatment of textile dyes. Chemosphere 72 (2008) 1816-1822.

[2.30] S.M.D.A.G.U. de Souza, K.A.S. Bonilla, A.A.U. de Souza, Removal of COD and color from hydrolyzed textile azo dye by combined ozonation and biological treatment. J. Hazard. Mater. 179 (2010) 35 – 42.

[2.31] M. J. Garcia, X. Domenech, J.A.H. Garcia, F. Torrades, J. Peral, The testing of several biological and chemical coupled treatments for cibacron red FN – R azo dye removal. J. Hazard. Mater. 154 (2008) 484 – 490.

[2.32] T.G. Bulc, A. Ojstrsek, The use of constructed wetland for dye-rich textile wastewater treatment. J. Hazard. Mater. 155 (2008) 76-82.

[2.33] N. Sheth, S. Dave, Enhanced biodegradation of reactive violet 5R manufacturing wastewater using down flow fixed film bioreactor. Biores. Technol. 101 (2010) 8627-8631

[2.34] T. M. Ting, N. Jamaludin, Decolorization and decomposition of organic pollutants for reactive and disperse dyes using electron beam technology: Effect of concentration of pollutants and irradiation dose. Chemosphere 73 (2008) 76-80.

[2.35] A. Gürses, A. Hassani, M. Kiranşan, Ö. Açişh, S. Karaca, Removal of methylene blue from aqueous solution using by untreated lignite as potential low – cost adsorbent: Kinetic, thermodynamic and equilibrium approach. J. Water Process Eng. 2 (2014) 10-21.

[2.36] S. Chen, J. Zhang, C. Zhang, Q.Y ue, Y. Li, C. Li, Equilibrium and kinetic studies of methyl orange and methyl violet adsorption on activated carbon derived from phargmitesaustralis. Desalination 252, (2010) 149-156.

[2.37] I.D. Mall, V.C. Srivastava, N.K. Agarwal, Adsorptive removal of auramine – O; Kinetic and equilibrium study. J. Hazard. Mater. 143(2007) 386-395

[2.38] A. Mittal, A. Malviya, D. Kaur, J. Mittal, L. Kurup, Studies on the adsorption kinetics and isotherms for the removal and recovery of methyl orange from waste waters using waste materials. J. Hazard. Mater. 148, (2007) 229-240.

[2.39] N. Sakkayawong, P. Thiravetyan, W. Nakbanpote, adsorption mechanism of synthetic reactive dye waste water by chitosan. J. Colloid Interface Sci. 286, 2005, 36-42.

[2.40] L. Wang, A. Wang, Adsorption characteristics of congo red onto the chitosan / montmorillonitenanocomposite. J. Hazard. Mater. 147 (2007) 979 – 985.

[2.41] S.L. Wan, H.C. Lee, Y. C. Jeong, B.C. Min, S.C. Lee, preparation and acid dye adsorption behavior of polyurethane/chitosan composite foams. Fibers and Polymers 10 (2009) 636 – 642.

[2.42] M.Y. Chang, R.S. Juang, Adsorption of tannic acid humic acid and dyes from water using the composite of chitosan and activated clay. J. Colloid Interface Sci. 278 (2004)18 – 25.

[2.43] W.S.W. Nag, N.F.M. Ariff, A. Hashim, M.A.K.M. Hanafiah, Malachite green adsorption onto chitosan coated bentonite beads: Isotherms, kinetic and mechanisms. Clean – Soil, Air, Water 38 (2010)394 – 400.

[2.44] N. Hoda, E. Bayram, E. Ayranci, Kinetic and equilibrium studies on the removal of acid dyes from aqueous solutions by adsorption onto activated carbon cloth. J. Hazard. Mater. B 137 (2006) 344-351.

[2.45] F. Deniz, S. Karaman, Removal of basic red 46 dye from aqueous solution by pine tree leaves. Chem. Eng. J. 170, (2011) 67-74.

[2.46] S.E. Subramani, N. Thinakaran, Isotherm, kinetic and thermodynamic studies on the adsorption behavior of textile dyes onto chitosan, Process Safety and Environmental Protection. 106 (2017) 1- 10.

[2.47] S.S. Tahir, N. Rauf, Removal of a cationic dye from aqueous solutions by adsorption onto bentonite clay. Chemosphere 63(2006) 1842 – 1848.

[2.48] S. Preethi, A. Sivasamy, S. Sivanesan, V. Ramamurthi, G. Swaminathan, Removal of safranin basic dye from aqueous solutions by adsorption onto corncob activated carbon. Ind. Eng. Chem. Res. 45 (2006) 7627 – 7632.

[2.49] C.Y. Shiau, C.C. Pan, Adsorption of basic dyes from aqueous solution by various adsorbents. Sep. Sci. Technol. 39(8) (2004) 1733 -1750.

[2.50] N. Ali, G. Maryam, Synthesis and performance evaluation of chitosan prepared from Persian Gulf shrimp shell in removal of reactive blue 29 from aqueous solution (isotherm, thermodynamic and kinetic study). Iran J. Chem. Chem. Eng. 36(3) (2017) 25 – 36.

[2.51] A.K. Jain, V.K. Gupta, A. Bhatnagar, A. Suhas, Comparative study of adsorbents prepared from industrial wastes for removal of dyes. Sep. Sci. Technol. 38 (2) (2003) 463 – 481.

[2.52] A. Rodriguez, J. Garcia, G. Ovejero, M. Mestanza, Adsorption of anionic and cationic dyes on activated carbon from aqueous solutions: Equilibrium and kinetics. J. Hazard. Mater. 172 (2009) 1311-1320.

[2.53] O. Gulnaz, A. Kaya, F. Matyar, B. Arikan, Sorption of basic dyes from aqueous solution by activatdsludge. J. Hazard. Mater. B 108 (2004) 183-188.

[2.54] I.D. Mall, V.C. Srivastava, G.V.A. Kumar, I.M. Mishra, Characterization and utilization of mesoporous fertilizer waste carbon for adsorptive removal of dyes from aqueous solution. Colloids and Surfaces A: Physicochem. Eng. Aspects 278 (2006) 175 – 187.

[2.55] D.K. Singh, B. Srivastava, Basic dye removal from waste water by adsorption on rice husk carbon. Indian J.Chem.Tech. 8 (2001) 133 – 139.

[2.56] T. Liu, Y. Li, Q. Du, J. Sun, Y. Jiao, G. Yang, Z. Wang, Y. Xia, W. Zhang, K. Wang, H. Zhu, Wu Dehai, Adsorption of methylene blue from aqueous solution by graphene. Colloids and Surfaces B: Biointerfaces 90 (2012) 197-203.

[2.57] D. Ghosh, K.G. Bhattacharyya, Adsorption of methylene blue on kaolinite. Appl. Clay Sci. 20 (2002) 295 – 300.

[2.58] M.K. Purkait, S. DasGupta, S. De, Adsorption of eosin dye on activated carbon and its surfactant based desorption. J. Environ. Management 76 (2005) 135 – 142.

[2.59] E.M. Terezinha, de Carvalho, D.A. Fungaro, C.P. Magdalene, P. Cunico, Adsorption of indigo carmine from aqueous solutions using coal fly ash and zeolite from fly ash. J. Radioanal Nucl. Chem. 289 (2011) 617 – 626.

[2.60] A. Olgun, N. Atar, Equilibrium and kinetic adsorption study of basic yellow 28 and basic red 46 by a boron industry waste. J. Hazard. Mater. 161 (2009) 148 – 156.

[2.61] A.B. Karim, B. Mounir, M. Hachkar, M. Bakasse, A. Yaacoubi, Removal of basic red 46 dye from aqueous solution by adsorption onto Moroccan clay. J. Hazard. Mater. 168 (2009) 304 – 309.

[2.62] I.D. Mall, V.C. Srivastava, N.K. Agarwal, I. M. Mishra, Adsorptive removal of malachite green dye from aqueous solution by bagasse fly ash and activated carbon. Kinetic study and equilibrium isotherm analyses. Colloid Surface A: Physicochem. Eng. Aspects 264 (2005) 17 – 28.

[2.63] I.D. Mall, V.C. Srivastava, N.K. Agarwal, I. M. Mishra, Removal of congo red from aqueous solution by bagasse fly ash and activated carbon: kinetic study and equilibrium isotherm analyses. Chemosphere 61 (2005) 492 – 501.

[2.64] I.D. Mall, V.C. Srivastava, N.K. Agarwal, I. M. Mishra, removal of orange G and methyl violet dyes by adsorption onto bagasse fly ash: kinetic study and equilibrium isotherm analyses. Dyes and Pigm. 69 (2006) 210 – 223.

[2.65] N. Kannan, M.M. Sundaram, Kinetics and mechanism of removal of methylene blue by adsorption on various carbons—a comparative study. Dyes and Pigm. 51 (2001) 25–40.

[2.66] N. Kannan, M.M. Sundaram, Adsorption of congo red on various activated carbons. Water Air Soil Pollut.138 (2002) 289 – 305.

[2.67] K.V. Kumar, S. Sivanesan, Comparison of linear and non – linear method in estimating the sorption isotherm parameters for safranin onto activated carbon. J. Hazard. Mater. B 123 (2005) 288 – 292.

[2.68] N.M. Mahmoodi, M. Arami, H. Bahrami, S. Khorramfar, Noval biosorbent(Canola hull): surface characterization and dye removal ability at different cationic dye concentrations. Desalination 264 (2010) 134 – 142.

[2.69] F. Deniz, S.D. Saygideger, Removal of a hazardous azo dye (basic red 46) from aqueous solution by princess tree leaf. Desalination 268 (2011) 6 – 11.

[2.70] F. Deniz, S.D. Saygideger, Investigation of adsorption characteristics of basic red 46 on to gypsum: equilibrium kinetics and thermodynamic study. Desalination 262 (2010) 161 – 165.

[2.71] H. Patel, R.T. Vashi, Fixed bed column adsorption of acid yellow 17 dye onto tamarind seed powder. Can. J. Chem. Eng. 90 (2012) 189 – 185.

[2.72] R. Han, Y. Wang, X. Zhao, Y. Wang, F. Xie, J. Cheng, M. Tang, Adsorption of methylene blue by phoenix tree leaf powder in a fixed – bed column: experiments and prediction of breakthrough curves. Desalination 245 (2009) 284 – 297.

[2.73] A.C.M.A. Rucha, I.B. Valentim, F.C. de. Abreu, indigo carmine removal from aqueous solution using natural bio polymer: fixed – bed column study. E. J. Sci. Technol. 4 (2015) 1-16

[2.74] N. Gopal, M. Asaithambi, P. Sivakumar, V. Sivakumar, Continuous fixed bed adsorption studies of rhodamine - B dye using polymer bound adsorbent. I. J. Chem. Technol. 23 (2016) 53 – 58.

[2.75] J.L. Cervantes, D. I. S. Machado, R. G. S. Duarte, and M. A.C. Murrieta, Study of a fixed-bed column in the adsorption of an azo dye from an aqueous medium using a chitosan– glutaraldehyde biosorbent. Adsorption Sci. Technol. 36 (1-2) (2017) 215 – 232.

[2.76] A.A. Ahmad, B. H. Hameed, Fixed-bed adsorption of reactive azo dye onto granular activated carbon prepared from waste. J. Hazard. Mater. 175 (2010) 298 – 303.

[2.77] K. S. Bharathi, S.P.T. Ramesh, Fixed – bed column studies on biosorption of crystal violet from aqueous solution by Citrulluslanatus rind and Cyperusrotundus. Appl. Water Sci. DOI 10.1007/s13201-013-0103

[2.78] I.J. Idan, L.C. Abdullah, S.N.A.B. Md. Jamil, M.K. Obaid, T.S.Y. Choong, Fixed – bed system for the adsorption of anionic acid dyes from binary solution onto quaternizedkenaf core fibre. BioResources 12 (4) (2107) 8870 – 8885.

[2.79] L. Markovska, V. Meshko, V. Noveski, Adsorption of basic dyes in a fixed bed column. Korean J. Chem. Eng., 18(2) (2001) 190-195.

[2.80] S. Rouf, M. Nagapadma, Modeling of Fixed Bed Column Studies for Adsorption of Azo Dye on Chitosan Impregnated with a Cationic Surfactant. Int. J. Sci. Eng. Res. 6 (2) (2015) 538 – 545.

[2.81] M.S. Sajab, C.H. Chia, S.Zakaria, M. Sillanpaa, Fixed-bed column studies for the removal of cationic and anionic dyes by chemically modified oil palm empty fruit bunch fibers: single- and multi-solute systems. Desalination Water Treatment, 55 (2015) 1372–1379.

[2.82] B. O. Isiuku1, C. A. Ojike1, O. U. Akakuru, F. C. Ibe1, Fixed-bed adsorptive removal of metanil yellow from simulated wastewater in a fixed-bed column by nitric acid-treated-H3PO4-activated carbon (NATPAAC) from oil palm fruit mesocarpfiber. World News of Natural Sciences 17 (2018) 157-172.

[2.83] K.Y. Foo, B.H. Hameed, Insights into the modeling of adsorption isotherm systems. Chem. Eng. J. 156, (2010) 2-10.

[2.84] H.M.F. Freundlich, Over the adsorption in solution. J. Phys. Chem. 57 (1906) 385-471.

[2.85] Z.J. Hu, N.X. Wang, J. Tan, J.Q. Chen, W.Y. Zhong, Kinetic and equilibrium of cefradine adsorption onto peanut husk. Desalination and Water Treatment 37 (2012) 160-168.

[2.86] I. Langmuir, The adsorption of gases on plane surface glass, mica and platinum. J. Am. Chem. Soc. 40 (1918) 1361-1403.

[2.87] D. O. Cooney, Adsorption design for waste water treatment. Lewis publishers. New York, 1999.

[2.88] C.J. Radke, J.M. Prausnitz, Adsorption of organic solutes from dilute aqueous solution on activated carbon. Ind. Eng. Chem. 11 (1972) 445.

[2.89] D.H. Lataye, I.M. Mishra, I.D. Mall, Pyridine sorption from aqueous solution by rice husk ash (RHA) and granular activated carbon (GAC): Parametric, kinetic, equilibrium and thermodynamic aspects. J. Hazard. Mater. 154 (2008) 858 – 870.

[2.90] V.C. Srivastava, I.D. Mall, I.M. Mishra, Adsorption thermodynamics and isosteric heat of adsorption of toxic metal ions onto bagasse fly ash (BFA) and rice husk ash (RHA). Chem. Eng. J. 132 (2007) 267-278.

[2.91] A.R. Khan, M.R. Riazi, Y.A. Al-Roomi, A thermodynamic model for liquid adsorption isotherms. Sepr. Purif. Technol. 18 (2000) 237-250.

[2.92] R. Watkins, D. Weiss, W. Dubbin, K. Peel, B. Coles, T. Arnold, Investigations into the kinetics and thermodynamics of Sb(III) adsorption on goethite (α -FeOOH). J. Colloid Interface Sci. 303 (2006) 639 – 646.

[2.93] S. Azizian, M. Haerifar, H. Bashiri, Adsorption of methyl violet onto granular activated carbon: Equilibrium, kinetics and modeling. Chem. Eng. J. 146, (2009) 36-41.

[2.94] N. Hoda, E. Bayram, E. Ayranci, Kinetic and equilibrium studies on the removal of acid dyes from aqueous solutions by adsorption onto activated carbon cloth. J. Hazard. Mater. B137 (2006) 344 – 351.

[2.95] H.C. Thomas, Heterogeneous ion exchange in a flowing system. J. Am. Chem.Soc. 66 (1944) 1664.

[2.96] H. C. Thomas, Chromatography: a problem in kinetics. Ann. N.Y. Acad. Sci. 49 (1948)161.

[2.97] A. P. Lim, A. Z. Aris, Continuous fixed – bed column study and adsorption modeling; removal of cadmium (II) and lead (II) ions in aqueous solution by dead calcareous skeletons. Biochem. Eng. J. 87 (2014) 50 -61.

CHAPTER 3
AIMS AND OBJECTIVES

Dyes are most widely used in industries such as textile, cosmetics, leather, plastic, printing and paper [3.1]. Rapid industrial development has resulted in increased discharge of effluents into the environment. The disposal of the effluent containing dyes into the water bodies affect the environmental ecology [3.2- 3.4]. The world is heading towards fresh water shortage as the resource is depleting due to industries, agriculture and domestic usage. Hence, these effluents should be treated to meet the requirements of environmental legislations before being discharged into the water bodies.

Many research activities have been carried out in the field of purification of waste water. Several treatment methods are available to remove dyes from effluents. These are broadly classified as physical, chemical and biological methods [3.5]. A brief discussion about the treatment methods have been presented in the chapter 1. The major advantages and disadvantages of the various treatment methods are summarized below.

The chemical treatment methods used are chemical oxidation, chemical precipitation, coagulation / flocculation. The advantages of these methods are ease of operate, and suitability for treatment of dyes. The volume of the waste water does not increase significantly in ozone treatment, the odors are greatly reduced and sludge formation is less. This process is however associated with the high energy consumption and chemical requirement. The chemical treatment of dyes also results in generating unwanted byproducts which cannot be used. In chemical treatment process, the total dissolved solids cannot be reduced and

dissolved solids level may raise which affect recycle of the treated effluent. The sludge generated leads to handling and disposal problems.

In biological treatment systems, the living and nonliving bio mass can be used as an adsorbent. The main draw backs are space requirement, high initial investment, and energy requirement for the supply of oxygen needed for aerobic digestion. Sludge generated is also high. The biological process are not very attractive because of more difficulty of maintaining operating conditions and inability to degrade the azo dyes. The literature study reveals that the biological treatments are ineffective for the many class of dyes.

Treatment of textile effluents via membrane technology is not widely acceptable process as it cannot efficiently remove low molecular weight dyes and soluble dyes. The treated effluent cannot be used directly as it requires further treatment. The disposal of the concentrated product is also a major concern. The major disadvantages are the high initial cost of the membrane, and the associated operating cost as the membrane operates at very high pressures. The frequent replacement of membrane is the other disadvantage of the method.

Adsorption is another technique for the treatment of dye effluents. . The process is less energy intensive unit operation compared to others. The method of operation is not complicated. These factors make it one of the attractive options for treatment of effluent in the industries [3.3]. Hence this study is focused on the adsorption technique for decolorization of effluent

The most common adsorbent is activated carbon. However, the cost of this adsorbent is high. Therefore, there is a need to identify the low cost adsorbent for dye removal. Interests are growing in recent years to find an alternate adsorbent to replace activated carbon to make the process more economical and effective [3.6 - 3.7].

In the past two decades, studies have focused on the use of agricultural waste materials and marine waste as adsorbent. Abundantly available marine based bio polymer, chitin may be used as a source of chitosan which is a low cost adsorbent. Chitosan shows good affinity for many classes of dyes. Due to the unique polycationic structure, chitosan finds extensive application in removal of anionic dyes such as acid, reactive and direct dyes from aqueous solution. Several million tons of sea food are processed every year. Nearly half of the sea food reject is generated as shell wastes. Therefore, it is essential to utilize bio materials generated from the sea food in a sustainable way. The application of chitin / chitosan in the area of removal of dyes gained significant development. Palmyra male inflorescence is another material which is abundantly available in the coastal area of Puducherry and Tamil Nadu region. Chitosan and the Palmyra male inflorescence are materials that have been considered as a source of adsorbents for dye removal in this study.

The anionic dyes like eosin Y, indigo carmine, and cationic dyes like orange G, safranine O, malachite green oxalate are continuously used in industries such as textiles, printing, paper and leather industries. The adsorbents developed in this study was used to decolorize solution produced by these dye compounds.

The objectives of the proposed research are presented in the following section.

- Development of new adsorbent:

  To develop low cost adsorbent material from agricultural waste, palmyra male inflorescence and sea food wastes such as crab and shrimp shells for the removal of dyes from aqueous solution. It has been noted that pretreatment often result in improvement of surface properties leading to higher uptake [3.8]. Therefore, the adsorbents were pretreated with different chemicals.

- Characterization of new adsorbent

  Characterization is important to understand and identify the physical structures and chemical properties. The newly prepared adsorbents were characterized using Fourier transform infrared spectroscopy (FTIR), particle size analyzer and BET instrument to determine the active sites, particle size, surface area, pore volume among others.

- Determining adsorption equilibrium of new adsorbent

  Knowledge of adsorption equilibrium is required to determine optimum amount of adsorbent required for removal of a given amount of solute for a given condition, design of contactor etc. Batch studies for various adsorbent-dye system were carried to investigate the effect of the parameters such as temperature, pH, solute concentration and adsorbent dose on adsorbed amount.

- Modeling of adsorption equilibrium data:

  Experimental determination of isotherm data at various temperatures is time intensive. Hence modeling of isotherm is essential for scaleup. The batch

equilibrium isotherm data was validated with the existing models available in the literature [3.9].

- Estimation of thermodynamic properties

  Thermodynamic properties are useful in identifying the nature of the adsorption process i.e. whether it is exothermic or endothermic, spontaneous among others. The thermodynamic behavior of the adsorption process is studied by determining the thermodynamic parameters such as Gibbs energy change (ΔG^o) enthalpy change(ΔH^o) and entropy change (ΔS^o) for the various adsorbent dye system [3.10-3.11]

- Determining adsorption kinetic parameters

  The uptake capacity choice of an adsorbent is determined by the rate at which the solute is adsorbing onto the adsorbent. This along with the understanding the mechanism of adsorption is required can be obtained from kinetic study.

- Development of new adsorption isotherm models

  The models used for correlating adsorption isotherm can be broadly classified as empirical models, chemical equilibrium based models and phase equilibrium based models. All these models require parameters such as quantity q_e (moles of adsorbate / mass of adsorbent) as a function of the adsorbate equilibrium concentration C_e (moles of adsorbate / volume of solution) in liquid. The relation between q_e and C_e at a temperature is known as adsorption isotherm. The conventional isotherm models (such Freundlich, Langmuir and other extended models) [3.12] correlate the adsorption data but does not account adsorbate – adsorbent properties in it. Such models have limited use in predicting the isotherm

data and can be used only within the concentration range examined. Therefore, there is a need to develop new adsorption isotherm models which accounts adsorbate - adsorbent properties. Such models would be useful in predicting isotherms at conditions beyond the concentration range examined.

- To investigate the breakthrough characteristics in a fixed bed using the existing models available in the literature [3.13].

  Fixed bed systems are more reliable and attractive in terms of time requirement and hence, are widely used in industries. The performance of the fixed bed system are represented in the form of breakthrough curves. The parameters such as time to breakthrough, stoichiometric wave front time, and exhaust time can be obtained from the breakthrough curves.

- Establishing equilibrium adsorption isotherms data in a fixed bed using frontal method.

  Single component adsorption isotherm data can be obtained accurately by batch experiments. Another technique to determine the same for fixed bed studies is by frontal analysis method [3.14-3.16] Frontal studies are not given much emphasis in literature, but this method is quite useful and simple technique for development of single solute adsorption isotherm.

References

[3.1] A. Rodriguez, J. Garcia, G. Ovejero, M. Mestanza, Adsorption of anionic and cationic dyes on activated carbon from aqueous solutions. Equilibrium and kinetics. J. Hazard. Mater. 172(2009) 1311-1320.

[3.2] S. Chen, J. Zhang, C. Zhang, Q. Yue, Y. Li, C. Li, Equilibrium and kinetic studies of methyl orange and methyl violet adsorption on activated carbon derived from phargmitesaustralis. Desalination 252 (2010) 149-156.

[3.3] A. Mittal, A. Malviya, D. Kaur, J. Mittal, L. Kurup, Studies on the adsorption kinetics and isotherms for the removal and recovery of methyl orange from waste waters using waste materials. J. Hazard. Mater. 148 (2007) 229-240.

[3.4] O. Gulnaz, A. Kaya, F. Matyar, B. Arikan, Sorption of basic dyes from aqueous solution by activated sludge. J. Hazard. Mater. B 108(2004) 183-188.

[3.5] N.M. Mahmoodi, B. Hayati, M. Arami, C. Lan, Adsorption of textile dyes on pine cone from colored wastewater: Kinetic, equilibrium and thermodynamic studies. Desalination 268 (2011) 117-125.

[3.6] T. Liu, Y. Li, Q. Du, J. Sun, Y. Jiao, G. Yang, Z. Wang, Y. Xia, W. Zhang, K. Wang, H. Zhu, Wu Dehai, Adsorption of methylene blue from aqueous solution by graphene. Colloids and Surfaces B: Biointerfaces 90 (2012) 197-203.

[3.7] A.S. Özcan, A. Özcan, Adsorption of acid dyes from aqueous solutions onto acid – activated bentonite. J. Colloid. Interface Sci. 276 (2004) 39 – 46.

[3.8] M. R. Lasheen, N.S. Ammar, H.S. Ibrahim, Adsorption / desorption of Cd (II), Cu (II) and Pb (II) using chemically modified orange peel: Equilibrium and kinetic studies. Solid State Sci. 14 (2012) 202 -210.

[3.9] K.Y. Foo, B.H. Hameed, Insights into the modeling of adsorption isotherm systems. Chem. Eng. J. 156. (2010) 2-10.

[3.10] A. Mittal, A. Malviya, D. Kaur, J. Mittal, L. Kurup, Studies on the adsorption kinetics and isotherms for the removal and recovery of methyl orange from waste waters using waste materials. J. Hazard. Mater. 148 (2007) 229-240.

[3.11] R. Watkins, D. Weiss, W. Dubbin, K. Peel, B. Coles, T. Arnold, Investigations into the kinetics and thermodynamics of Sb(III) adsorption on goethite (α -FeOOH). J. Colloid Interface Sci. 303 (2006) 639 – 646.

[3.12] D. O. Cooney, Adsorption design for waste water treatment. Lewis publishers, New York. (1999).

[3.13] A. P. Lim, A. Z. Aris, Continuous fixed – bed column study and adsorption modeling; removal of cadmium (II) and lead (II) ions in aqueous solution by dead calcareous skeletons. Biochem. Eng. J. 87 (2014) 50 -61

[3.14] A. L. Hines, R.N. Maddox, Mass transfer fundamental and applications. Prentice Hall Inc., NJ.1985.

[3.15] D.L.A. Fernandes, M.R.B. Xavier, A.D. Silva, C.M. Silva, Dynamic and equilibrium adsorption experiments. J. Chem. Edu. 82(6) (2005) 919 – 923.

[3.16] O. Lisec, P. Hugo, A.S. Morgenstern, Frontal analysis method to determine competitive adsorption isotherms. J. Chromatogr. A 908 (2001) 19-34.

CHAPTER 4
CHARACTERIZATION
OF
ADSORBENTS

This study was carried out to understand the physical structures and properties of the adsorbents developed from the agricultural and sea food waste. The instruments used for characterization were particle size analyzer, Brunauer-Emmett and Teller (BET) and Fourier Transform Infrared Spectroscopy (FTIR). Particle size analyzer was used to estimates the average particle size, BET instrument to determine the specific surface area, pore volume, average pore diameter, whereas FTIR analysis was used to identify various functional groups on the adsorbent surface.

4.1 Materials and methods

The commercial activated carbon (CAS No. 7440 -44 -0) was purchased from Merck. The material was washed thoroughly with distilled water and dried in an oven at 383.15 K. This material was used as such for adsorption studies. Palmyra male inflorescence was collected from a village near Puducherry. The material is washed with distilled water, sun dried and subjected to further processing. The crab and shrimp shells were collected from the local fish market in Cuddalore, Tamil Nadu. The materials are washed with distilled water and dried in sunlight and subjected to further processing. More details about the processing methods about palmyra male inflorescence and chitosan are discussed in the following section.

4.1.1 Preparation of palmyra male inflorescence carbon

The Palmyra male inflorescences was collected from Vaduvakuppam village in Puducherry, India. The flow sheet for preparation of palmyra male inflorescence carbon is shown in figure 4.1.

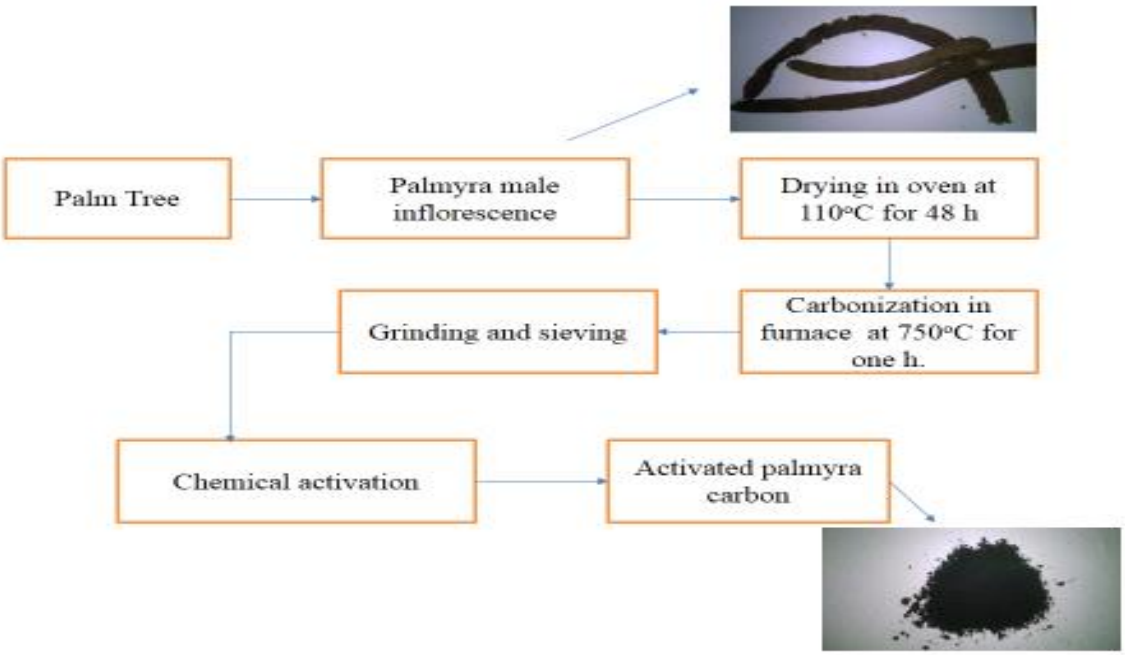

Figure 4.1 Preparation of activated palmyra male inflorescence carbon.

The material was washed with distill water and dried in an oven. The carbonization was carried in a muffle furnace under airtight condition at 750° C for one hour. The palmyra male inflorescence was chemically activated with 0.1N solution of KOH, H_3PO_4 and $ZnCl_2$ respectively (1:10 w/v) and washed till the solution reached neutral pH. The samples were dried at 110°C, powdered and sieved.

4.1.2 Preparation of chitosan

The bio polymer chitosan was prepared from chitin from the waste of crab and shrimp shells [4.1- 4.2]. This waste is available abundantly from local fish market of Cuddalore, Tamil Nadu. These are the marine source of Bay of Bengal, India. The procedure for the preparation of chitosan was the same as used by Subramani and Thinakaran [4.3]. It is depicted here figure 4.2.

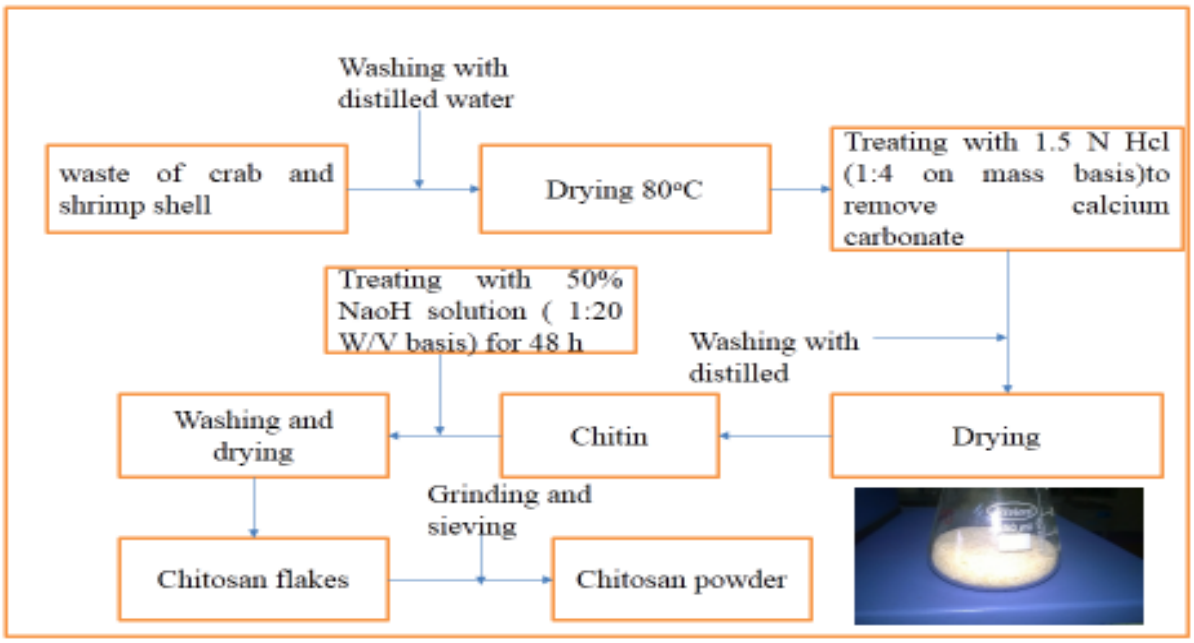

Figure 4.2 Preparation of chitosan from crab and shrimp shells.

The collected crab and prawn shells were washed with distilled water and then sun dried for a week. The dried material was then dried for one day at 80^{o} C in an electrical oven. It was then soaked in 1.5 N HCL for 24 h in ratio of 1:4 (mass basis) to remove calcium carbonate and then thoroughly washed with distilled water. The chitin obtained was dried further to remove the moisture. The chitosan was obtained by treating the chitin with 50% NaoH (1:20w/v) for 2 days. The alkali was drained and washed with distilled water until the washing reached the neutral pH. The chitosan was dried at 80^{o}C, powdered and sieved.

4.2 Results and Discussion

The surface area and pore size of activated carbon was evaluated using Brunauer-Emmet-Teller (BET) instrument (Beckman Coulter®; ASAP 2020 V4.03 (V4.03 H)). The value of surface area was calculated by BET method. The mesopore volume and size was calculated by Barret, Joyner, and Halenda (BJH) technique [4.4 – 4.5]

4.2.1 Activated carbon characterization

The commercial activated carbon surface area and pore size was evaluated using Brunauer-Emmet-Teller (BET) instrument. Figure 4.3 (a) and 4.3 (b) shows the nitrogen adsorption and desorption isotherm at 77 K, and pore area against pore diameter respectively. The value of surface area determined by BET method was 1155.20 m^2/g and that of the total pore volume was 0.7233 cm^3/g.

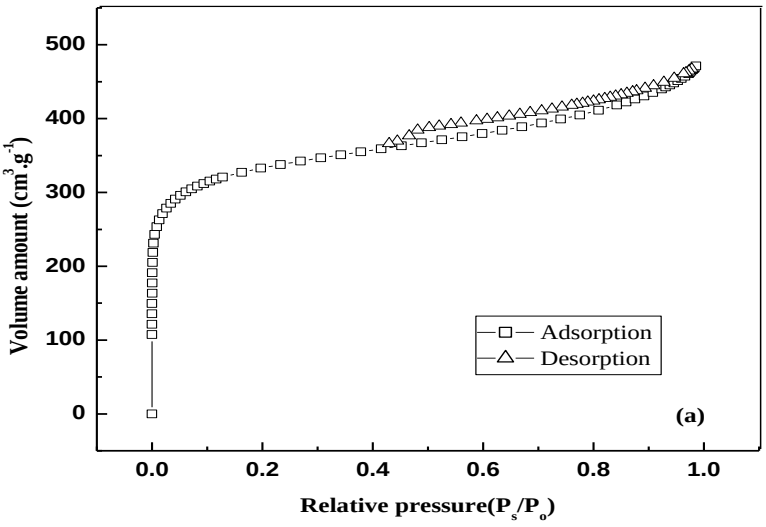

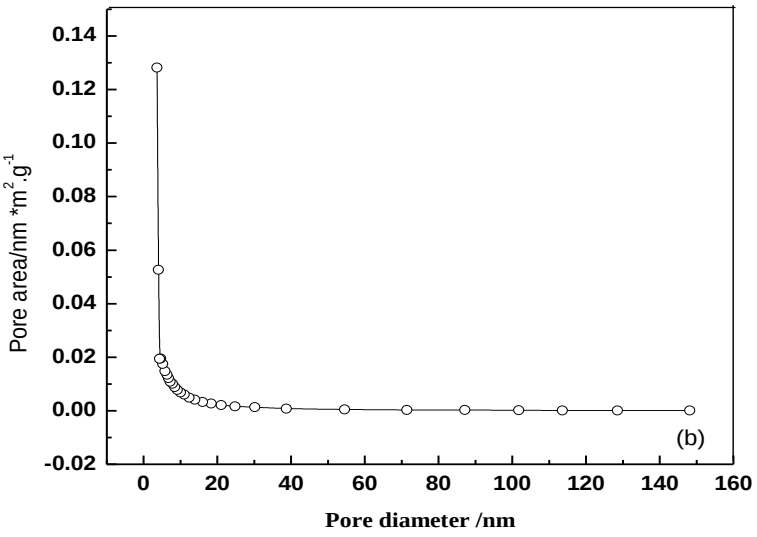

Figure 4.3 (a) Activated carbon hysteresis isotherm (BET) **(b)** Activated carbon pore area vs. pore diameter (BET).

Figure 4.4 (a) and 4.4 (b) shows the pore size distribution and particle size distribution respectively. The average particle size is found to be 26.514µm. The average particle size was analyzed using HORIBA® laser scattering particle size distribution Analyzer model LA-960.

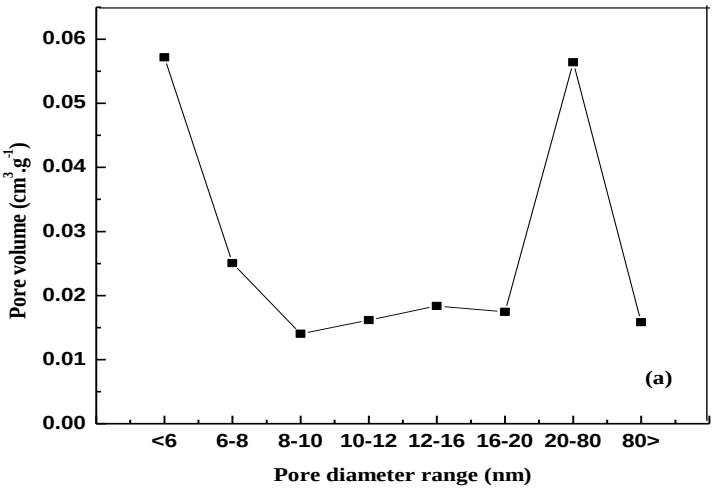

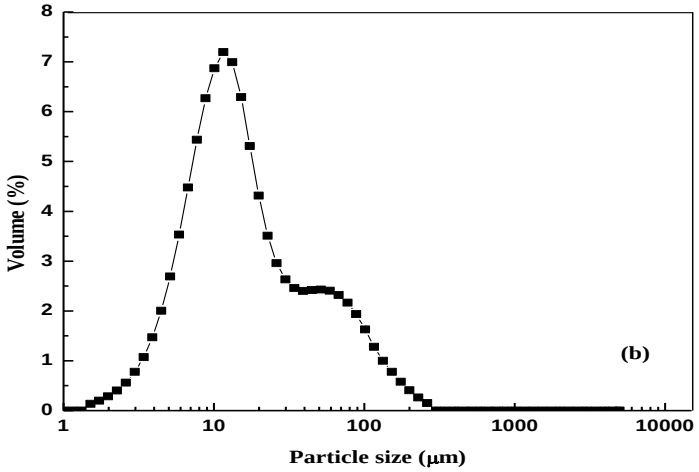

Figure 4.4 (a) Pore size distribution of activated carbon (BET) (b) Particle size distribution of activated carbon (HORIBA LA90).

4.2.2 Palmyra male inflorescence carbon characterization

The palmyramale inflorescence carbon surface area and pore size was evaluated using Brunauer-Emmet-Teller (BET) instrument (ASAP 2020 V4.03 (V4.03 H). The value of surface area and the total pore volume calculated by BET method were 2.4732 m^2/g and 0.007016 cm^3/g respectively whereas the average pore size was 113.4807 Å. Figure 4.5 (a) and 4.5 (b) shows the nitrogen adsorption and desorption isotherm at 77 K, and pore area against pore diameter respectively.

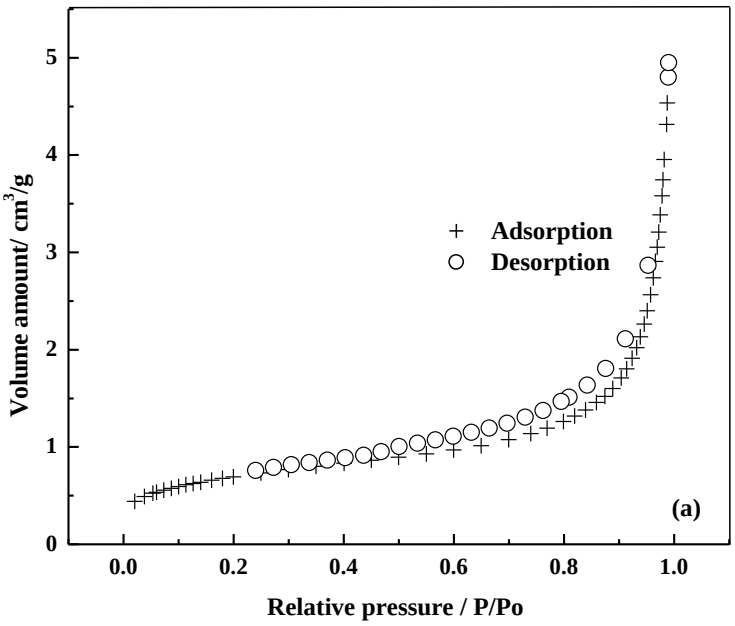

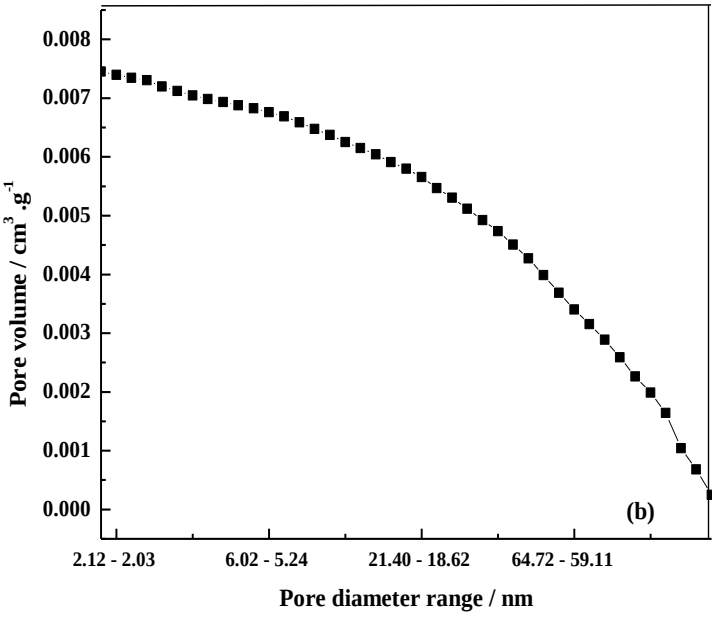

Figure 4.5 (a) Palmyra male inflorescence carbon (KOH) hysteresis isotherm (BET). (b) Pore size distribution (BET)

The average particle size is 6.81335 μm. Figure 4.6 (a) and 4.6 (b) shows the pore size distribution and particle size distribution respectively.

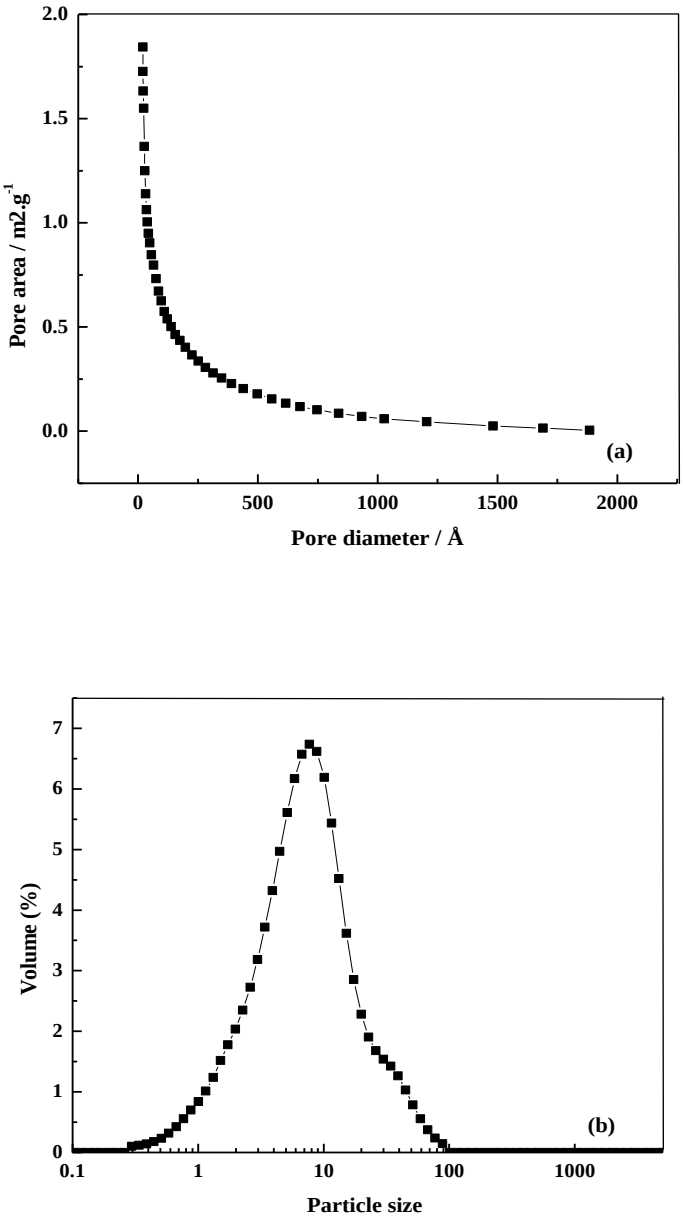

Figure 4.6 (a) Palmyra male inflorescence carbon (KOH) pore area vs pore diameter. (b) Particle size distribution (Horiba LA90)

4.2.2 (a) Fourier Transform infrared spectroscopy (FTIR) study of palmyra male influroscence carbon

FTIR was used for structural analysis of organic compounds. In this technique, the identification of the various structural groups available in the compounds is possible as the infrared radiation is selectively adsorbed by the various bonds within the compound. The structures can be identified by various peaks at different wave numbers. The FTIR spectrum of raw palmyra male inflouresece carbon and the chemically treated carbon is shown in the figure 4.7. The raw palmyra male inflouresece carbon shows the absence of the fuctional groups. The carbon treated with various chemicals undergo changes in the funtional groups. For the chemically treated palmyra male influrosence carbon, the absorbance at the wave number (cm^{-1}) 1000 – 1250 (cm^{-1}) indicates the stretching of C-O bonds which is attributed by the hydroxyl and unsaturated ethers. The bending of O-H and C-H between 1350 and 1430(cm^{-1}) indicates the presence of hydroxyl, carboxylic acid, olefins and methyl group. The stretching of C = C between 1600 and 1700(cm^{-1}) shows the olefinic structures, and the wave number at 1750(cm^{-1})represents the presence of C = O which shows the presence of carbonyl groups. The stretching of O – H, N – H at 3000 – 3600 cm^{-1}shows hydroxyl and carboxylic acid groups [4.6].

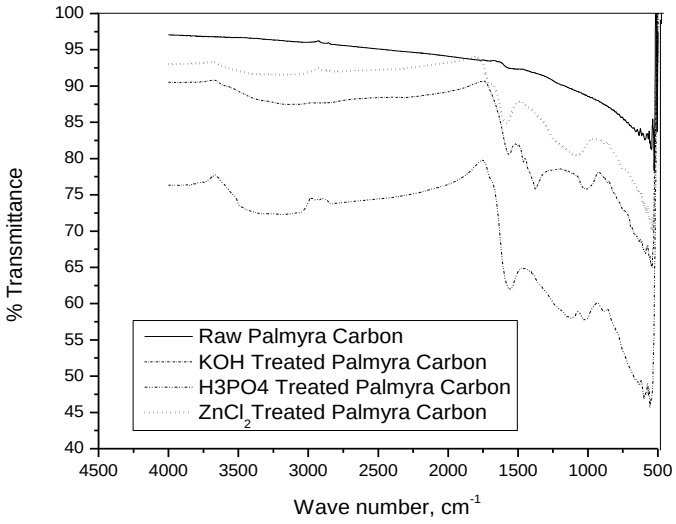

Figure 4.7 FTIR spectroscopy of palmyra male inflorescence carbon

4.2.3 Chitosan characterisation

The chitin was deacetylated with 50 % sodium hydroxide solution to get chitosan. Figure 4.8 shows the FTIR spectrum of chitosan. The degree of deacetylation of the chitosan was determined by Fourier transform infrared (FTIR) spectroscope using the following equation [4.7].

$$DD = 97.67 - \left[26.486\left(A_{1655}/A_{3450}\right)\right] \qquad (4.1)$$

Where A_{1655} and A_{3450} are absorbency values at 1655 and 3450 cm^{-1} for carbonyl and hydroxyl peaks. The degree of deacetylation of the chitosan sample was found to be 55.44 percent (figure 4.8). The chemical structure of chitosan is shown in figure 4.9.

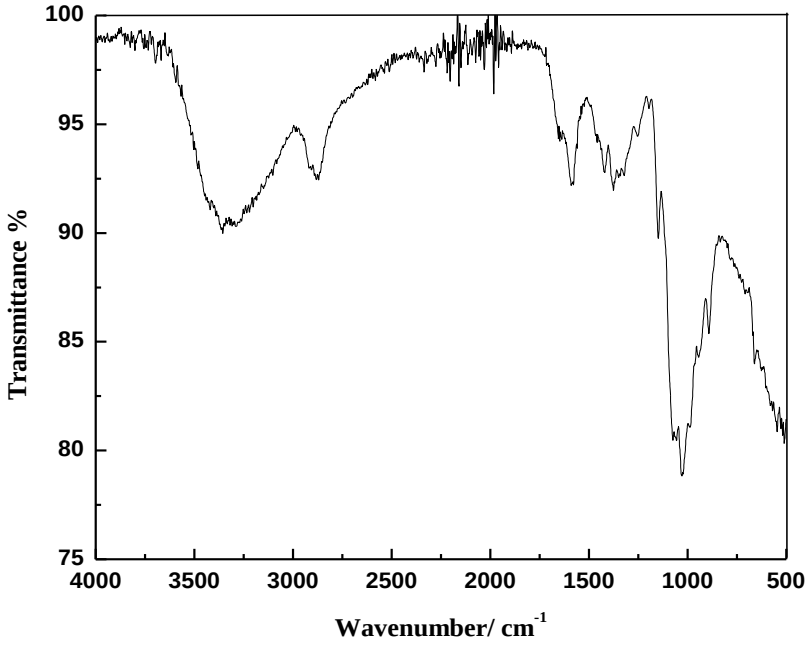

Figure 4.8 The FTIR spectrum of chitosan sample.

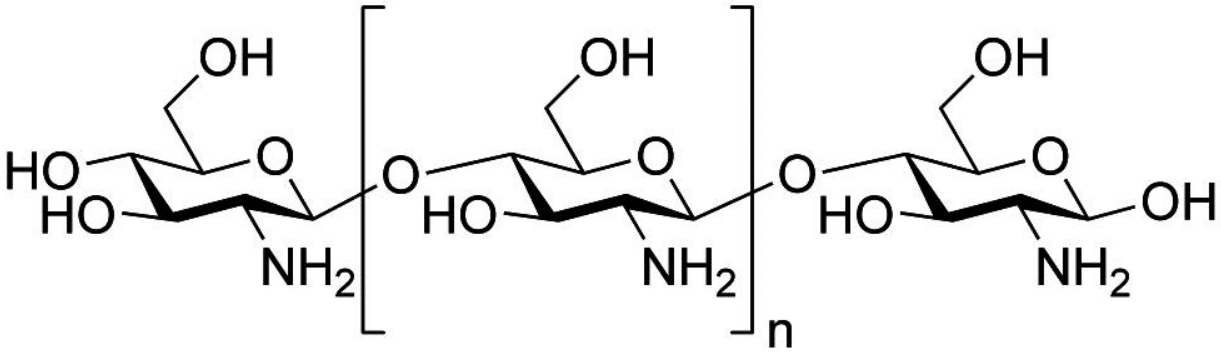

Figure 4.9 Chemical structure of chitosan.

The chitosan surface area 0.5305 m^2/g and pore size 176.3554 Å was evaluated using Brunauer-Emmet-Teller (BET) instrument (ASAP 2020 V4.03 (V4.03 H). The total pore volume was 0.000007cm^3/g. Figure 4.10 (a) and 4.10 (b) shows the nitrogen adsorption and desorption isotherm at 77 K, and pore area against pore diameter respectively. The average particle size is 48.18440. Figure 4.11 (a) and 4.11(b) shows the pore size distribution and particle size distribution respectively.

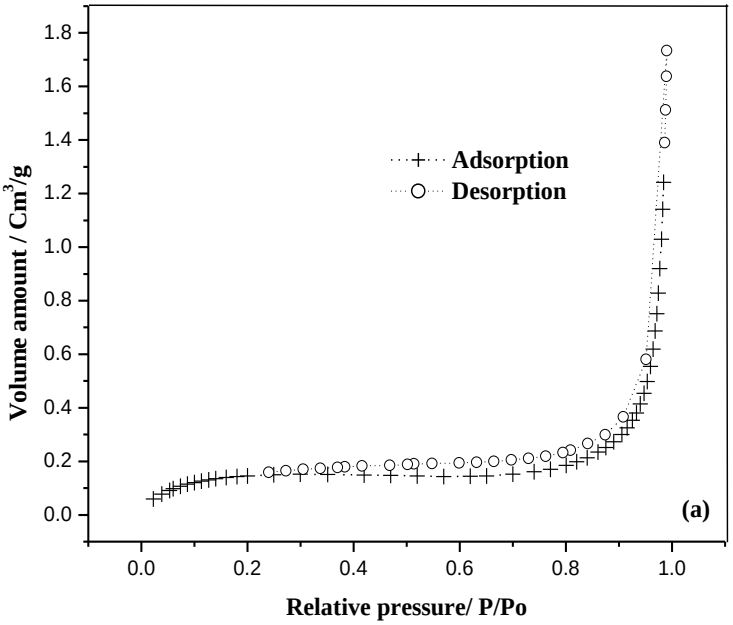

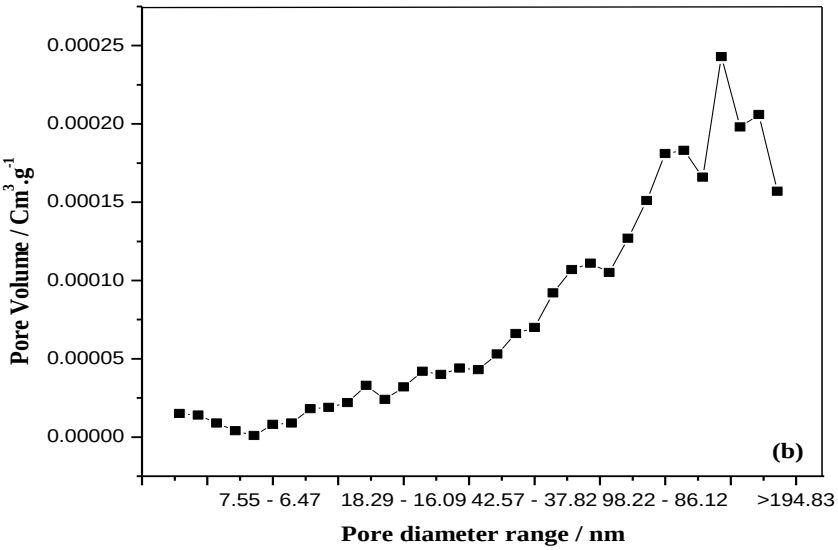

Figure 4.10 (a) Chitosan hysteresis isotherm (BET). (b) Pore size distribution of chitosan (BET)

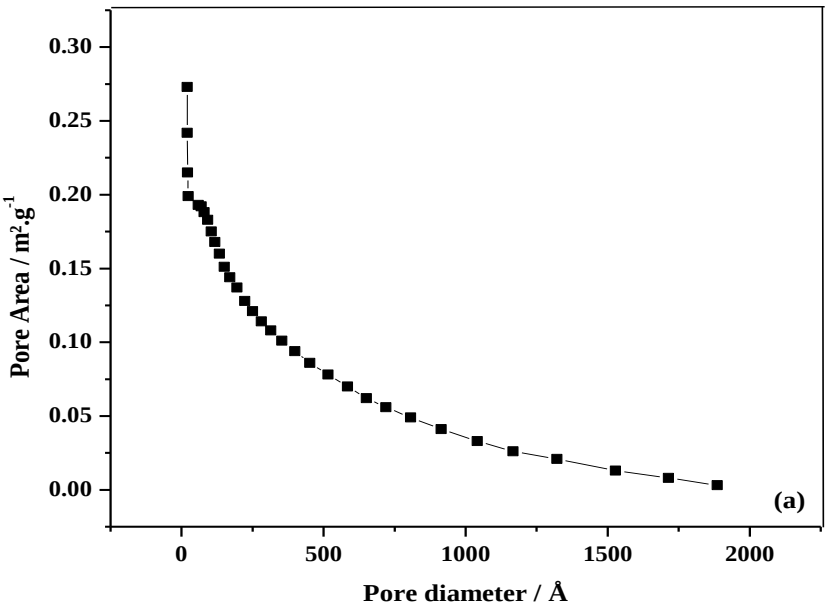

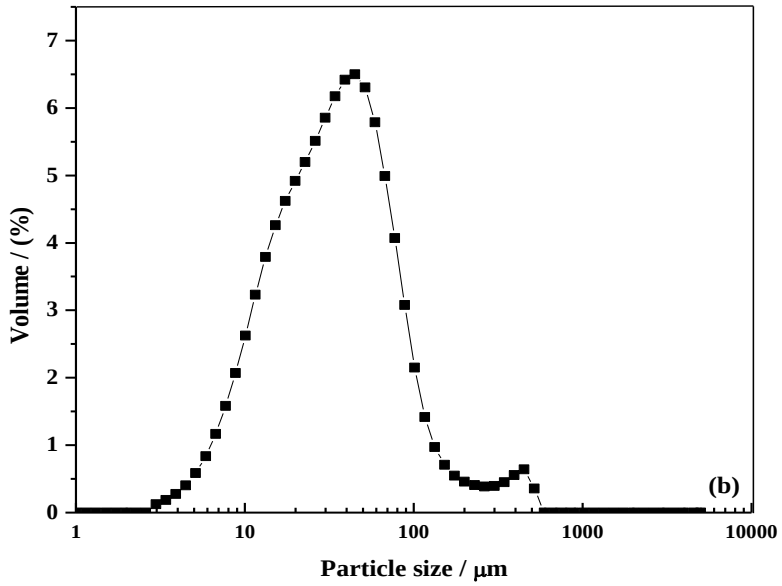

Figure 4.11 (a) Chitosan pore area vs pore diameter. (b) Particle size distribution of chitosan (Horiba LA90)

Reference

[4.1] M.N.V.R. Kumar, A. review of chitin and chitosan applications. Reactive & Functional Polymers 46 (2000) 1-27.

[4.2] C. Gerente, V.K.C. Lee, P. Le Cloirec, McKay, Critical Reviews in Environmental Science and Technology 37 (2007) 41 – 127.

[4.3] S.E. Subramani, N. Thinakaran, Isotherm, kinetic and thermodynamic studies on the adsorption behavior of textile dyes onto chitosan. Process Safety and Environmental Protection 106 (2017) 1- 10.

[4.4] A.F. Freitas, M.F. Mendes, G.L.V. Coelho, Thermodynamic study of fatty acids adsorption on different adsorbents. J. Chem. Thermodyn. 39 (2007) 1027 -1037.

[4.5] A. Rodriguez, J. Garcia, G. Ovejero, M. Mestanza, Adsorption of anionic and cationic dyes on activated carbon from aqueous solutions: Equilibrium and kinetics. J. Hazard. Mater. 172 (2009) 1311-1320.

[4.6] V.C. Srivastava, I.D. Mall, I.M. Mishra, Adsorption thermodynamics and isosteric heat of adsorption of toxic metal ions onto bagasse fly ash (BFA) and rice husk ash (RHA). Chem. Eng. J. 132 (2007) 267- 278.

[4.7] A.G.S. Prado, J.C. Torres, E.A. Faria, S.C.L. Dias, Comparative adsorption studies of indigo carmine dye on chitin and chitosan. J. Colloid Interface Sci. 277 (2004) 43 – 47.

CHAPTER 5
BATCH ADSORPTION STUDIES

Batch equilibrium studies for adsorption of dyes from aqueous solution onto various adsorbents (commercial activated carbon, palmyra male inflorescence carbon and chitosan) were performed. The influence of solute concentration in the aqueous phase, temperature, and pH on the adsorption process were investigated. The adsorption isotherm experimental results were fitted with the conventional adsorption models. The thermodynamics parameters such as Gibbs energy change $\left(\Delta G^{o}\right)$, enthalpy change $\left(\Delta H^{o}\right)$ and entropy change $\left(\Delta S^{o}\right)$ were estimated. Kinetic studies were carried out to determine the rate parameters. The adsorption kinetics was examined with pseudo first order, pseudo second order, and intra particle diffusion model.

5.1 Materials and methods

5.1.1 Adsorbate

The dyes safranine O (CAS NO. 477-73-6, mass fraction purity 0.95, λ_{max} 520 nm) was purchased from Himedia (India). Malachite green oxalate (CAS No. 2437-29-8, mass fraction purity 0.988, λ_{max} 617 nm), and indigo carmine (CAS No. 860-22-0, mass fraction purity 0.98, λ_{max} 611nm) were both purchased from Loba Chemie (India). Orange G (CAS NO. 1936-15-8,mass fraction purity, λ_{max} 480 nm) and eosin Y (CAS No. 17372-87-1, mass fraction purity 0.88 λ_{max} 517nm) was purchased from Nice India. All of them were used without further purification.

5.1.2 Adsorbents

The activated carbon (CAS No.7440-44-0) was purchased from Merck. The adsorbents - palmyra male inflorescence and chitosan used in the experiments were prepared in the laboratory as mentioned in the chapter 4.

5.2 Analytical measurements

Concentrations of the dye solution were determined by finding out the absorbance at the characteristic wavelength using UV – vis spectrophotometer (Jasco UV model V-630) [5.1]. The calibration of the spectrophotometer was carried out with standard dye solution prepared by dissolving accurately weighed amounts of dye in distilled water. The UV- vis spectrophotometer is shown in figure 5.1. The UV response curves and calibration graphs for the dye compounds used for the experiments are shown in the figures 5.2 – figure 5.6.

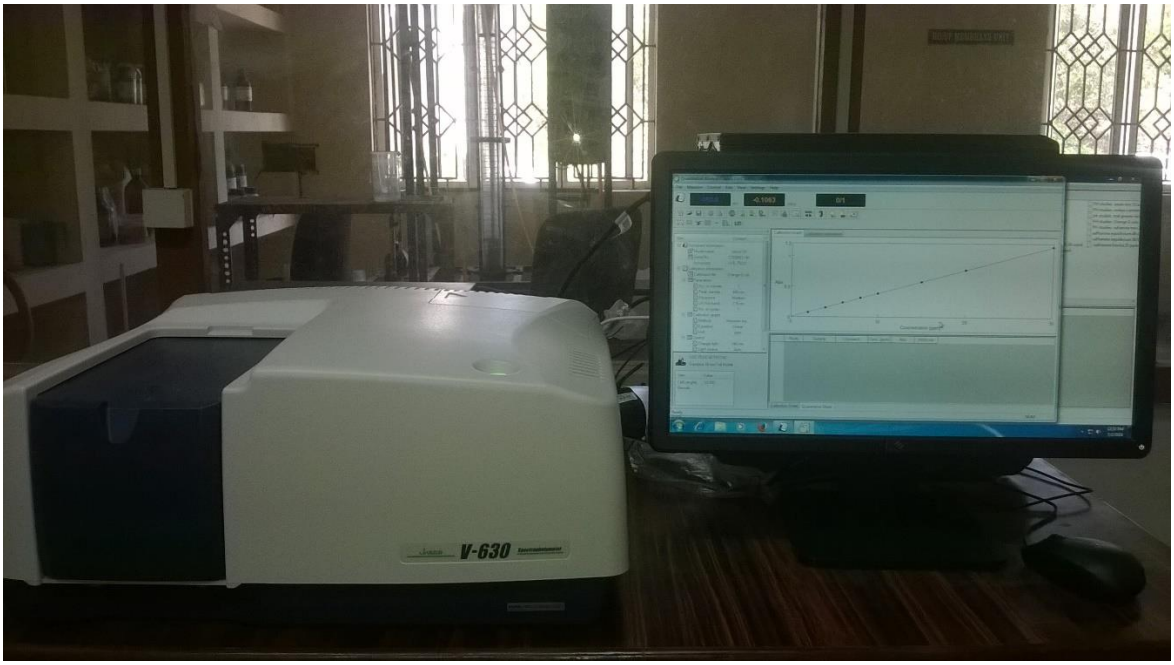

Figure 5.1 The photograph of UV – vis spectrophotometer.

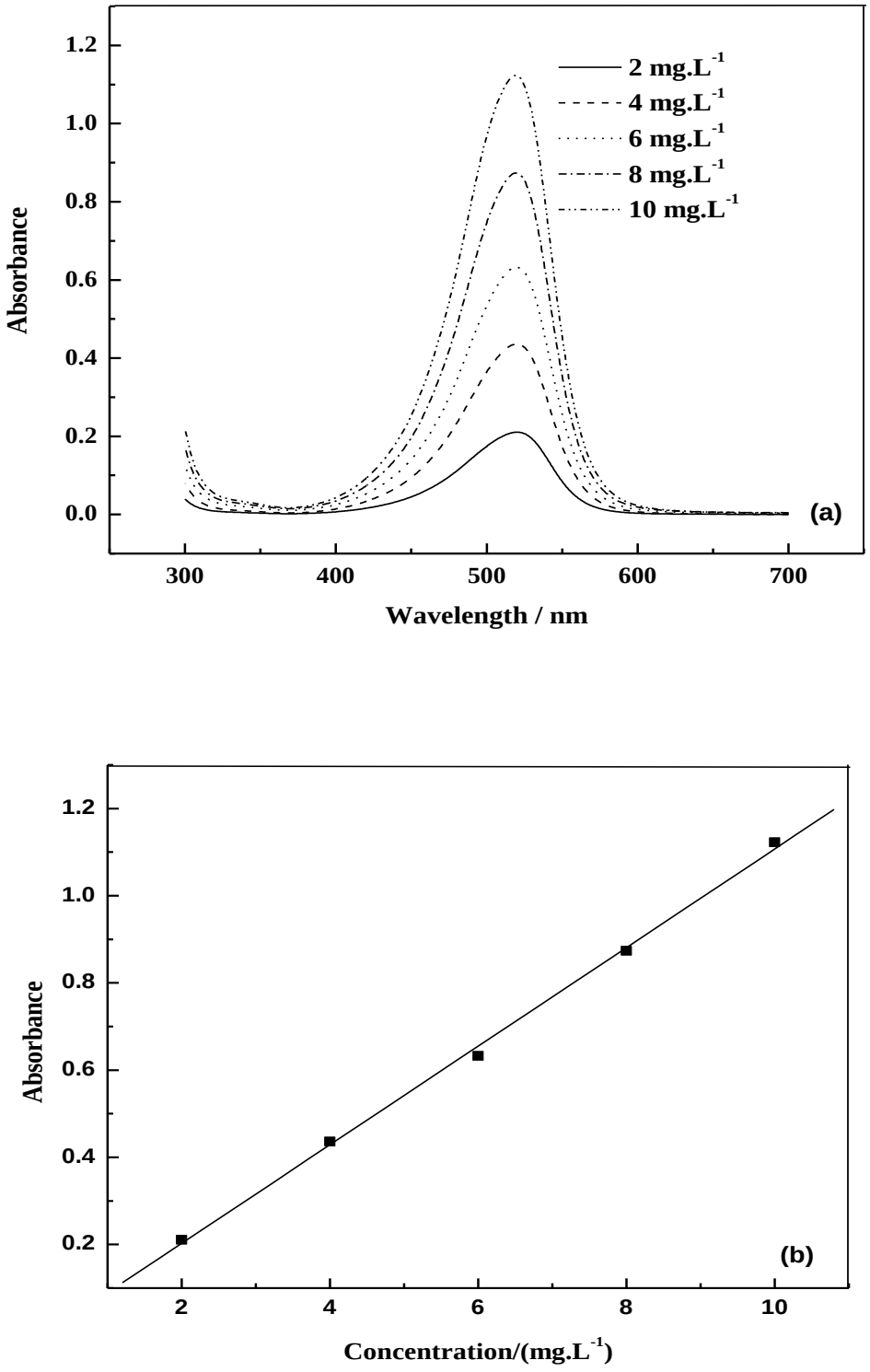

Figure 5.2 (a) Absorbance versus wavelength for safranine O. (b) Absorbance versus concentration for safranine O.

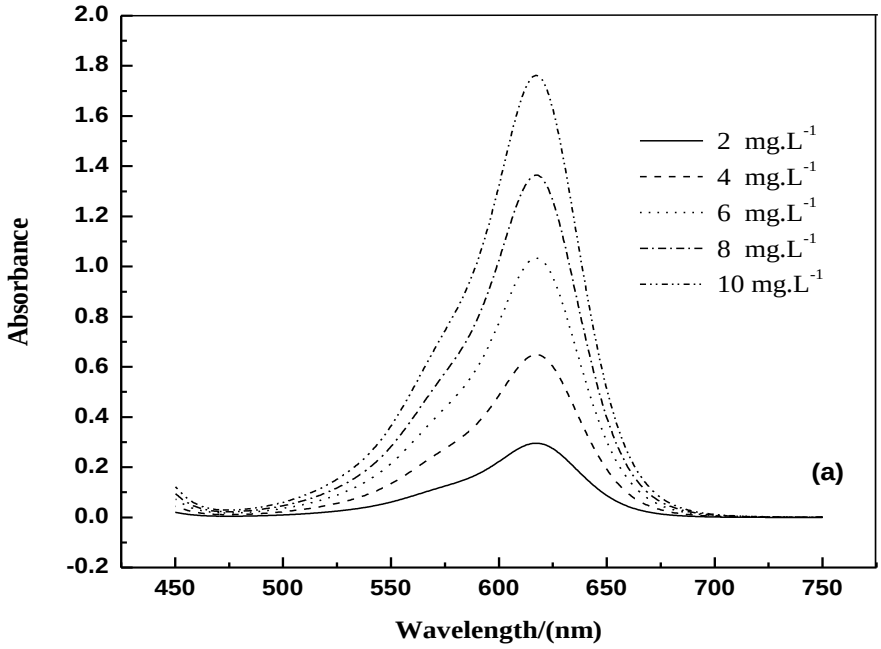

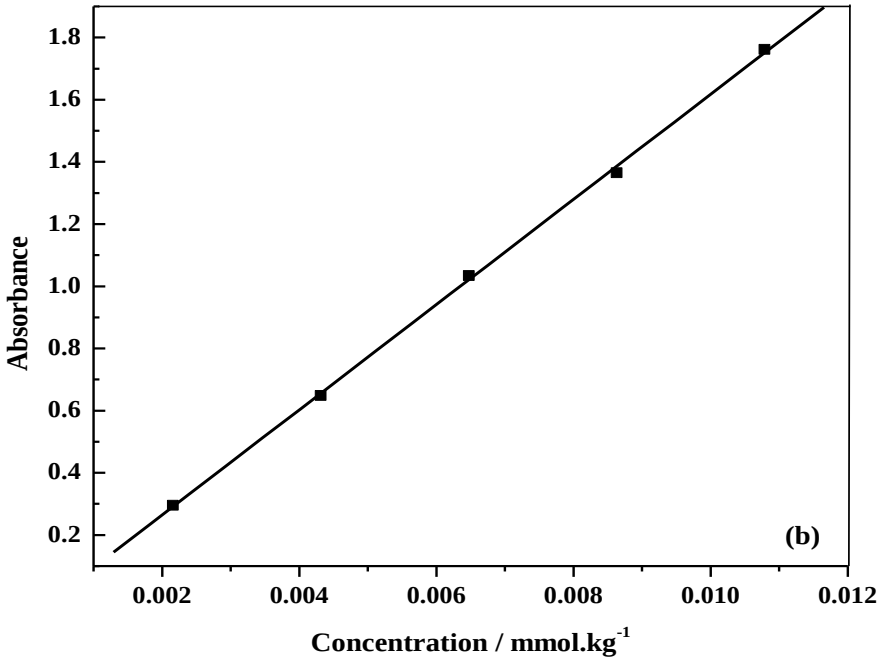

Figure 5.3 (a) Absorbance versus wavelength for malachite green oxalate. (b) Absorbance versus concentration for malachite green oxalate.

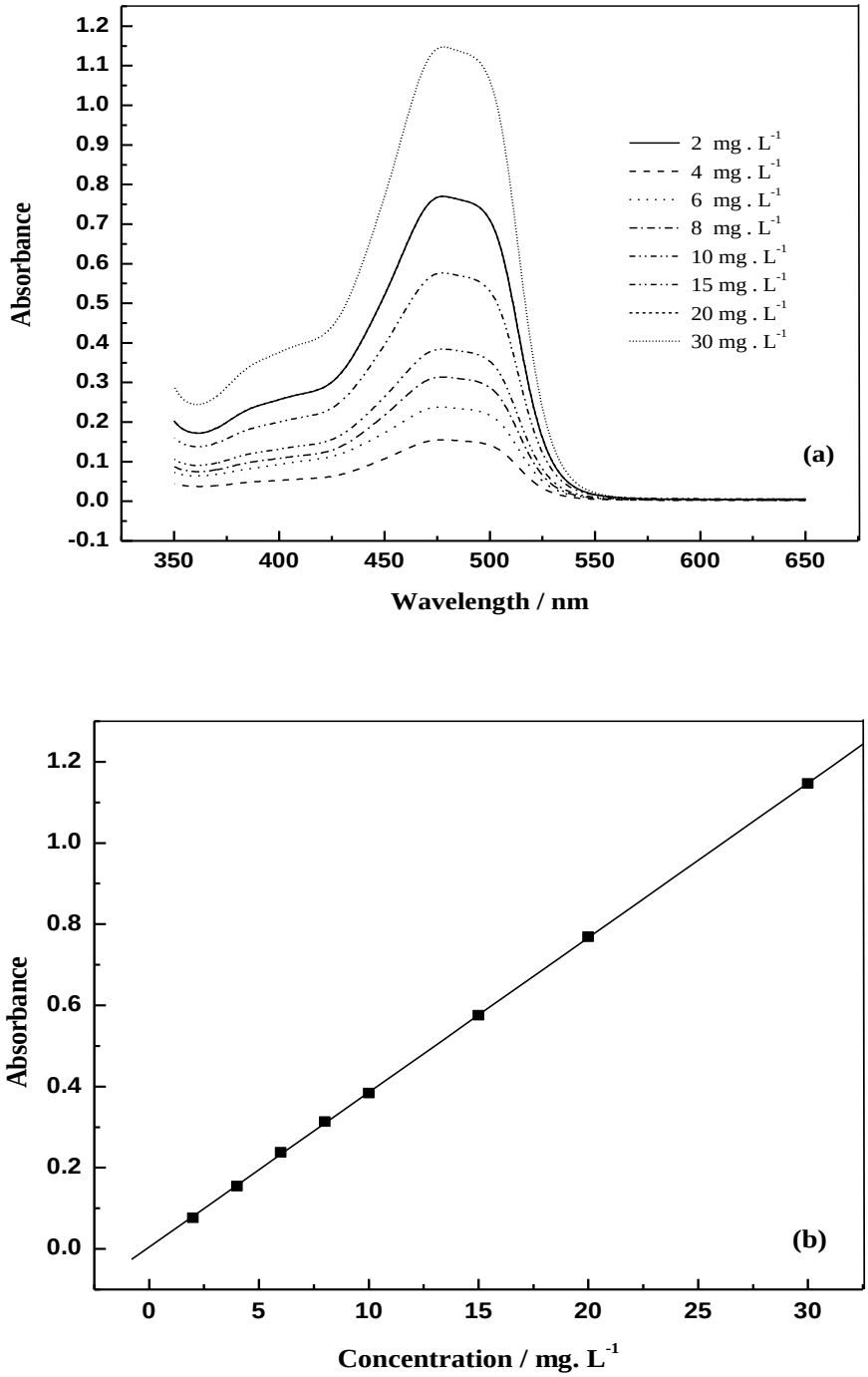

Figure 5.4 (a) Absorbance vs. wavelength for orange G. (b) Absorbance Vs. concentration for orange G.

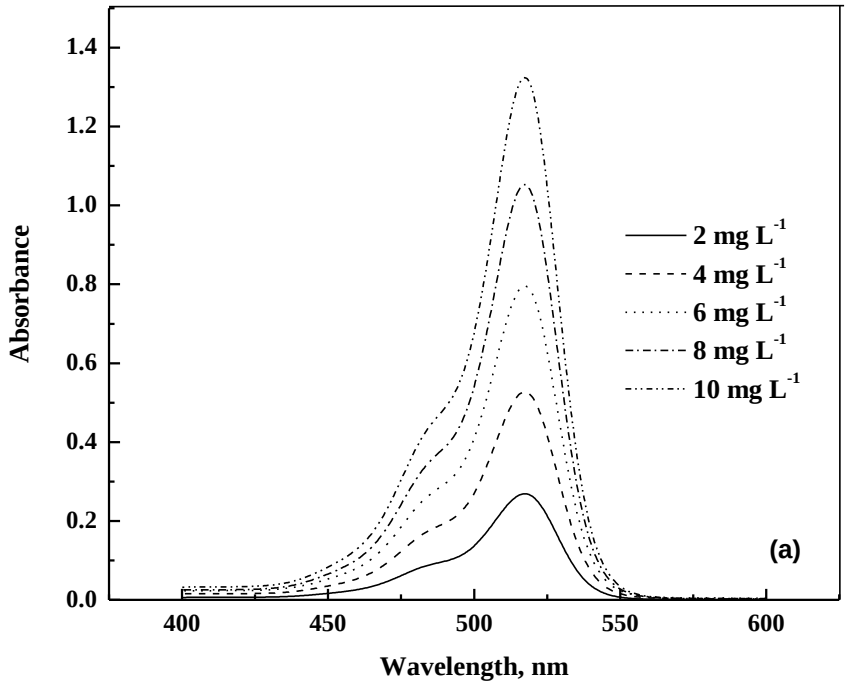

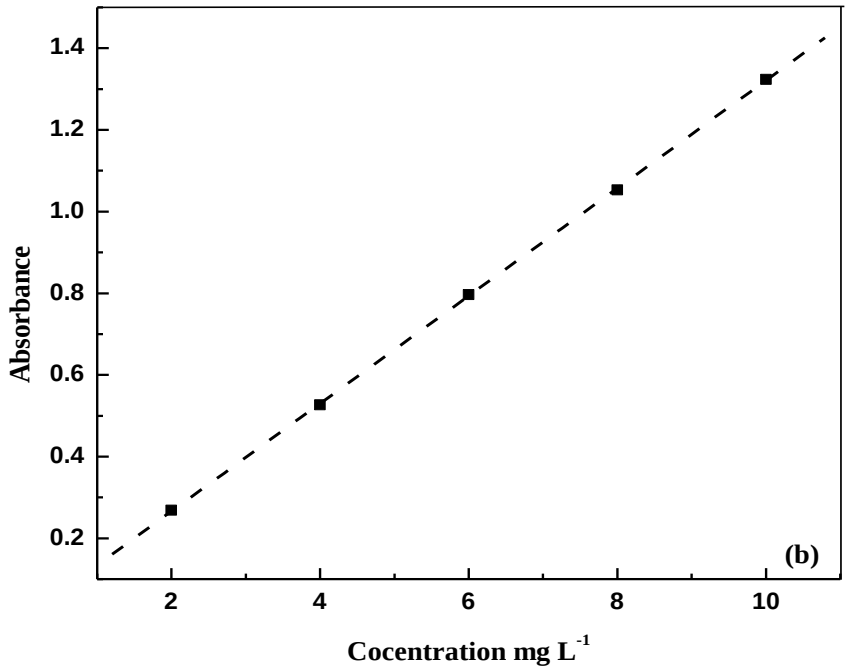

Figure 5.5 (a) Absorbance versus wavelength for eosin Y. (b) Absorbance versus concentration for eosin Y.

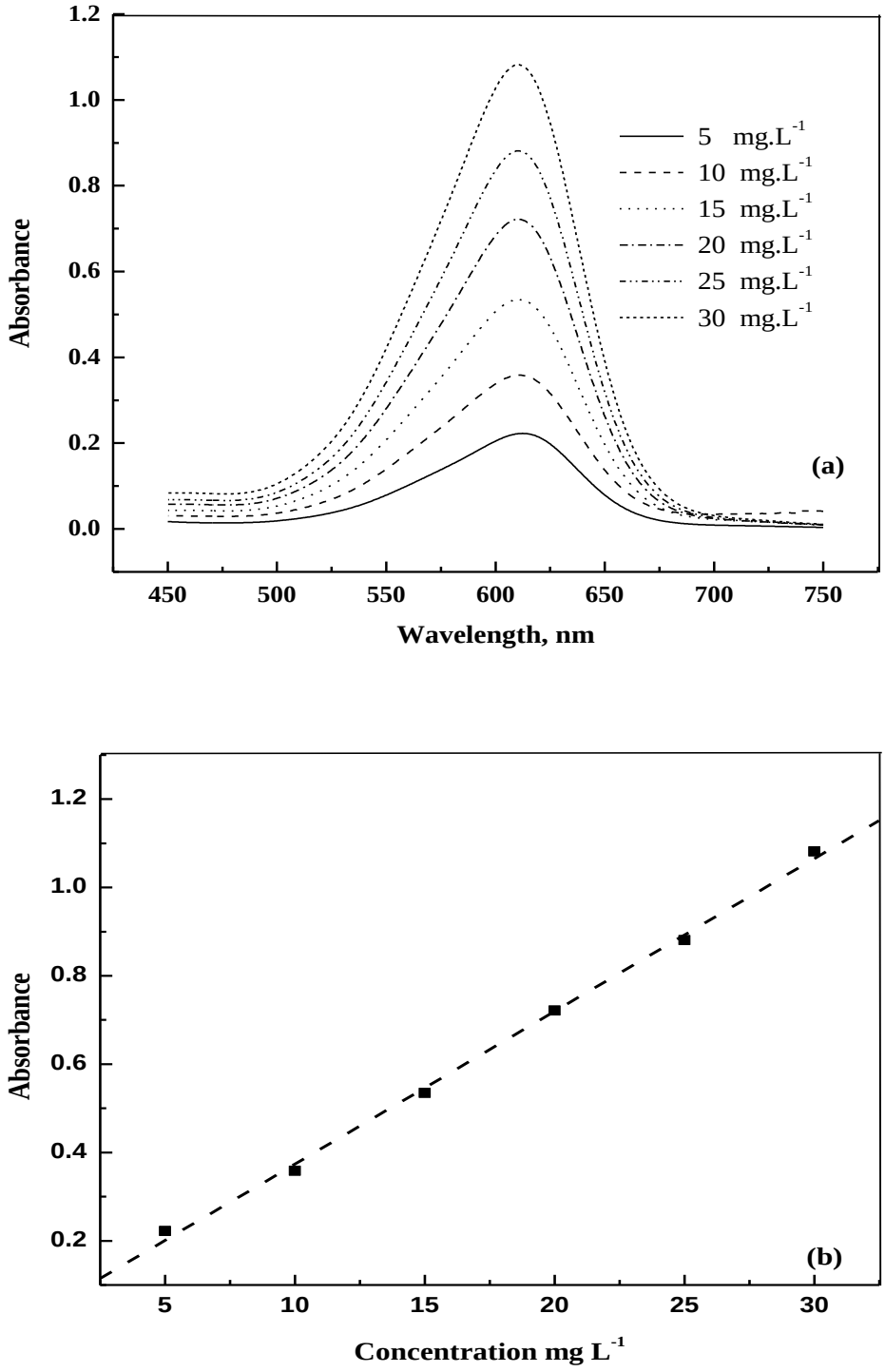

Figure 5.6 (a) Absorbance versus wavelength for indigo carmine (b) Absorbance versus concentration for indigo carmine.

5.3 Experimental section

5.3.1 Equilibrium studies

Activated carbon, palmyra male inflorescence carbon and chitosan ranging from 0.1 -0.6 g were taken in a 250 ml stoppered conical flask. Fifty mL of aqueous dye solutions of known initial concentration was added to the flask and the contents shaken for three days in a temperature controlled water bath [5.2 – 5.4]. In order to observe the effect of temperature on dye adsorption, the experiments were performed at three different temperatures (303 K, 313 K and 323 K). The equilibrium concentration of the dye in the solution was accurately measured by spectrophotometer. The removal of dyes from the aqueous solution and the equilibrium uptake on to activated carbon were calculated using the following relations.

$$\% \text{ adsorbate removal} = \frac{C_o - C_e}{C_o} \times 100 \qquad (5.1)$$

$$q_e = \frac{(C_o - C_e)v}{w} \qquad (5.\ 2)$$

Where, C_o is the initial concentration of dye in aqueous solution (mg L^{-1}), C_e is the the equilibrium dye concentration (mg L^{-1}), v is the volume of the solution (m^3) and W is the weight of the activated carbon (g) [5.2].

5.4 Results and discussions

5.4.1 Effect of pH

The effect of pH on adsorption was studied by varying the pH of the aqueous solution from 2.0 to 12.0 at 303 K [5.5 – 5.6]. Dilute NaOH and HCl of 0.1 N was used to adjust the pH. The experimental results for activated carbon – dye system are shown in figures 5.7 to 5.11. In figure 5.7, the effect of pH on the removal of orange g onto activated carbon was investigated. The dye removal was found in the range from 95% - 82% when the pH of the system varied from 2 to 12. Moderate decrease in adsorption capacity for orange G was observed under basic conditions. The maximum removal was 96 % observed at pH 4.0. Similar adsorption behavior with variation in solution pH has been reported in the literature [5.5] for orange G-bagasse fly ash system. The dye adsorption efficiency moderately decreased with increase in solution pH. The main interaction between activated carbon and dye molecule is electrostatic in nature. The reduction in dye adsorption at highly basic conditions can be attributed to electrostatic repulsion between the negatively charged activated carbon and the deprotonated dye molecules [5.6]. Figure 5.8 shows the effect of pH for safranine O. The removal percentage varied from 91 % -98 % for the variation in the pH from 2 to 12. Maximum adsorption is noted at pH around 6. Figure 5.9 depicts the effect of pH for malachite green oxalate dye. The removal of dyes varies from 98.4% to 95.8% for the pH range 2 to 12, and maximum removal of 98.8% was observed at pH 6. The effect of pH for the removal of eosin Y is represented in figure 5.10. For the pH range 2 to 12 the removal of dyes varied from 99.5% -82% and the maximum removal was observed at pH 2. Figure

5.11 shows the removal of indigo carmine dye. The removal varied from 94% – 78% For variation of pH from 2 to 12. Maximum removal was observed at pH 2.

At acidic pH a high electrostatic attraction exits between the acid dyes and the positively charged surface of the adsorbents. Hence for the acid dyes the maximum removal was observed at lower pH.

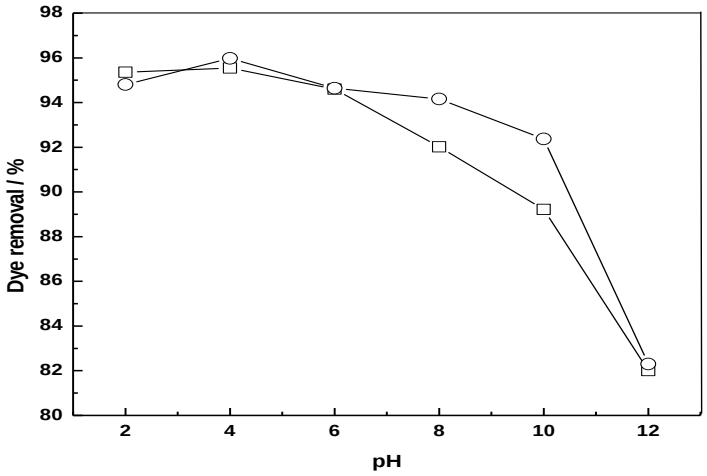

Figure 5.7 Effect of pH on the removal of orange G dye by activated carbon at a dosage of 0.5 g and volume of 5×10^{-4} m^3 at T = 303 K: □, 50 $mg\ L^{-1}$; ○, 75 $mg\ L^{-1}$.

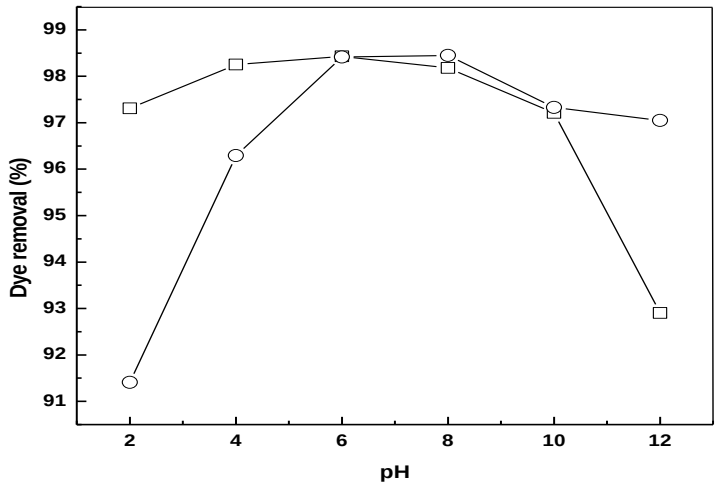

Figure 5.8 Effect of pH on the removal of safranine O dye by activated carbon at a dosage of 0.5 g and volume of 5×10^{-4} m^3 at T = 303 K: □, 50 $mg\ L^{-1}$; ○, 75 $mg\ L^{-1}$.

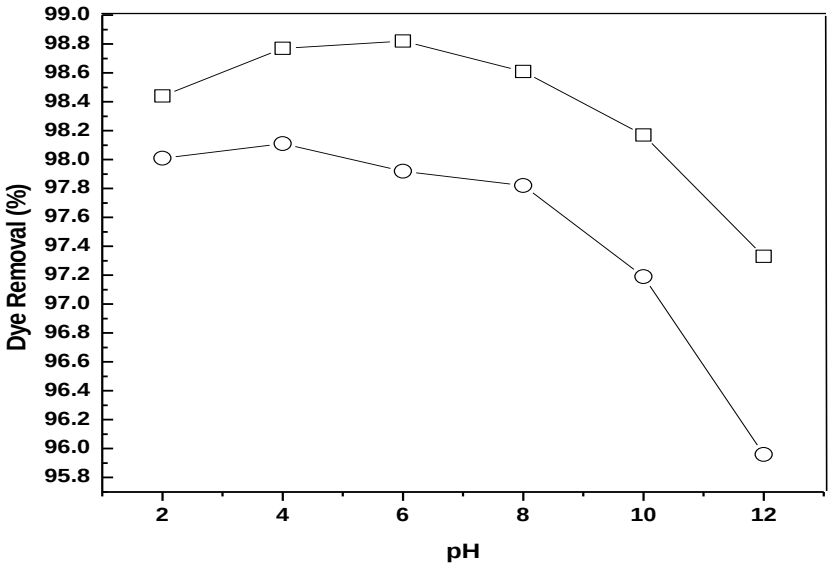

Figure 5.9 Effect of pH on the removal of malachite green oxalate dye by activated carbon at a dosage of 0.5 g and volume of 5×10^{-4} m^3 at T = 303 K: □, 50 $mg\ L^{-1}$; ○, 75 $mg\ L^{-1}$.

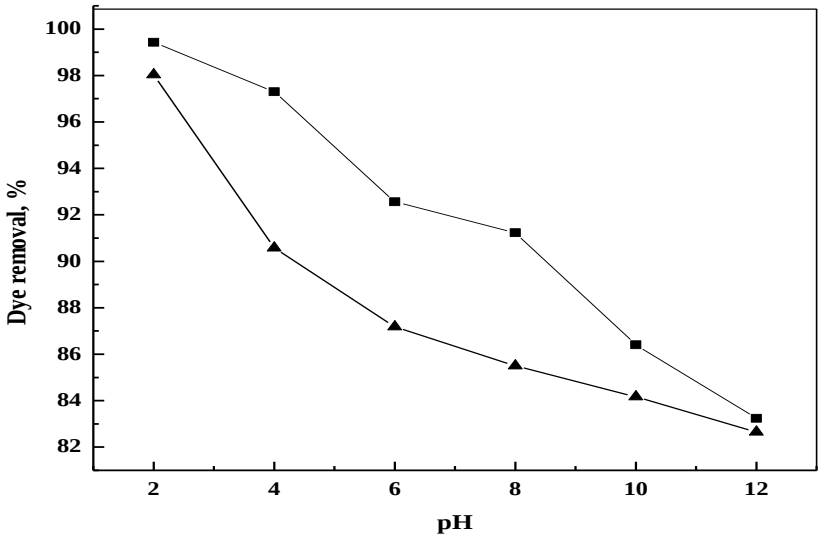

Figure 5.10 Effect of pH on the removal of eosin Y dye by activated carbon at a dosage of 0.5 g and volume of 5×10^{-4} m^3 at T = 303 K: □, 50 $mg\ L^{-1}$; ○, 75 $mg\ L^{-1}$.

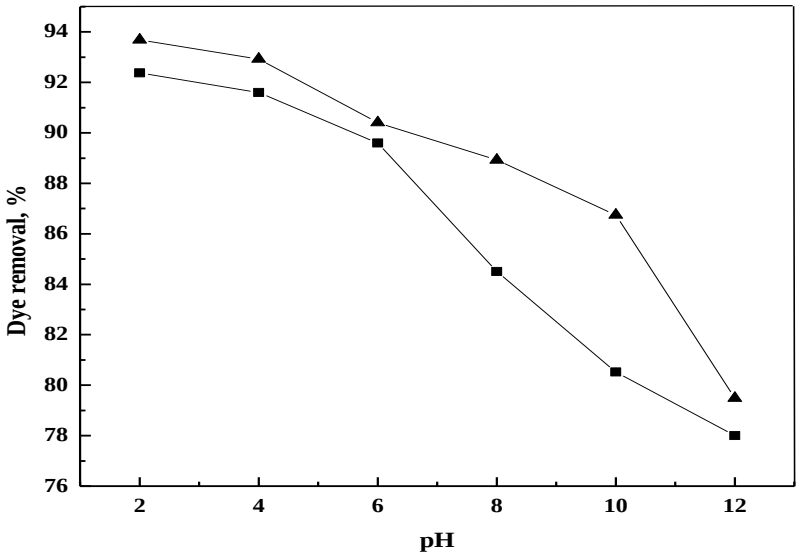

Figure 5.11 Effect of pH on the removal of indigo carmine dye by activated carbon at a dosage of 0.5 g and volume of 5×10^{-4} m^3 at T = 303 K: □, 50 $mg\ L^{-1}$; ○, 75 $mg\ L^{-1}$.

Figure 5.12 shows the effect of pH for chitosan eosin Y and indigo carmine dye system. The percentage of dye removed varied from 97% - 92% for the pH range 4 to 12. The maximum uptake of dye was observed at pH 6. For indigo carmine dye the removal varies from 97 % - 72% when the solution pH varied from 4 to 12 with maximum dye removal at pH 6. The dye removal efficiency at pH 4 was slightly lower when compared to pH 6 because of the solubility of chitosan [5.7].

The effect of variation of pH on the removal of malachite green oxalate and safranine O onto palmyra male inflorescence carbon is represented in figure 5.13 and figure 5.14 respectively. For the malachite green oxalate treated with KOH, the removal was around 97%, for H_3PO_4 the removal of dye ranged from 65% - 98% and for $ZnCl_2$ it was in the range of 68% - 80%. For safranine O dye treated with KOH the removal was around 80%, for H_3PO_4. The dye removal was between 76% - 78.5% and for $ZnCl_2$ the removal was observed between 74.5% - 75.5%. The maximum removal was observed at pH 6 for KOH and H_3PO_4 treated and at higher pH for $ZnCl_2$ treated.

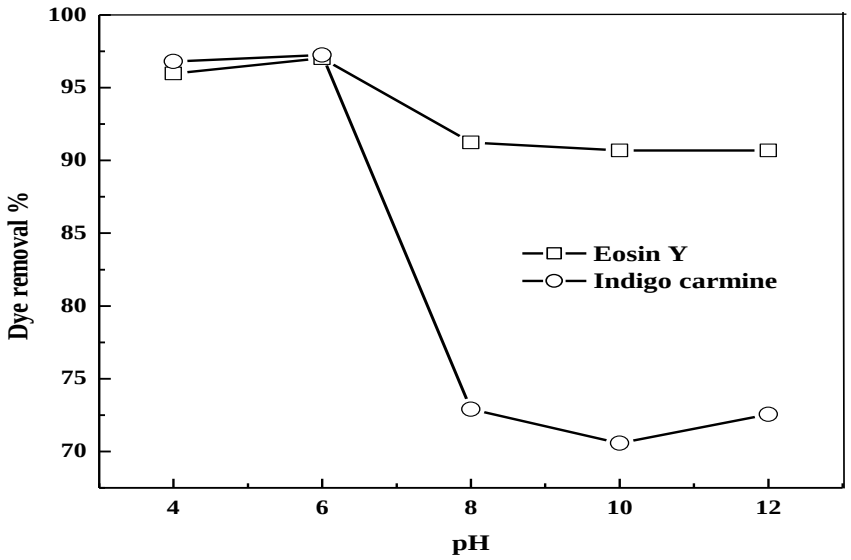

Figure 5.12 Effect of pH on the removal of eosin and indigo carmine dye by chitosan at a dosage of 0.5 g and volume of 5×10^{-4} m^3 at T = 303 K.

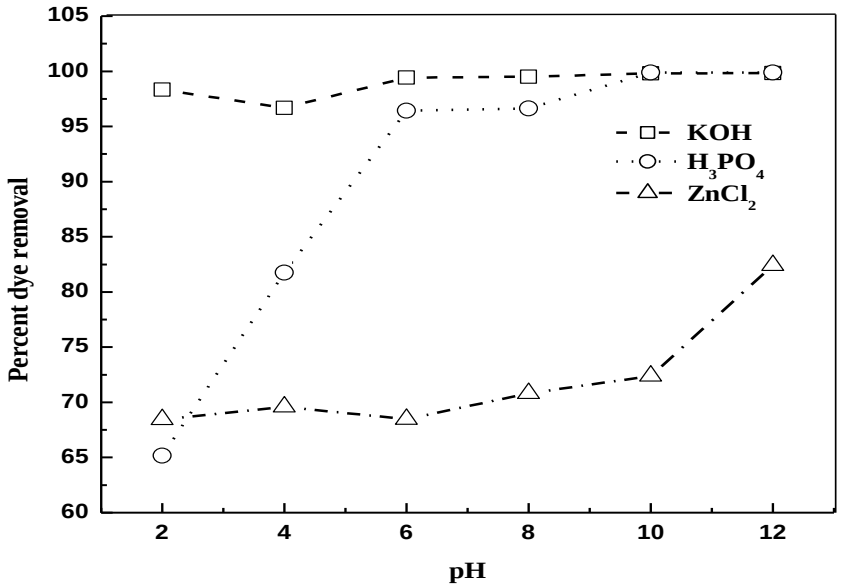

Figure 5.13 Effect of pH on the removal of malachite green oxalate by palmyra male inflorescence carbon at a dosage of 2 g and volume of 5×10^{-4} m3 at T = 303K

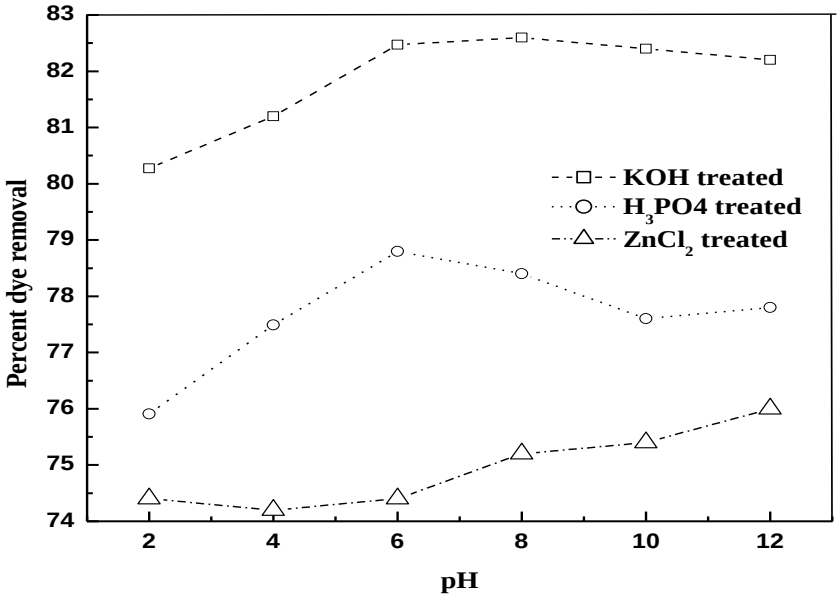

Figure 5.14 Effect of pH on the removal of safranine O by Palmyra male inflorescence carbon at a dosage of 2 g and volume of 5×10-4 m3 at T = 303K

5.4.2 Batch kinetic studies

Kinetic studies are important as it provides information about the mechanism of adsorption [5.8]. Experiment was performed in a beaker fitted with a stirrer with 500 ml dye solution at temperature 303 K. Samples were withdrawn at various time intervals and the dye concentration was measured. The kinetic data was modeled by pseudo first order, second order and intraparticle diffusion kinetic model. The calculated parameters are shown in the table 5.1 (a), 5.1 (b) and 5.1 (c) for activated carbon dye systems. As seen from table 5.1 (a), the pseudo first-order rate constant k_1 increased with the decrease in the dye concentrations for most of the cases. The kinetic constant k_1 values varies from 0.033 min^{-1} - 0.0464 min^{-1} for activated carbon - eosin Y system. For indigo carmine the constant k_1 values varies from 0.0307 min^{-1} - 0.1975 min^{-1}, for safranine O the constant k_1

values varies from 0.315 min^{-1} - 0.0569 min^{-1}, for malachite green oxalate the k_1 values varies from 0.0153 min^{-1} - 0.3917 min^{-1} and for orange G the k_1 values are in the range of 0.008 min^{-1} - 0.0462 min^{-1}. It can be noted that there is a wide difference with the calculated and the experimentally determined q_e values. The regression coefficients show that the pseudo first order model is poorly correlating.

Table 5.1 (b) shows the kinetic parameters for activated carbon system. From this table it can be found that the q_e values calculated were comparable with the experimental ones for all the dye systems studied with activated carbon. The value of the correlation coefficient is nearly equal to one for nearly all the data indicating that the pseudo second order provides better correlation to the experimental values. The values of the pseudo second order kinetic constants k_2 were in the range of 0.0048 $g.mg^{-1} min^{-1}$ – 0.0323 $g.mg^{-1} min^{-1}$ for eosin Y, 0.0154 $g.mg^{-1} min^{-1}$ – 0.5239 $g.mg^{-1} min^{-1}$ for indigo carmine, 0.0143 $g.mg^{-1} min^{-1}$ – 0.5739 $g.mg^{-1} min^{-1}$ for safranine O, 0.01039 $g.mg^{-1} min^{-1}$ – 0.3347 $g.mg^{-1} min^{-1}$ for malachite green oxalate and 0.00672 $g.mg^{-1} min^{-1}$ – 0.1482 $g.mg^{-1} min^{-1}$ for orange G. Similar kinetic behavior has been reported in the literature for orange G-bagasse-fly ash system, and orange G-mesoporous-fertilizer plant waste carbon system [5.5 – 5.6].

Figures 5.15 to figures 5.19 shows the second order kinetic plot for activated carbon dye system. The results for activated carbon dyes system indicates that the adsorption mechanism was second order.

The table 5.1 (c) represent the values for the intraparticle diffusion model. The values of the regression coefficients are not consistent and there were variation in the

experimental and the calculated q_e values. This suggest that the model is not appropriate of determining adsorption kinetic.

Table 5.1 (a) Pseudo first order kinetic rate constants for activated carbon dye system.

Name of the dye	Concentration $\left(\text{mg L}^{-1}\right)$	First order kinetic model			
		$q_{e(\exp)}\left(\text{mg g}^{-1}\right)$	$k_1\left(\text{min}^{-1}\right)$	$q_{e(cal)}\left(\text{mg g}^{-1}\right)$	R^2
Eosin Y	50	46.62	0.0464	20.43	0.88
	75	70.27	0.0357	15.67	0.91
	100	86.61	0.033	10.37	0.82
Indigo Carmine	50	47.02	0.0419	8.32	0.65
	75	66.89	0.1975	11.33	0.65
	100	82.801	0.0307	10.87	0.62
Safranine - O	50	49.0	0.315	1.66	0.69
	75	74.36	0.1888	49.79	0.57
	100	83.416	0.0569	33.95	0.85
	125	100.94	0.0569	33.95	0.85
Malachite Green Oxalate	50	49.0	0.39174	3.006	0.65
	75	73.99	0.167	2.256	0.38
	100	96.68	0.0153	3.781	0.856
	125	120.57	0.0213	7.636	0.907
Orange G	50	40.30	0.008	0.395	0.754
	75	48.24	0.0462	3.645	0.932
	100	62.47	0.0421	13.585	0.767
	125	63.6	0.0326	15.059	0.689

Table 5.1 (b) Pseudo second order kinetic rate constants for activated carbon – dye system.

Name of the dye	Concentration $\left(\text{mg L}^{-1}\right)$	Second order kinetic model			
		$q_{e(\exp)}$ $\left(\text{mg g}^{-1}\right)$	k_2 $\left(\text{g mg}^{-1}\text{min}^{-1}\right)$	$q_{e(cal)}$ $\left(\text{mg g}^{-1}\right)$	R^2
Eosin Y	50	46.62	0.0063	48.11	0.999
	75	70.27	0.0048	71.97	0.999
	100	86.61	0.0323	86.88	0.999
Indigo Carmine	50	47.02	0.0173	47.46	0.999
	75	66.89	0.5239	66.93	0.999
	100	82.801	0.0154	82.58	0.999
Safranine O	50	49.0	0.5739	49.04	0.999
	75	74.36	0.0143	74.906	0.999
	100	83.416	0.0362	84.033	0.999
	125	100.94	0.00776	102.14	0.999
Malachite Green Oxalate	50	49.0	0.0488	49.019	0.999
	75	73.99	0.3347	74.07	0.999
	100	96.68	0.0149	96.81	0.999
	125	120.57	0.01039	120.89	0.999
Orange G	50	40.31	0.1482	40.333	0.999
	75	48.25	0.0730	48.38	0.999
	100	62.47	0.00962	63.34	0.999
	125	63.6	0.00672	64.97	0.999

Table 5.1 (c) Intraparticle diffusion kinetic rate constants for activated carbon dye system

Name of the dye	Concentration $\left(\text{mg L}^{-1}\right)$	Intraparticle diffusion kinetic model			
		$q_{e(\text{exp})}$ $\left(\text{mg}\cdot\text{g}^{-1}\right)$	k_p $\left(\text{mg}\cdot\text{g}^{-1}\text{min}^{-0.5}\right)$	C	R^2
Eosin Y	50	46.62	1.19	34.81	0.94
	75	70.27	1.11	59.05	0.937
	100	86.61	0.199	84.64	0.918
Indigo Carmine	50	47.02	0.290	43.99	0.924
	75	66.89	0.019	66.71	0.702
	100	82.801	0.401	78.18	0.92
Safranine O	50	49.0	0.0397	48.64	0.444
	75	74.36	0.7225	67.336	0.865
	100	83.416	0.5803	78.434	0.285
	125	100.94	1.264	88.79	0.86
Malachite Green Oxalate	50	49.0	0.0040	48.96	0.3801
	75	73.99	0.0206	73.786	0.614
	100	96.68	0.388	92.135	0.879
	125	120.57	0.7189	112.89	0.9716
Orange G	50	40.31	0.0346	39.987	0.732
	75	48.25	0.298	45.44	0.760
	100	62.47	0.885	53.815	0.8967
	125	63.6	1.320	50.92	0.8337

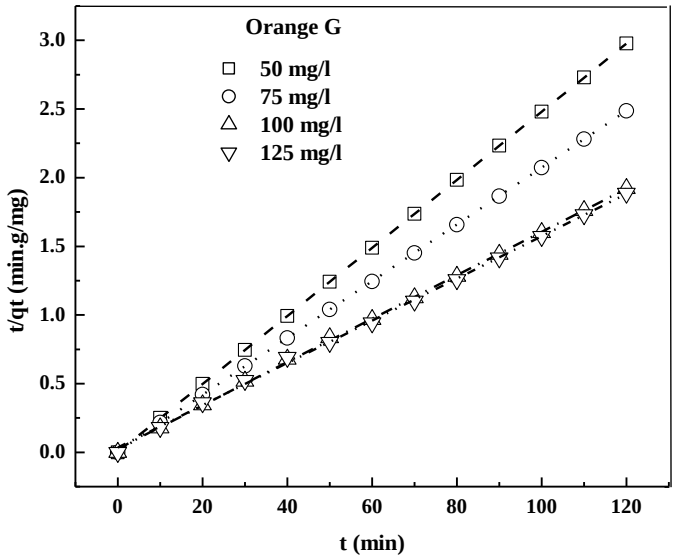

Figure 5.15 Pseudo second order adsorption kinetics of orange G onto activated carbon at a dose of 0.5 g and solution volume of $5\times10^{-4}m^3$ at T = 303 K.

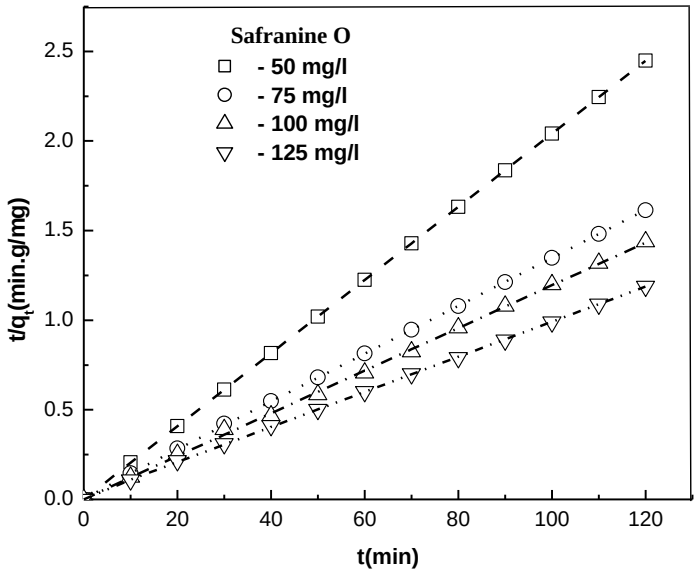

Figure 5.16 Pseudo second order adsorption kinetics of safranine O onto activated carbon at a dose of 0.5 g and solution volume of $5\times10^{-4}m^3$ at T = 303 K.

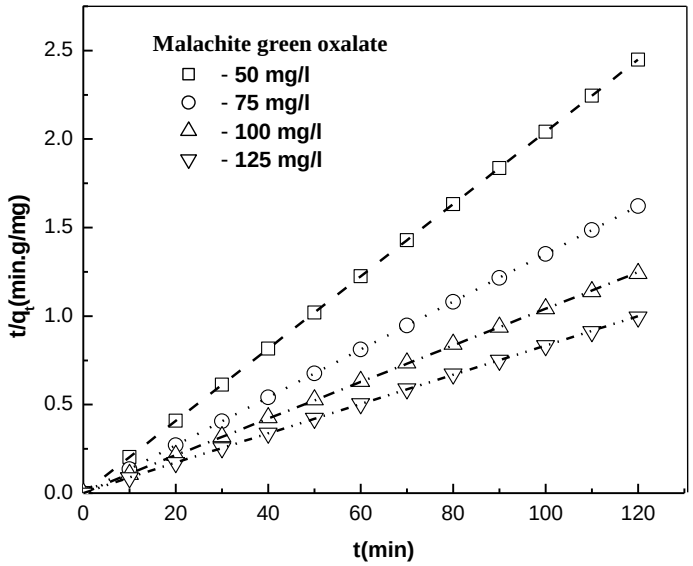

Figure 5.17 Pseudo second order adsorption kinetics of malachite green oxalate onto activated carbon at a dose of 0.5 g and solution volume of $5\times10^{-4}m^3$ at T = 303 K.

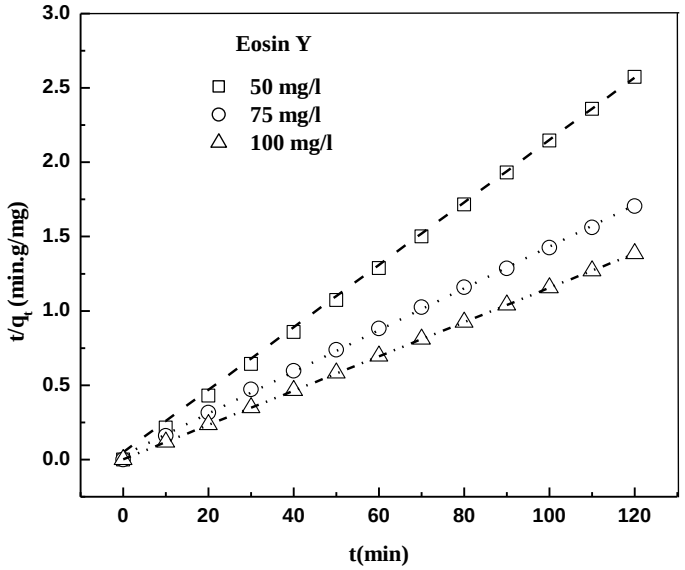

Figure 5.18 Pseudo second order adsorption kinetics of eosin Y onto activated carbon at a dose of 0.5 g and solution volume of $5\times10^{-4}m^3$ at T = 303 K.

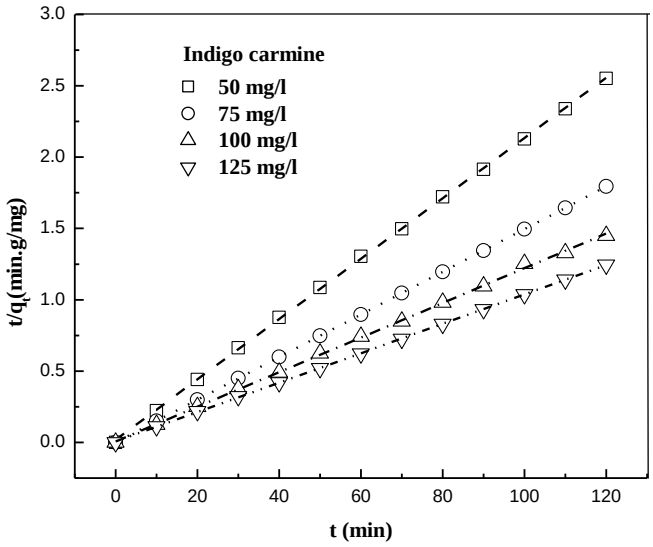

Figure 5.19 Pseudo second order adsorption kinetics of indigo carmine onto activated carbon at a dose of 0.5 g and solution volume of $5\times10^{-4}m^3$ at T = 303 K.

The kinetic parameters for the chitosan with eosin Y and indigo carmine are reported in table 5.2. The pseudo first order kinetic constant k_1 values are 0.0266 min^{-1} and 0.034 min^{-1} for eosin Y and indigo carmine respectively. The experimental q_e value and the calculated q_e values are not consistent due to poor prediction of the pseudo first order kinetic model. Pseudo second order kinetics rate constant k_2 are 0.2183 $g.mg^{-1}$ min^{-1} and 0.3512 $g.mg^{-1}$ min^{-1} for eosin Y and indigo carmine respectively. The parameter, q_e determined from the experiment and the model are comparable. The results indicate that the chitosan – dye system studied follows the pseudo second order. Figure 5.20 shows kinetic plots for the eosin and indigo carmine dyes.

Table 5.2 Kinetic rate constants obtained for chitosan – dye system at 303 K.

Kinetic model	Name of the compound	
	Eosin Y	Indigo Carmine
Pseudo first order		
$q_{e(\exp)}\ (\mathrm{mg\ g^{-1}})$	22.82	14.225
$k_1\ (\mathrm{min^{-1}})$	0.02266	0.034
$q_{e(cal)}\ (\mathrm{mg\ g^{-1}})$	0.2449	4.415
R^2	0.956	0.813
Pseudo second order		
$k_2\ (\mathrm{g \cdot mg^{-1} min^{-1}})$	0.2183	0.3512
$q_{e(cal)}\ (\mathrm{mg\ g^{-1}})$	22.841	14.388
R^2	0.999	0.999
Intraparticle diffusion model		
$k_p\ (\mathrm{mg \cdot g^{-1} min^{-0.5}})$	1.172	0.744
C	8.629	5.053
R^2	0.576	0.615

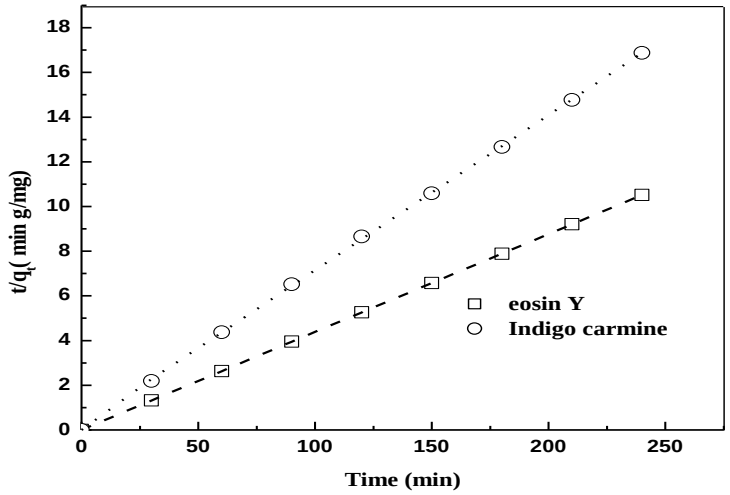

Figure 5.20 Pseudo second order adsorption kinetics of eosin Y and indigo carmine dye on chitosan a dose of 2 g and solution volume of $5\times10^{-4}m^3$ at T = 303 K. Dye concentration:100 $mg\ L^{-1}$

The kinetic parameters for the palmyra male inflorescence carbon with malachite green oxalate and safranine O are shown in table 5.3 and table 5.4 respectively. The pseudo first order kinetic model and intraparticle diffusion model poorly correlate the experimental data. The pseudo second order kinetic constant k_2 for palmyra male inflorescence carbon malachite green oxalate dye were 0.0467 g mg^{-1} min^{-1}, 0.0152 g mg^{-1} min^{-1}, 0.0056 g mg^{-1} min^{-1} for KOH, H_3PO_4 and $ZnCl_2$ activated carbon respectively. The experimental q_e values of 124.58 mg g^{-1}, 116.6 mg g^{-1} and 72.65 mg. g^{-1} were comparable with the model values of 124.67 mg g^{-1}, 120.11 mg g^{-1} and 74.766 mg g^{-1} for the KOH, H_3PO_4 and $ZnCl_2$ activated carbon respectively. For palmyra male inflorescence carbon safranine O dye the magnitude of k_2 was found to be 0.00067 g mg^{-1} min^{-1}, 0.00058 g mg^{-1} min^{-1}, 0.00198 g mg^{-1} min^{-1} for KOH, H_3PO_4 and $ZnCl_2$ activated carbon respectively. The experimental q_e values of 48.25 mg g^{-1}, 45.65 mg g^{-1} and 35.05 mg g^{-1} were comparable with the model values of 48.54 mg g^{-1}, 46.77 mg g^{-1} and 36.02

mg g^{-1} for the KOH, H_3PO_4 and $ZnCl_2$ activated carbon respectively. The pseudo second order kinetics gives better correlation for the systems studied. Figure 5.21 and figure 5.22 shows the kinetic plots for the palmyra male inflorescence carbon with malachite green oxalate and safranine O dye system..

Table 5.3 Kinetic rate constants obtained for malachite green oxalate -palmyra male inflorescence carbon system at 303 K.

Kinetic model	Chemical activation with		
	KOH	H_3PO_4	$ZnCl_2$
Pseudo first order			
$q_{e(\exp)}\ (\text{mg g}^{-1})$	124.58	116.6	72.65
$k_1\ (\text{min}^{-1})$	0.0284	0.0221	0.0517
$q_{e(cal)}\ (\text{mg g}^{-1})$	2.455	2.86	89.747
R^2	0.896	0.82	0.71
Pseudo second order			
$k_2\ (\text{g mg}^{-1}\text{min}^{-1})$	0.046716	0.015212	0.000562
$q_{e(cal)}\ (\text{mg g}^{-1})$	124.67	120.11	74.766
R^2	0.999	0.999	0.999
Intraparticle diffusion model			
$k_p\ (\text{mg g}^{-1}\text{min}^{-0.5})$	0.0878	3.165	3.456
C	123.42	77.66	28.05
R^2	0.918	0.504	0.727

Table 5.4 Kinetic rate constants obtained for safranine O -palmyra male inflorescence carbon system at 303 K.

Kinetic model	Chemical activation with		
	KOH	H_3PO_4	$ZnCl_2$
Pseudo first order			
$q_{e(\exp)}\ (\mathrm{mg\ g^{-1}})$	48.25	45.65	35.05
$k_1\ (\mathrm{min^{-1}})$	0.0084	0.0157	0.0269
$q_{e(cal)}\ (\mathrm{mg\ g^{-1}})$	3.808	11.023	26.176
R^2	0.669	0.901	0.665
Pseudo second order			
$k_2\ (\mathrm{g \cdot mg^{-1} min^{-1}})$	0.0006741	0.000583	0.001981
$q_{e(cal)}\ (\mathrm{mg\ g^{-1}})$	48.54	46.77	36.02
R^2	0.999	0.999	0.999
Intraparticle diffusion model			
$k_p\ (\mathrm{mg\ \ g^{-1} min^{-0.5}})$	0.225	0.433	0.833
C	44.36	38.62	23.44
R^2	0.845	0.922	0.92

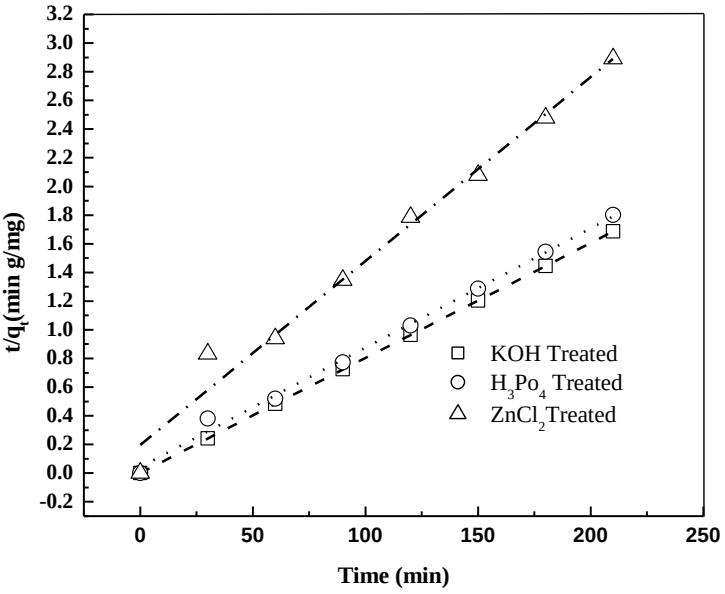

Figure 5.21 Pseudo second order adsorption kinetics of malachite green oxalate dye onto palmyra male inflorescence at a dose of 2 g and solution volume of $5\times10^{-4}m^3$ at T = 303 K. Dye concentration:500 mg L^{-1}

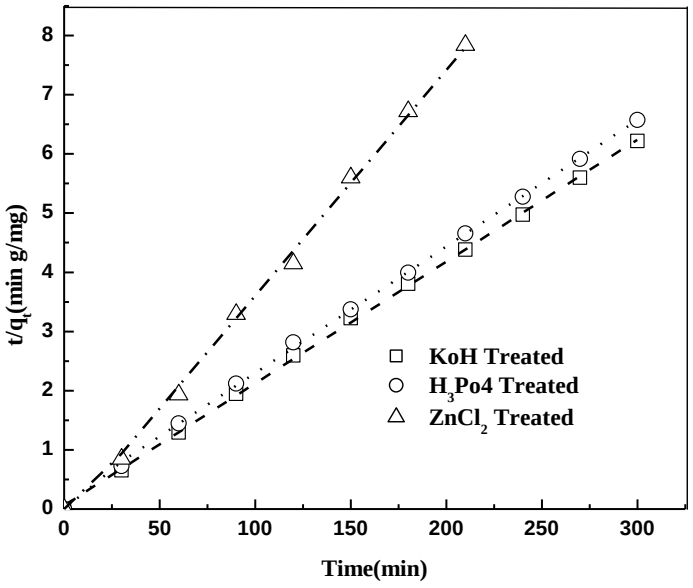

Figure 5.22 Pseudo second order adsorption kinetics of safranine O dye onto palmyra male inflorescence at a dose of 2 g and solution volume of $5\times10^{-4}m^3$ at T = 303 K. Dye concentration:500 mg L^{-1}

5.4.3 Thermodynamic studies

The values of thermodynamic parameters, enthalpy change (ΔH^o), Gibbs energy change (ΔG^o) and entropy change (ΔS^o) of the adsorption process of the different adsorbent – adsorbate system were evaluated based on equations 2.13 – 2.15. The thermodynamic parameters for activated carbon dye system in reported in table 5.5.

Table 5.5 Thermodynamic parameters for the removal of dye compounds on activated carbon.

Name of the dye	T/(K)	$-\Delta G^o$ (J mol^{-1})	$-\Delta H^o$ (J mol^{-1})	ΔS^o $(\text{J mol}^{-1}\text{K}^{-1})$
Eosin Y	303	29485.45	28456.5	3.38
	313	30785.35		7.42
	323	32677.29		13.05
Indigo Carmine	303	29012.7	12009.1	56.09
	313	30286.6		58.37
	323	31637.3		60.74
Safranine O	303	30366.61	2286.61	92.63
	313	31473.28		93.20
	323	32551.35		93.66
Malachite green oxalate	303	34252.12	3981.27	99.85
	313	35606.27		100.99
	323	36869.41		101.77
Orange G	303	25704.58	4087.71	71.31
	313	26551.33		71.73
	323	27529.74		72.54

The table 5.6 and table 5.7 shows the thermodynamic parameters of palmyra male inflorescence carbon and chitosan – dye system respectively. The value of Gibbs energy change was found to be negative for all the adsorbent dyes systems investigated in this study. The magnitude of Gibbs energy change decreases with the increase in the temperature for the adsorption system. The negative value of Gibbs energy change $\left(\Delta G^{o}\right)$ indicates that the process is spontaneous [5.7]. The decrease in the values of ΔG^{o} with increase in temperature indicates that the adsorption process is favored at high temperature. The entropy change is related to randomness of the system. The entropy values are found to be positive in all the cases. The entropy values increase with the increase in temperature. The positives value for entropy change ΔS^{o} indicates that the basic dye molecules are in more randomic condition at the solid solution interface,[5.8 – 5.9] . The enthalpy values obtained for all the adsorbent dye systems studied shows the negative values. The negatives values of ΔH^{o} indicates an exothermic process as is common in most adsorption processes [5.10].

Table 5.6 Thermodynamic parameters for the removal of dye compounds on palmyra male inflorescence carbon.

Name of the dye	T/(K)	$-\Delta G^o$ $(J\ mol^{-1})$	$-\Delta H^o$ $(J\ mol^{-1})$	ΔS^o $(J\ mol^{-1}K^{-1})$
Safranine O				
KOH	303	20791.48	1266.50	64.41
	313	21476.65		64.54
	323	22202.92		64.79
H_3PO_4	303	21207.24	2403.22	77.88
	313	21950.87		77.77
	323	22575.09		77.29
$ZnCl_2$	303	20354.39	11755.62	105.92
	313	20685.56		103.59
	323	20970.73		101.27
Malachite				
green oxalate ,	303		11323.48	58.61
KOH		29091.55		
	313	30405.16		60.93
	323	31737.70		63.17
H_3PO_4	303	22314.68	1210.57	69.62
	313	23013.31		71.92
	323	23786.86		74.47
$ZnCl_2$	303	20162.30	5367.75	48.80
	313	20888.698		49.56
	323	21727.16		50.62

Table 5.7 Thermodynamic parameters for the removal of dye compounds on chitosan

Name of the dye	T/(K)	$-\Delta G^o$ (J mol^{-1})	$-\Delta H^o$ (J mol^{-1})	ΔS^o (J mol^{-1}K^{-1})
Eosin Y	303	29750.31	2560.18	89.69
	313	30696.72		89.85
	323	31758.74		90.36
Indigo Carmine	303	25822.87	4679.25	69.75
	313	26598.50		69.99
	323	27597.31		70.92

5.4.4 Adsorption equilibrium isotherms

The q_e vs C_e data obtained from batch experiments is optimized with the isotherm models to obtain correlations for the equilibrium isotherms [5.11]. The equilibrium isotherm equations, namely Freundlich, Langmuir, Redlich – Peterson, Temkin and Toth are tested for their efficacy to represent the adsorption data [5.12]. The related parameters of the isotherm equations and their correlation coefficients for activated carbon-dye system are reported in Tables 5.8 to 5.12, and in Tables 5.13 and 5.14 for chitosan dye system. Tables 5.15 (a), 5.15 (b) and 5.15 (c) for palmyra male inflorescence-malachite green oxalate dye system, Tables 5.16(a), 5.16(b) and 5.16 (c) for palmyra male inflorescence carbon-safranine O system. All the models investigated in this study were successful in correlating the experimental data expect in few cases. The Langmuir model was observed to be consistent for all the systems investigated. The

effect of temperature on the adsorption system were studied by varying the temperature from 303 – 333 K. The Langmuir adsorption capacity for activated carbon eosin system varies from 90.57 mg g^{-1} to 100.88 mg g^{-1} and the value of K_L varied from 0.1206 L mg^{-1} to 0.1914 L mg^{-1}. For indigo carmine the adsorption capacity was found in the range of 246.98 mg g^{-1} to 253.31 mg g^{-1} and K_L varied from 0.099 L mg^{-1} to 0.130 L mg^{-1}. The adsorption capacity for safranine O was observed in the range of 127.95 mg $g^{-1}$to 141.42 mg g^{-1} and K_L varied from 0.171 L mg^{-1} to 0.183 L mg^{-1}. For malachite green oxalate the adsorption capacity varied from 151.91 mg g^{-1} to 159.14 mg $g^{-1}$and K_L varied from 0.798 L mg^{-1} to 0.912 L mg^{-1}. For orange G the value varied from 127.613 mg $g^{-1}$to 147.217 mg g^{-1} and K_L varied from 0.0268 L mg^{-1} to 0.02819 L mg^{-1}. The adsorption capacity and the value of K_L found to increase with the increase in temperature. For palmyra male inflorescence carbon malachite green oxalate system maximum adsorption of 343.50 mg g^{-1} and 129.03 mg g^{-1} was obtained with the H_3PO_4 and $ZnCl_2$ treated carbon respectively. Similarly for safranine O treated with palmyra male inflorescence carbon maximum adsorption of 258.93 mg g^{-1} and 60.98 mg g^{-1} was obtained with the KOH and $ZnCl_2$ treated carbon respectively. From the tables it is clearly evident that the Langmuir adsorption capacity of the dye compound by palmyra male inflorescence carbon is higher compared to activated carbon. The maximum Langmuir adsorption capacity obtained in this study for the safranine O and malachite green treated with palmyra male inflorescence carbon found to be 258.93 mg g-1 (KOH treated) and 343.50 mg g^{-1} (H_3PO_4 treated) respectively whereas the activated carbon the values are found to be 141.42mg g^{-1} and 159.139 mg g^{-1}. The maximum Langmuir adsorption capacity for the chitosan was found to be 21.574 mg g^{-1} and 24.876 mg g^{-1} for eosin Y and indigo

carmine respectively and these is comparable with the literature studied adsorbents [5.13]. The plot of the experimental equilibrium data and the Langmuir model predictions are represented in the figures from 5.23 to 5.31. The equilibrium isotherm of activated carbon dye system is shown in the figure 5.23 to 5.27, the figure 5.28 and 5.29 for chitosan dye system. For palyra male inflorescence carbon the equilibrium isotherm is shown in figure 5.30 (a), 5.30(b), 5.30 (c) and 5.31(a), 5.21 (b), 5.31 (c).

Table 5.8 Isotherm constants for eosin Y dye adsorption onto activated carbon at different temperatures

Name of the Isotherm	T/K		
	303	313	323
Freundlich			
$K_F\left((mg/g)/(mg/L)^{\frac{1}{n}}\right)$	26.1	27.31	32.08
1/n	0.261	0.274	0.261
R^2	0.905	0.854	0.838
Langmuir			
$q_m\left(mg\ g^{-1}\right)$	90.57	95.99	100.88
$K_L\left(L\ mg^{-1}\right)$	0.1206	0.1367	0.1914
R^2	0.998	0.999	0.999
Redlich Peterson			
$K_R\left(L\ mg^{-1}\right)$	19.848	17.557	28.544
β_R	0.903	0.942	0.933
a_R	0.3585	0.2435	0.3905
R^2	0.999	0.999	0.999
Toth			
a_τ	2.01	4.11	2.01
T	0.883	0.942	0.916
$K_\tau\left(mg\ g^{-1}\right)$	56.47	76.49	73.22
R^2	0.999	0.999	0.999
Temkin			
$K_T\left(L\ mg^{-1}\right)$	2.96	2.86	4.75
B1	14.80	16.25	16.27
R^2	0.968	0.936	0.934

Table 5.9 Isotherm constants for indigo carmine dye adsorption onto activated carbon at different temperatures

Name of the Isotherm	T/K		
	303	313	323
Freundlich			
$K_F\left((mg/g)/(mg/L)^{\frac{1}{n}}\right)$	34.55	37.02	40.14
1/n	0.517	0.302	0.302
R^2	0.907	0.985	0.910
Langmuir			
$q_m\left(mg\ g^{-1}\right)$	246.98	250.16	253.31
$K_L\left(L\ mg^{-1}\right)$	0.099	0.1127	0.130
R^2	0.985	0.985	0.984
Redlich Peterson			
$K_R\left(L\ mg^{-1}\right)$	26.779	29.638	33.477
B_R	0.9403	0.9616	0.986
a_R	0.1367	0.1367	0.1388
R^2	0.985	0.985	0.984
Toth			
a_τ	2.01	10.04	8.58
T	1.0	0.993	0.986
$k_\tau\left(mg\ g^{-1}\right)$	247.298	245.591	244.544
R^2	0.985	0.985	0.984
Temkin			
$K_T\left(L\ mg^{-1}\right)$	0.939	1.0645	1.232
B1	55.272	55.901	0.987
R^2	0.987	0.987	0.988

Table 5.10 Isotherm constants for safranine O dye adsorption onto activated carbon at different temperatures

Name of the Isotherm	T/K		
	303	313	323
Freundlich			
$K_F\left((mg/g)/(mg/L)^{\frac{1}{n}}\right)$	44.16	45.88	47.47
1/n	0.302	0.302	0.302
R^2	0.932	0.934	0.939
Langmuir			
$q_m\left(mg\ g^{-1}\right)$	127.95	134.53	141.42
$K_L\left(L\ mg^{-1}\right)$	0.171	0.178	0.183
R^2	0.999	0.999	0.999
Redlich Peterson			
$K_R\left(L\ mg^{-1}\right)$	42.38	49.775	58.528
β_R	0.930	0.920	0.909
a_R	0.4829	0.5627	0.6633
R^2	0.999	0.999	0.999
Toth			
a_τ	7.20	1.78	1.51
T	0.930	0.921	0.910
$k_\tau\left(mg \cdot g^{-1}\right)$	94.30	96.03	96.97
R^2	0.999	0.999	0.999
Temkin			
$K_T\left(L\ mg^{-1}\right)$	9.44	9.41	9.27
B1	17.25	18.24	19.29
R^2	0.987	0.989	0.992

Table 5.11 Isotherm constants for malachite green oxalate dye adsorption onto activated carbon at different temperatures

Name of the Isotherm	T/K		
	303	313	323
Freundlich			
$K_F\left((mg/g)/(mg/L)^{1/n}\right)$	68.44	70.60	71.94
1/n	0.231	0.242	0.251
R^2	0.704	0.766	0.779
Langmuir			
$q_m\left(mg \cdot g^{-1}\right)$	151.91	156.497	159.139
$K_L\left(L \cdot mg^{-1}\right)$	0.798	0.8695	0.912
R^2	0.999	0.999	0.999
Redlich Peterson			
$\mathrm{K_R}\left(\mathrm{L \cdot mg^{-1}}\right)$	165.986	195.55	203.57
β_R	0.958	0.951	0.952
a_R	1.309	1.530	1.553
R^2	0.999	0.999	0.999
Toth			
a_τ	0.764	0.654	0.644
T	0.958	0.951	0.952
$k_\tau\left(\mathrm{mg\ g^{-1}}\right)$	132.344	134.322	137.60
R^2	0.999	0.999	0.999
Temkin			
$K_T\left(\mathrm{L\ mg^{-1}}\right)$	32.518	31.099	29.734
B1	20.99	22.16	22.97
R^2	0.860	0.909	0.919

Table 5.12 Isotherm constants for orange G dye adsorption onto activated carbon at different temperatures

Name of the Isotherm	T/K		
	303	313	323
Freundlich			
$K_F\left((mg/g)/(mg/L)^{\frac{1}{n}}\right)$	14.76	14.40	14.82
1/n	0.390	0.415	0.43
R^2	0.930	0.998	0.907
Langmuir			
$q_m\left(mg \cdot g^{-1}\right)$	127.613	137.86	147.217
$K_L\left(L \cdot mg^{-1}\right)$	0.0268	0.02685	0.02819
R^2	0.999	0.998	0.996
Redlich Peterson			
$K_R\left(\mathrm{L} \cdot \mathrm{mg}^{-1}\right)$	6.755	7.095	7.631
β_R	0.837	0.8297	0.8282
a_R	0.1366	0.1367	0.1367
R^2	0.992	0.989	0.987
Toth			
a_τ	11.09	11.099	11.099
T	0.865	0.860	0.861
$k_\tau\left(\mathrm{mg} \cdot \mathrm{g}^{-1}\right)$	68.147	72.63	78.86
R^2	0.994	0.991	0.989
Temkin			
$K_T\left(\mathrm{L} \cdot \mathrm{mg}^{-1}\right)$	0.2528	0.2376	0.245
B1	28.25	31.32	33.77
R^2	0.977	0.975	0.975

Table 5.13 Isotherm constants for indigo carmine dye adsorption onto chitosan at different temperatures

Name of the Isotherm	T/K		
	303	313	323
Freundlich			
$K_F\left((mg/g)/(mg/L)^{\frac{1}{n}}\right)$	1.714	1.713	1.802
1/n	0.528	0.54	0.536
R^2	0.973	0.973	0.971
Langmuir			
$q_m\left(mg \cdot g^{-1}\right)$	23.364	24.691	24.876
$K_L\left(L \cdot mg^{-1}\right)$	0.02815	0.02734	0.02891
R^2	0.995	0.99	0.99
Redlich Peterson			
$K_R\left(\mathrm{L} \cdot \mathrm{mg}^{-1}\right)$	1.4215	0.9978	1.055
β_R	0.654	0.7466	0.7554
a_R	0.333	0.1367	0.1367
R^2	0.98	0.99	0.99
Toth			
a_τ	11.09	11.099	11.099
T	0.798	0.781	0.777
$k_\tau\left(\mathrm{mg} \cdot g^{-1}\right)$	0.099	0.1058	0.1153
R^2	0.98	0.987	0.987
Temkin			
$K_T\left(\mathrm{L} \cdot \mathrm{mg}^{-1}\right)$	0.2204	0.2178	0.2297
B1	5.686	5.965	6.0175
R^2	0.995	0.995	0.995

Table 5.14 Isotherm constants for eosin Y dye adsorption onto chitosan at different temperatures

Name of the Isotherm	T/K		
	303	313	323
Freundlich			
$K_F\left((mg/g)/(mg/L)^{\frac{1}{n}}\right)$	5.623	5.669	5.772
1/n	0.297	0.321	0.35
R2	0.98	0.979	0.979
Langmuir			
$q_m\left(mg \cdot g^{-1}\right)$	20.57	21.249	21.574
$K_L\left(L \cdot mg^{-1}\right)$	0.1337	0.1319	0.1360
R2	0.99	0.99	0.99
Redlich Peterson			
$K_R\left(\mathrm{L} \cdot \mathrm{mg}^{-1}\right)$	12.195	12.195	12.195
β_R	0.77	0.77	0.77
a_R	1.659	1.659	1.659
R^2	0.999	0.999	0.999
Toth			
a_τ	9.577	9.096	9.615
T	0.94	0.738	0.750
$k_\tau\left(\mathrm{mg} \cdot \mathrm{L}^{-1}\right)$	1.659	3.0644	2.208
R^2	0.999	0.999	0.999
Temkin			
$K_T\left(\mathrm{L} \cdot \mathrm{mg}^{-1}\right)$	1.633	1.5895	1.3732
B1	4.096	4.3366	4.786
R^2	0.99	0.983	0.97

Table 5.15 (a) Isotherm constants for malachite green oxalate dye adsorption onto palmyra male inflorescence carbon activated with KOH at different temperatures

Name of the isotherm	T/ K		
	303	313	323
Freundlich			
$K_F\left((mg/g)/(mg/L)^{\frac{1}{n}}\right)$	39.646	41.679	44.256
1/n	0.36	0.362	0.362
R^2	0.99	0.99	0.98
Langmuir			
$q_m\left(mg\ g^{-1}\right)$	217.39	222.22	226.24
$K_L\left(L\ mg^{-1}\right)$	0.1037	0.1184	0.1348
R^2	0.99	0.98	0.98
Redlich Peterson			
$K_R\left(L\ mg^{-1}\right)$	322.58	338.98	357.14
β_R	0.6642	0.6599	0.655
a_R	7.463	7.463	7.463
R^2	0.999	0.999	0.999
Toth			
a_τ	1.01	1.01	1.01
T	0.9047	0.894	0.887
$K_\tau\left(mg\ g^{-1}\right)$	133.03	135.03	136.47
R^2	0.97	0.97	0.97
Temkin			
$K_T\left(L\ mg^{-1}\right)$	1.882	2.078	2.341
B1	35.78	36.95	37.79
R^2	0.96	0.96	0.96

Table 5.15 (b) Isotherm constants for malachite green oxalate dye adsorption onto palmyra male inflorescence carbon activated with H_3PO_4 at different temperatures

Name of the isotherm	T/ K		
	303	313	323
Freundlich			
$K_F\left((mg/g)/(mg/L)^{\frac{1}{n}}\right)$	5.07	5.02	5.06
1/n	0.666	0.69	0.718
R^2	0.976	0.98	0.99
Langmuir			
$q_m\left(mg\ g^{-1}\right)$	270.23	303.03	343.50
$K_L\left(L\ mg^{-1}\right)$	0.0073	0.007	.0069
R^2	0.99	0.99	0.98
Redlich Peterson			
$K_R\left(L\ mg^{-1}\right)$	3.294	3.422	3.702
β_R	0.5843	0.566	0.5468
a_R	0.1367	0.1367	0.1367
R^2	0.97	0.97	0.97
Toth			
a_τ	2.009	2.009	2.009
T	0.465	0.4435	0.417
$k_\tau\left(mg\ g^{-1}\right)$	24.459	26.04	28.93
R^2	0.953	0.95	0.97
Temkin			
$K_T\left(L\ mg^{-1}\right)$	0.111	0.120	0.134
B1	45.51	47.18	49.71
R^2	0.95	0.94	0.93

Table 5.15 (c) Isotherm constants for malachite green oxalate dye adsorption onto palmyra male inflorescence carbon activated with $ZnCl_2$ at different temperatures

Name of the Isotherm	T/K		
	303	313	323
Freundlich			
$K_F\left((mg/g)/(mg/L)^{\frac{1}{n}}\right)$	1.685	1.748	1.868
1/n	0.628	0.627	0.62
R^2	0.99	0.99	0.98
Langmuir			
$q_m\left(mg\ g^{-1}\right)$	128.21	130.208	129.03
$K_L\left(L\ mg^{-1}\right)$	0.003	0.003	0.0033
R^2	0.99	0.99	0.99
Redlich Peterson			
$K_R\left(\mathrm{L\ mg^{-1}}\right)$	0.8191	0.8489	0.9057
β_R	0.5463	0.5477	0.5472
a_R	0.1367	0.1367	0.1367
R^2	0.97	0.97	0.97
Toth			
a_τ	2.009	2.009	2.009
T	0.458	0.459	0.469
$k_\tau\left(\mathrm{mg\ g^{-1}}\right)$	6.84	7.07	7.45
R^2	0.97	0.97	0.97
Temkin			
$K_T\left(\mathrm{L\ mg^{-1}}\right)$	0.0281	0.0291	0.0301
B1	28.0	28.28	28.56
R^2	0.99	0.99	0.99

Table 5.16 (a) Isotherm constants for safranine O dye adsorption onto palmyra male inflorescence carbon activated with KOH at different temperatures

Name of the isotherm	T/K		
	303	313	323
Freundlich			
K_F $\left((mg/g)/(mg/L)^{\frac{1}{n}}\right)$	2.533	2.577	2.635
1/n	0.7	0.7065	0.7118
R^2	0.98	0.98	0.98
Langmuir			
$q_m\left(mg\ g^{-1}\right)$	238.09	250.0	258.93
$K_L\left(L\ mg^{-1}\right)$	0.0038	0.0038	0.0039
R^2	0.98	0.98	0.98
Redlich Peterson			
$K_R\left(\mathrm{L\ mg^{-1}}\right)$	1.624	1.6809	1.745
β_R	0.52	0.5191	0.516
a_R	0.1367	0.1367	0.1367
R^2	0.944	0.944	0.947
Toth			
a_τ	101.99	101.99	101.99
T	0.83	0.8197	0.818
$k_\tau\left(\mathrm{mg\ g^{-1}}\right)$	0.0120	0.0127	0.0136
R^2	0.97	0.97	0.974
Temkin			
$K_T\left(\mathrm{L\ mg^{-1}}\right)$	0.0402	0.0414	0.04273
B1	49.57	51.104	52.534
R^2	0.99	0.998	0.997

Table 5.16 (b) Isotherm constants for safranine O dye adsorption onto palmyra male inflorescence carbon activated with H_3PO_4at different temperatures

Name of the Isotherm	T/K		
	303	313	323
Freundlich			
K_F $\left((mg/g)/(mg/L)^{\frac{1}{n}}\right)$	1.853	1.893	1.848
1/n	0.544	0.543	0.549
R^2	0.95	0.95	0.958
Langmuir			
$q_m\left(mg\ g^{-1}\right)$	71.098	71.24	72.763
$K_L\left(L\ mg^{-1}\right)$	0.0045	0.0046	0.0045
R^2	0.975	0.972	0.975
Redlich Peterson			
$K_R\left(\mathrm{L\ mg^{-1}}\right)$	0.7629	0.779	0.764
β_R	0.615	0.618	0.6124
a_R	0.1367	0.1367	0.1367
R^2	0.957	0.9547	0.959
Toth			
a_τ	40.93	42.178	41.4
T	0.898	0.9085	0.895
$k_\tau\left(\mathrm{mg\ g^{-1}}\right)$	0.0098	0.0098	0.0098
R^2	0.97	0.967	0.9725
Temkin			
$K_T\left(\mathrm{L\ mg^{-1}}\right)$	0.03386	0.0343	0.033
B1	17.69	17.742	18.036
R^2	0.98	0.978	0.983

Table 5.16 (c) Isotherm constants for safranine O dye adsorption onto palmyra male inflorescence carbon activated with $ZnCl_2$at different temperatures

Name of the Isotherm	T/K		
	303	313	323
Freundlich			
K_F $\left((mg/g)/(mg/L)^{\frac{1}{n}}\right)$	1.791	1.697	1.613
1/n	0.558	0.589	0.62
R^2	0.97	0.97	0.987
Langmuir			
$q_m\left(mg\ g^{-1}\right)$	50.76	55.56	60.98
$K_L\left(L\ mg^{-1}\right)$	0.0032	0.003	0.0025
R^2	0.974	0.975	0.984
Redlich Peterson			
$K_R\left(\mathrm{L\ mg^{-1}}\right)$	0.403	0.369	0.3342
β_R	0.5859	0.561	0.5348
a_R	0.1367	0.137	0.1367
R^2	0.9611	0.962	0.9731
Toth			
a_τ	22.67	22.30	21.839
T	0.856	0.837	0.8159
$k_\tau\left(\mathrm{mg\ L^{-1}}\right)$	0.0098	.0098	0.0098
R^2	0.969	0.970	0.98
Temkin			
$K_T\left(\mathrm{L\ mg^{-1}}\right)$	0.02411	0.021	0.0201
B1	12.608	13.51	14.406
R^2	0.984	0.989	0.996

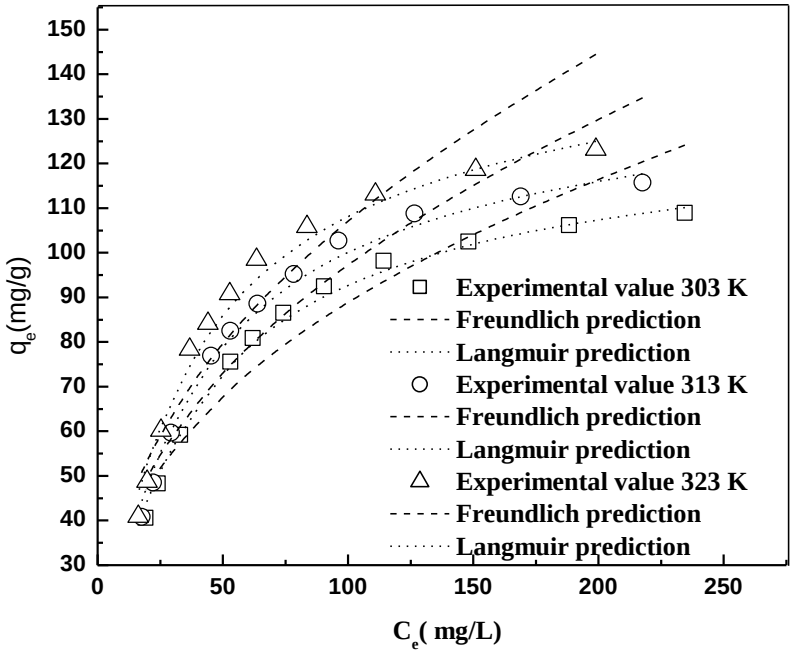

Figure 5.23 Equilibrium isotherm for adsorption of orange G onto activated carbon

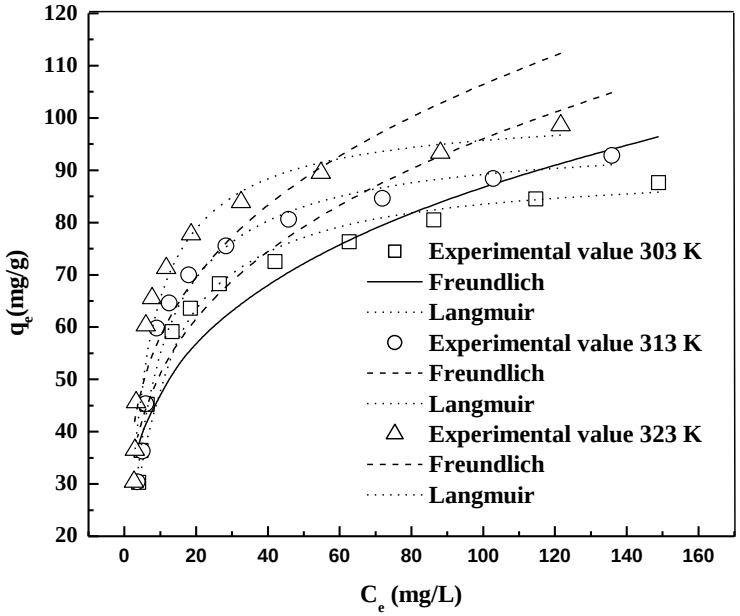

Figure 5.24 Equilibrium isotherm for adsorption of eosin Y onto activated carbon

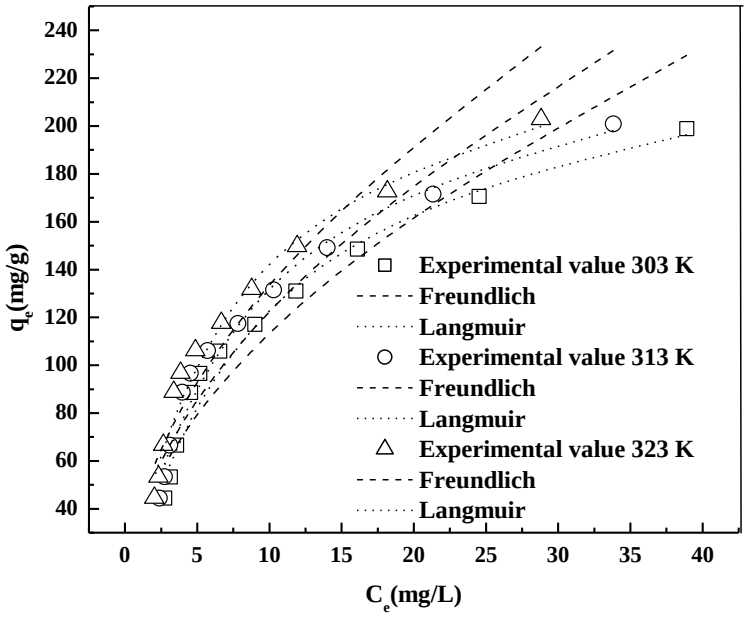

Figure 5.25 Equilibrium isotherm for adsorption of indigo carmine onto activated carbon

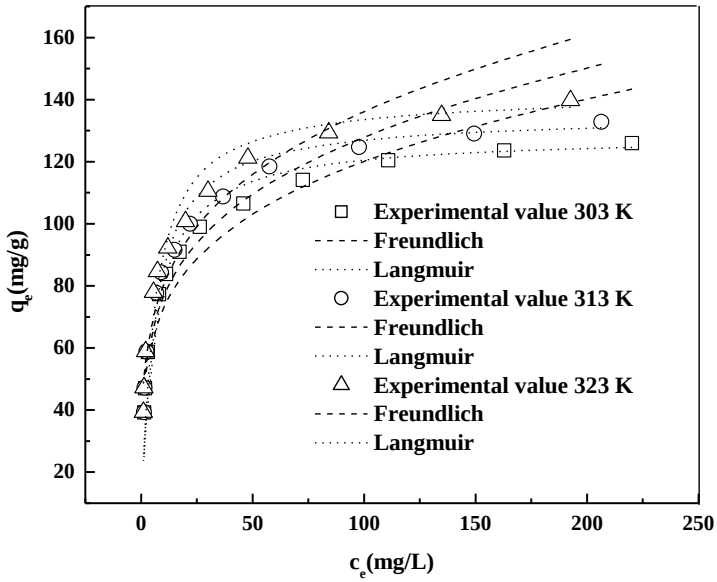

Figure 5.26 Equilibrium isotherm for adsorption of safranine O onto activated carbon

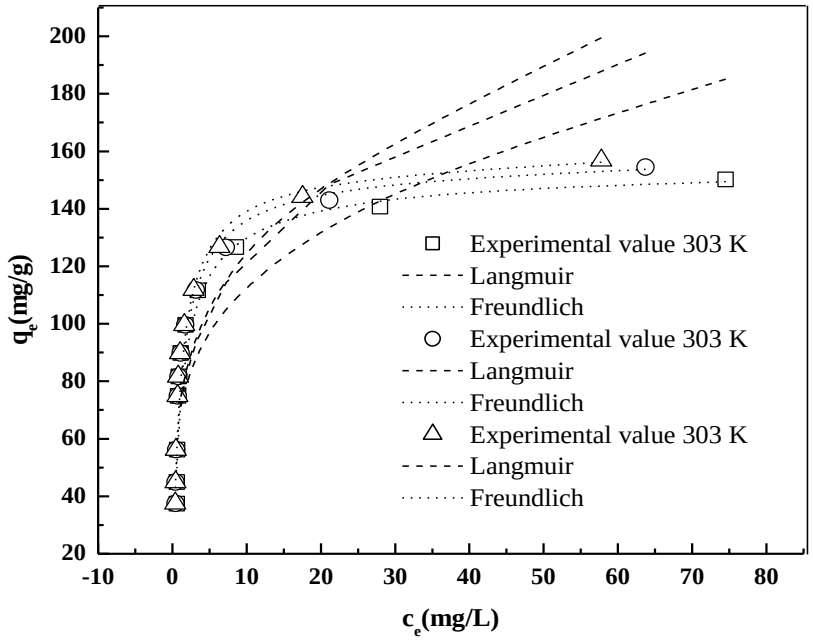

Figure 5.27 Equilibrium isotherm for adsorption of malachite green oxalate onto activated carbon

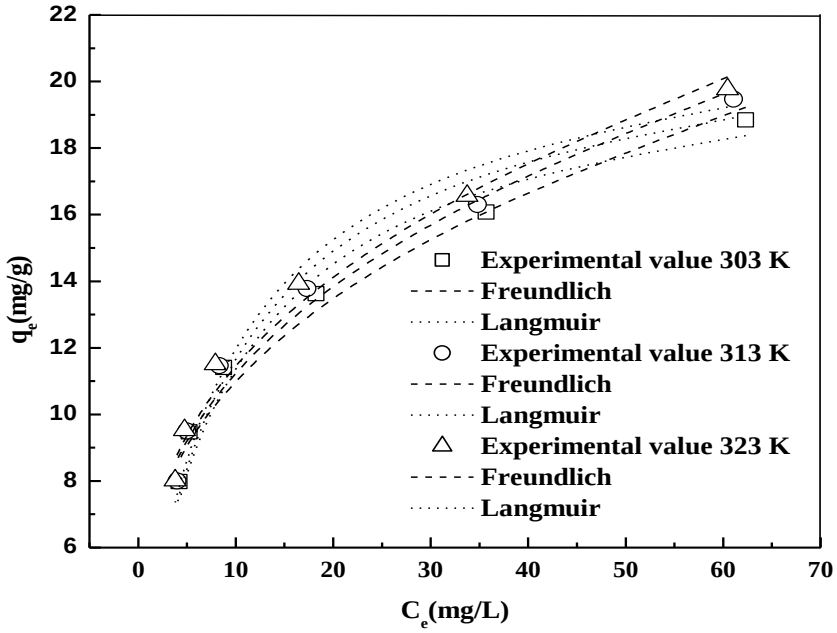

Figure 5.28 Equilibrium isotherm for adsorption of eosin Y onto Chitosan

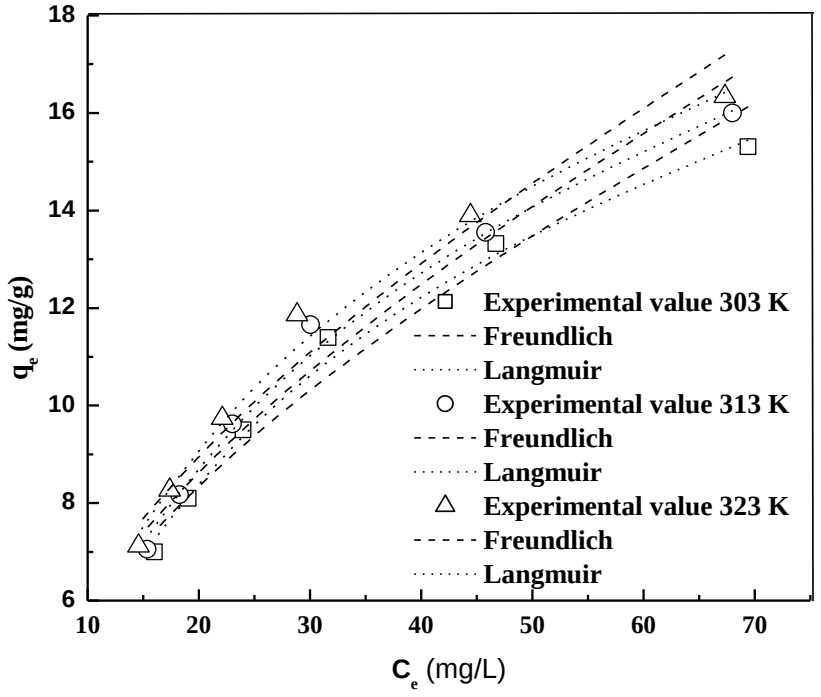

Figure 5.29 Equilibrium isotherm for adsorption of indigo carmine onto chitosan

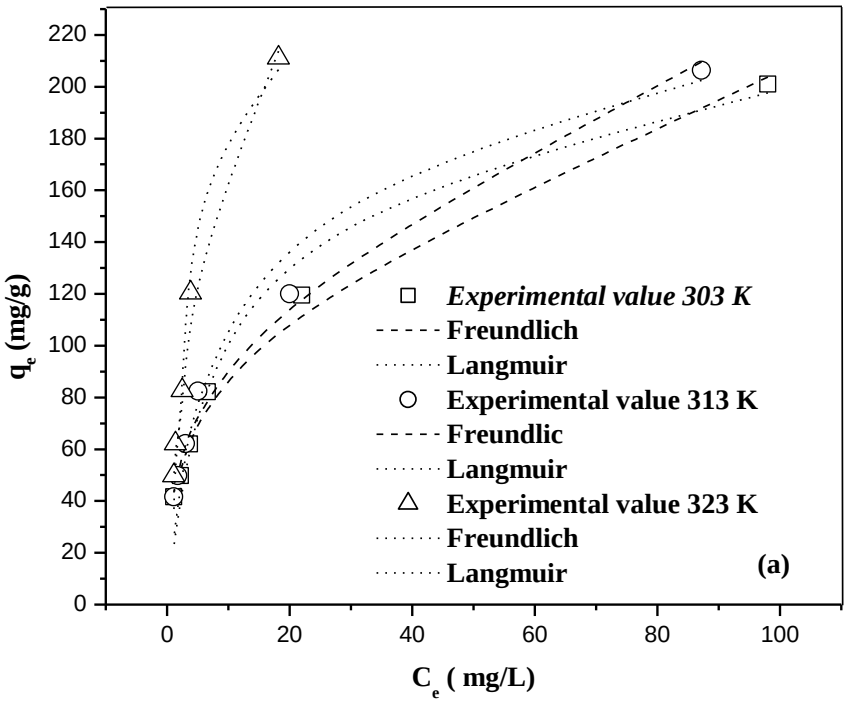

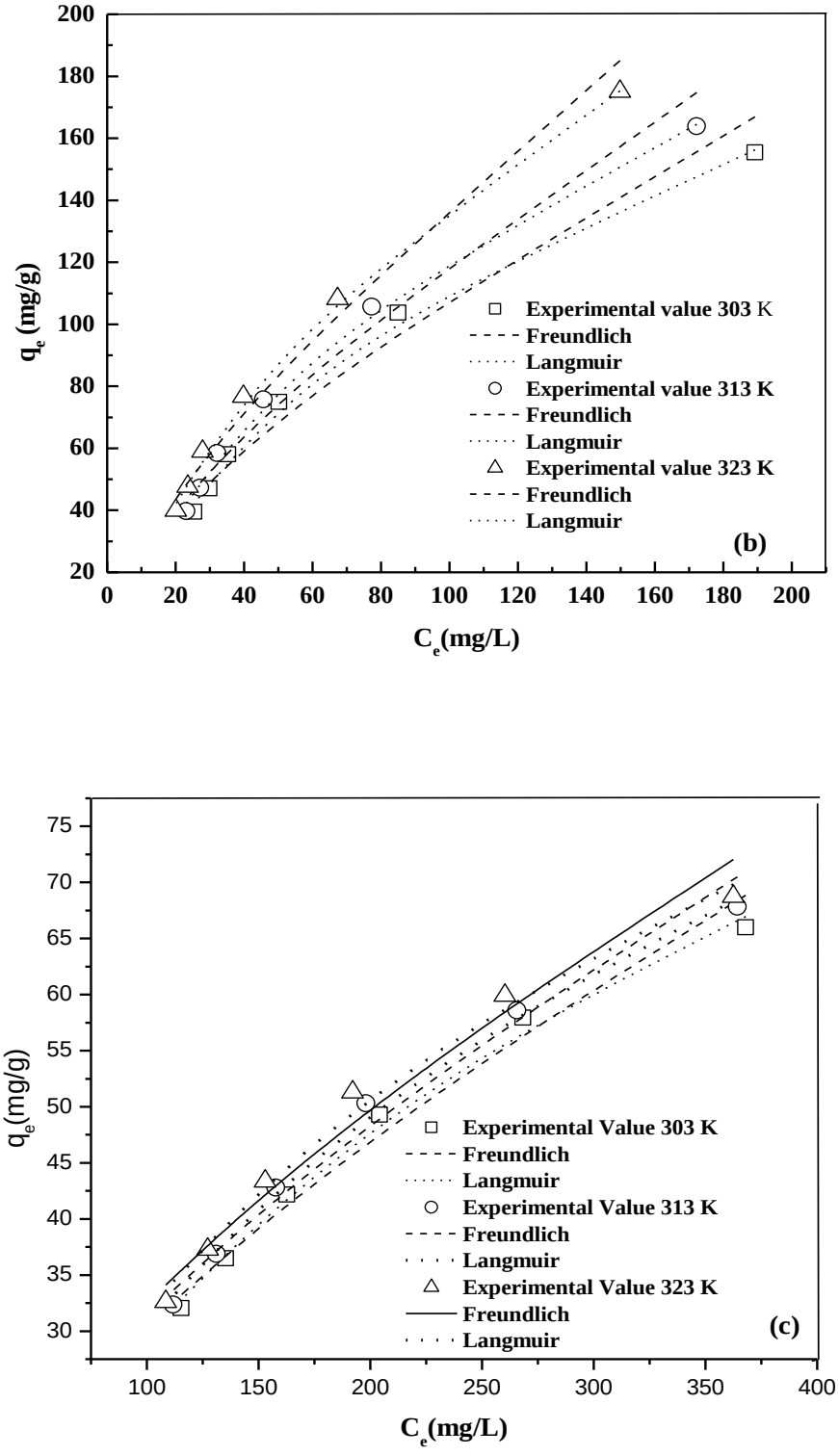

Figure 5.30 Equilibrium isotherm for adsorption of malachite green oxalate onto palmyra male inflorescence carbon. (a) KOH treated (b) H_3PO_4 treated (c) $ZnCl_2$ treated.

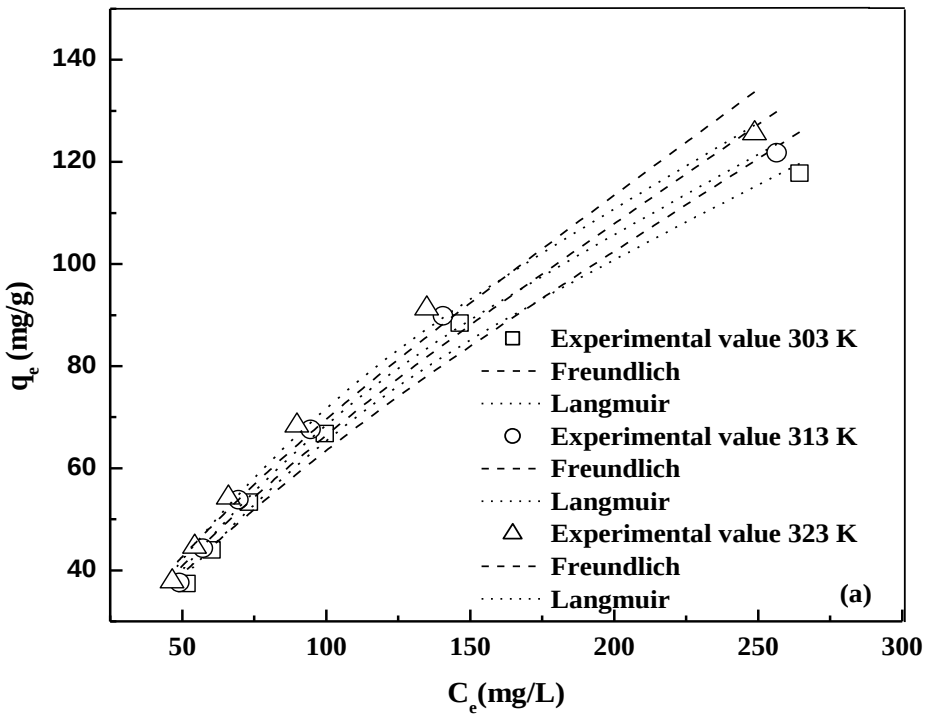
140
120
100
80
60
40
50
100
150
200
250
300
q_e (mg/g)
C_e(mg/L)
Experimental value 303 K
Freundlich
Langmuir
Experimental value 313 K
Freundlich
Langmuir
Experimental value 323 K
Freundlich
Langmuir
(a)

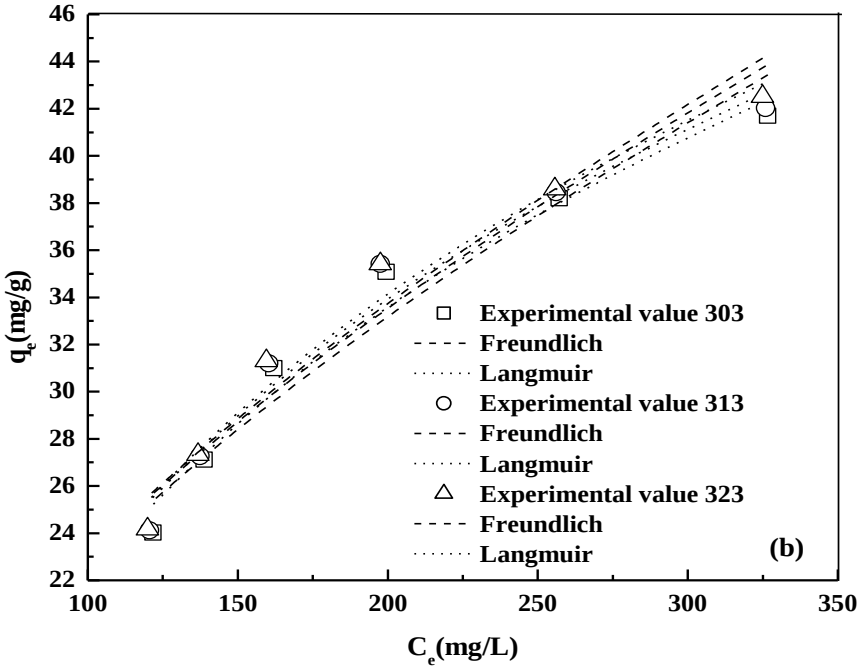
46
44
42
40
38
36
34
32
30
28
26
24
22
100
150
200
250
300
350
q_e (mg/g)
C_e(mg/L)
Experimental value 303
Freundlich
Langmuir
Experimental value 313
Freundlich
Langmuir
Experimental value 323
Freundlich
Langmuir
(b)

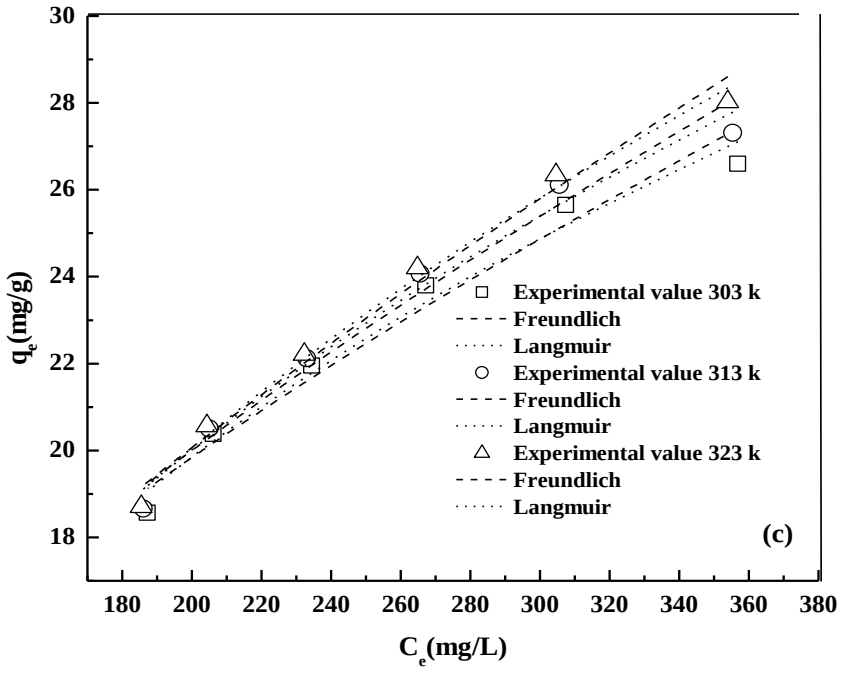

Figure 5.31 Equilibrium isotherm for adsorption of safranine O onto palmyra male inflorescence carbon. (a) KOH treated (b) H_3PO_4 treated (c) $ZnCl_2$ treated.

5.5 Conclusions

In this work, batch studies are performed. The effect of parameters such as pH, adsorbent dose and temperatures were investigated. Their thermodynamic parameters evaluated reveals that the adsorption process is favorable with the adsorbents studied. Kinetic studies are performed in a mechanically stirred vessel to determine the rate parameters. The adsorption process is well represented by pseudo second order kinetics. The various existing equilibrium isotherm models are used to evaluate the experimental data. The correlated results shows that the new adsorbent palmyra male inflorescence carbon is found to be better than the commercial available adsorbent. The maximum Langmuir adsorption capacity of safranine O and malachite green treated with palmyra male inflorescence carbon found to be 258.93 mg g^{-1} and 343.50 mg g^{-1} respectively

whereas the activated carbon the values are found to be 141.42 mg g^{-1} and 159.139 mg g^{-1}. The maximum Langmuir adsorption capacity of the chitosan developed in this work found to be 21.574 mg g^{-1} and 24.876 mg g^{-1} for eosin Y and indigo carmine respectively and these is comparable with the literature studied adsorbents.

Reference

[5.1] I.D. Mall, V.C. Srivastava, N.K. Agarwal, Adsorptive removal of auramine – O; Kinetic and equilibrium study. J. Hazard. Mater. 143 (2007) 386-395.

[5.2] D. O. Cooney, Adorption design for waste water treatment. Lewis Publishers, New York, 1999.

[5.3] A.S. Özcan, A. Özcan, Adsorption of acid dyes from aqueous solutions onto acid – activated bentonite. J. Colloid. Interface Sci. 276 (2004) 39 - 46.

[5.4] F. Deniz, S. Karaman, Removal of basic red 46 dye from aqueous solution by pine tree leaves. Chem. Eng. J. 170 (2011) 67-74.

[5.5] I.D. Mall, V.C. Srivastava, N.K. Agarwal, Removal of Orange G and methyl violet dyes by adsorption onto bagasse fly ash-kinetic study and equilibrium isotherm analyses. Dyes and Pigm. 69 (2006) 210-223.

[5.6] Y.S.A. Degs, M.I.E. Barghouthi, A.H.E. Sheikh, G.M. Walker, Effect of solution pH, ionic strength and temperature on adsorption behavior of reactive dyes on activated carbon. Dyes and Pigm.77 (2007) 16-23.

[5.7] S.E. Subramani, N.Thinakaran, Isotherm, kinetic and thermodynamic studies on the adsorption behavior of textile dyes onto chitosan. Process Safety and Environmental Protection 106 (2017) 1 – 10.

[5.8] D.H. Lataye, I.M. Mishra, I.D. Mall, Pyridine sorption from aqueous solution by rice husk ash (RHA) and granular activated carbon (GAC), Parametric, kinetic, equilibrium and thermodynamic aspects. J. Hazard. Mater. 154 (2008) 858 – 870.

[5.9] D.H. Lataye, I.M. Mishra, I.D. Mall, Adsorption of α - picoline onto rice husk ash and granular activated carbon from aqueous solution, Equilibrium and thermodynamic study. Chem. Eng. J. 147 (2008) 139-149.

[5.10] A.F. Freitas, M.F. Mendes, G.L.V. Coelho, Thermodynamic study of fatty acids adsorption on different adsorbents. J. Chem. Thermodyn. 39 (2007) 1027-1037.

[5.11] Z.J. Hu,N.X. Wang, J. Tan, J.Q. Chen, W.Y. Zhong, Kinetic and equilibrium of cefradine adsorption onto peanut husk. Desalination and Water Treatment 37 (2012) 160-168.

[5.12] K.Y. Foo, B.H. Hameed, Insights into the modeling of adsorption isotherm systems. Chem. Eng. J. 156 (2010) 2-10.

[5.13] A.G.S. Prado, J.C. Torres, E.A. Faria, S.C.L. Dias, Comparative adsorption studies of indigo carmine dye on chitin and chitosan. J. Colloid Interface Sci. 277 (2004) 43 – 47.

CHAPTER 6

MODELING OF BATCH ADSORPTION

In this chapter, the theoretical basis for the development of new adsorption isotherm models based on phase equilibrium criterion has been presented. The adsorption equilibrium data obtained for the various adsorbent – adsorbate systems (activated carbon – safranine O, malachite green oxalate and orange G and chitosan – eosin Y and indigo carmine) were used correlate the proposed new models. The new models were compared with the only existing phase equilibrium model proposed by Khan et al [6.1].

6.1 New Models

6.1.1 Phase equilibrium model -1

In this model, we assume that the sorbate (solute) molecules are uniformly absorbed on an adsorbent, which is highly porous. The solid phase is treated as a solid solution of solute well distributed into the porous adsorbent [6.1- 6.2]. Applying the basic criterion for equilibrium in terms of fugacity to the solid-liquid system gives:

$$f_i^L = f_i^S \qquad (6.1)$$

Where, f_i^L is the fugacity of the sorbate (component i) in the liquid phase (L) and f_i^S is its fugacity in the solid phase (S).

Solid phase activity coefficient for component *i* can be defined as follows

$$\gamma_i^S = \frac{f_i^S}{z_i f_i^{OS}} \qquad (6.2)$$

where z_i is the mole fraction of the sorbate "*i*" in the solid phase; f_i^{OS} is the fugacity of solid, *i* at standard state that may be considered as pure solid state i.

Liquid phase activity coefficient for component i can be defined as follows:

$$\gamma_i^L = \frac{f_i^L}{x_i f_i^{OL}} \tag{6.3}$$

where x_i is the mole fraction of the sorbate "i" in the liquid phase; f_i^{OL} is the fugacity of liquid i at standard state that may be considered as pure liquid state i.

Substituting equations (6.2) and (6.3) into equation (6.1) gives:

$$x_i \ \gamma_i^L \ f_i^{OL} = z_i \ \gamma_i^S \ f_i^{OS} \tag{6.4}$$

The liquid phase activity coefficient γ_i^L can be estimated from regular solution theory [6.3].

$$RT \ln\left(\gamma_i^L\right) = v_i^L \phi_j \left(C_{ii} + C_{jj} - 2C_{ij}\right) \tag{6.5}$$

$$\phi_j = \frac{x_j v_j^L}{\left(x_i v_i^L + x_j v_j^L\right)} \tag{6.6}$$

$$C_{ii} = \frac{\Delta H_{vi} - RT}{v_i^L} \tag{6.7}$$

$$C_{jj} = \frac{\Delta H_{vj} - RT}{v_j^L} \tag{6.8}$$

$$C_{12} = \left(1 - l_{ij}\right)\sqrt{C_{ii} C_{jj}} \tag{6.9}$$

Where *i* is the sorbate (solute) and *j* is the solvent, v_i^L is the molar volume of the solute, v_j^L is the molar volume of the solvent; ΔH_{vi} is the enthalpy of vaporization of the solute, ΔH_{vj} is the enthalpy of vaporization of the solvent, l_{ij} is the correction factor.

The solid phase activity coefficient can be obtained from truncated Redlich-Kister expansion [6.2].

$$\ln\left(\gamma_{\mathrm{i}}^{\mathrm{S}}\right)=\left(1-z_{\mathrm{i}}\right)^{2}\left(A'+B'z+C'z^{2}\right) \tag{6.10}$$

where $\left(1-z_{\mathrm{i}}\right)$ is the mole fraction of the adsorbent, A' B' and C' are temperature – dependent parameters related to constants in the relation for excess Gibbs energy, G^{E}. The solid phase activity coefficient is similar to the four-suffix Margules equation for liquid systems.

Equation (6.4) is rearranged to give:

$$x_{\mathrm{i}}=z_{\mathrm{i}}\left(\frac{\gamma_{\mathrm{i}}^{\mathrm{S}}}{\gamma_{\mathrm{i}}^{\mathrm{L}}}\right)\left(\frac{f_{\mathrm{i}}^{\mathrm{OS}}}{f_{\mathrm{i}}^{\mathrm{OL}}}\right) \tag{6.11}$$

B. Wang et al. [6.4] and Q. Li et al.[6.5] suggested an equation relating fugacity of the pure solid and fugacity of the pure liquid at the temperature (T) and pressure of the system in terms of solute melting temperature, T_{m} and heat of fusion, ΔH_{f} as

$$\ln\left(\frac{f_i^{OS}}{f_i^{OL}}\right)=\frac{-\Delta H_f}{RT}\left(\frac{T}{T_m}-1\right)$$

Therefore

$$\frac{f_{\mathrm{i}}^{\mathrm{OS}}}{f_{\mathrm{i}}^{\mathrm{OL}}}=\exp\left[\frac{-\Delta H_{\mathrm{f}}}{RT}\left(\frac{T}{T_{\mathrm{m}}}-1\right)\right] \tag{6.12}$$

Substituting equations (6.10) and (6.12) into equation (6.11) gives

$$x_i = z_i \left(\frac{\exp\left\{(1-z_i)^2 \left(A' + B'\ z_i + C'\ z_i^2\right)\right\}}{\gamma_i^L} \right) \exp\left[\frac{-\Delta H_f}{RT} \left\{ \frac{T}{T_m} - 1 \right\} \right] \qquad (6.13)$$

If the heat of fusion ΔH_f is not available for a compound of interest, the term $6.54\left(1-\frac{T}{T_m}\right)$ may be used as a rough approximation of the term $\frac{\Delta H_f}{RT}\left(\frac{T}{T_m}-1\right)$ in equation (6.13) [6.6]. Hence,

$$\frac{f_i^{OS}}{f_i^{OL}} = \exp\left\{-6.54\left(1-\frac{T_m}{T}\right)\right\} \qquad (6.14)$$

Substituting equations (6.12) and (6.14) into equation (6.11) gives

$$x_i = z_i \left(\frac{\exp\left((1-z_i)^2 \left(A' + B'\ z_i + C'\ z_i^2\right)\right)}{\gamma_i^L} \right) \exp\left[-6.54 \left\{ 1 - \frac{T_m}{T} \right\} \right] \qquad (6.15)$$

Usually the adsorption data available in terms of q_e and m_e from such data z can be calculated from the following

$$z = \frac{q_e/\text{mol kg}^{-1}}{1000/12 + \left(q_e/\text{mol kg}^{-1} \right)} \qquad (6.16)$$

where q_e is moles of solute adsorbed / kg of adsorbent.

Similarly, x is the mole fraction of the solute in the liquid phase which can be calculated from the experimental data on solute concentration (m_e). If m_e is in the units of mol kg^{-1} then x is calculated by the following expression

$$x = \frac{m_e/\text{mol kg}^{-1}}{1000/18 + \left(m_e/\text{mol kg}^{-1} \right)} \qquad (6.17)$$

Solid solute molar volume was measured by additivity method of Immirzi and Perini [6.6]. Liquid solute molar volume can be calculated by multiplying the solids molar volume with a factor 1.02 [6.4].

6.1.2 Phase equilibrium model -2

In this model we assume that adsorbent is highly porous. Solute is well distributed in the porous adsorbent, and the solute molecules are uniformly absorbed on an adsorbent. The solid phase is treated as a solid solution [6.1- 6.2]. At equilibrium the fugacity of sorbate in liquid and solid can be equated as,

$$\hat{f}_A^L = \hat{f}_A^S \qquad (6.18)$$

In equation (6.18), subscript A is the solute and superscripts (L) and (S) represents the liquid and solid phase respectively. Equation (6.18) can be rewritten in terms of the activity coefficients as,

$$\hat{f}_A^L = \gamma_A^L x_A f_A^L \qquad (6.19a)$$

$$\hat{f}_A^S = \gamma_A^S z_A f_A^S \qquad (6.19b)$$

where γ_A^L and γ_A^S are the activity coefficients of solute in liquid and solid phase. x_A and z_A are the mole fractions of solute in liquid and solid phase, respectively. f_A^L and f_A^S are pure component fugacity of solute in the respective phases.

For dilute systems the liquid phase activity coefficient γ_A^L may be treated as infinite dilution (i.e., $\gamma_A^{\infty L}$) and it has been used as an adjustable parameter in this model.

The solid phase activity coefficient can be obtained from truncated Redlich-Kister expansion as suggested by Riazi and Khan [6.2].

$$\ln\left(\gamma_A^S\right) = \left(1 - z_A\right)^2 \left(A' + B' \quad z + C' \quad z^2\right) \qquad (6.20)$$

where $(1 - z_A)$ is the mole fraction of the adsorbent, A' B' and C' are temperature–dependent parameters related to constants in the relation for excess Gibbs free energy, G^E. Equation (6.18), equation (6.19a) and equation (6.19b), were combined and rearranged to give

$$x_i = z_i \left(\frac{\gamma_A^S}{\gamma_A^{\infty L}}\right)\left(\frac{f_A^S}{f_A^L}\right) \qquad (6.21)$$

Fugacity of the pure solid and fugacity of the pure liquid at system pressure and temperature [6.4] as

$$\ln\left(\frac{f_A^S}{f_A^L}\right) = \frac{-\Delta H_f}{RT}\left(\frac{T}{T_m} - 1\right) \qquad (6.22)$$

If the physical properties are not available for a compound of interest, the term $\alpha - \frac{\beta}{T}$ may be used as an alternate of the term $\Delta H_f / RT(T/T_m - 1)$ in equation (6.22), hence,

$$f_A^S / f_A^L = \exp\left(\alpha - \beta / T\right) \qquad (6.23)$$

where α and β are constants.

Combining equation (6.20), equation (6.21) and equation (6.23), gives

$$x_A = z_A \left(\frac{\exp\left((1 - z_A)^2 \left(A' + B'\ z_A + C'\ z_A^2\right)\right)}{\gamma_A^{\infty L}} \right) \left(\exp\left(\alpha - \beta / T\right) \right) \qquad (6.24)$$

In general the adsorption equilibrium data's are reported in terms of q and C from such data x_A and z_A can be calculated from the following equations

$$x_A = \frac{C / M}{C / M + \rho_B \left(1 - C / M\rho_A\right)} \qquad (6.25)$$

$$z_A = \frac{q / M}{1000 / 12 + q / M} \qquad (6.26)$$

where C is sorbate (i.e., solute) concentration in liquid, q is solute adsorbed per unit weight of adsorbent and M molar mass of the solute. ρ_B is the molar density of the pure solvent, ρ_A is the molar density of the pure liquid solute (*A*) of interest. Solid density can be measured by additively method of Immirzi and Perini [6.2]. For pure liquids density can be calculated by dividing the solids density with a factor 1.02 [6.4]

6.1.3. Phase equilibrium model -3

In this model we have assumed that solute is uniformly distributed into the adsorbent. The solid phase is treated as a solid solution [6.1 – 6.2]. At equilibrium the chemical potential of sorbate in liquid and solids can be equated as

$$\mu_1^L = \mu_1^S \tag{6.27}$$

In equation (6.27) subscript 1 is the adsorbate and superscript L and S are liquid and solid phases respectively. Equation (6.27) can be rewritten in terms of activity as

$$\mu_1^L = G_1^{oL} + RT \ln \hat{a}_1^L \tag{6.28}$$

$$\mu_1^S = G_1^{oS} + RT \ln \hat{a}_1^S \tag{6.29}$$

Where $\hat{a}_1^L$ and $\hat{a}_1^S$ are activity of the solute in liquid and solid phase. For liquid phase the equation is modified by introducing the activity coefficient as

$$\hat{a}_1^L = \frac{\hat{f}_1^L}{f_1^{oL}} = \gamma_1^L x_1 \frac{f_1^L}{f_1^{oL}} \tag{6.30}$$

$$\hat{a}_1^S = \frac{\hat{f}_1^S}{f_1^{oS}} = \gamma_1^S z_1 \frac{f_1^S}{f_1^{oS}} \tag{6.31}$$

where x_1 is mole fraction of the solute in the liquid phase, z_1 is the mole fraction of the solute in solid solution (i.e., on adsorbent), γ_1^L is the activity coefficient of the solute in the liquid phase, γ_1^S is the activity coefficient of the solute in solid phase, f_1^L and f_1^{oL} represent fugacity of pure liquid 1 at temperature T, and pressure p and p^o, respectively. Similarly, both f_1^S and f_1^{oS} represent fugacity of pure solid 1 (i.e., solid solution) at temperature T, and pressure p and p^o, respectively. Except in the critical region, pressure has little effect on the properties of liquids as well as on solid solutions therefore

the ratio f_1^L / f_1^{oL} and f_1^S / f_1^{oS} is often taken as unity [6.7]. Equation (6.30) and (6.31) reduced as

$$\hat{a}_1^L = \gamma_1 x_1 \tag{6.32}$$

$$\hat{a}_1^S = \gamma_1 z_1 \tag{6.33}$$

Combining equation (6.27), (6.28), (6.29), (6.30) and equation (6.31) gives

$$G_1^{oL} + RT \ln x_1 \gamma_1^L = G_1^{oS} + RT \ln z_1 \gamma_1^S \tag{6.34}$$

Rearranging equation (6.34) gives

$$x_1 \gamma_1^L = z_1 \gamma_1^S \exp\left(\frac{\Delta G_1^{S-L}}{RT}\right) \tag{6.35}$$

where ΔG_1^{S-L} is Gibbs energy change (i.e., (G_1^{oS}-G_1^{oL})) when solute transferred from liquid to solids solution.

The solid phase activity coefficient can be obtained from truncated Redlich-Kister expansion [6.2].

$$\ln\left(\gamma_1^{\mathrm{S}}\right) = (1 - z_1)^2 (\mathrm{D} + \mathrm{E}\ z_1 + \mathrm{F} z_1^2) \tag{6.36}$$

where $(1 - z_1)$ is the mole fraction of the adsorbent, D, E and F are temperature – dependent parameters relates to constants in the relation for excess Gibbs energy, G^{E} further solid phase activity coefficient are similar to the four-suffix Margules equation for liquid systems [6.3].

Equation (6.35) and Equation (6.36) combined and rearranged to give

$$x_1 = z_1 \left(\frac{\exp\left((1 - z_1)^2 \left(\mathrm{D} + E\ z_1 + \mathrm{F}\ z_1^2\right)\right)}{\gamma_1^{\mathrm{L}}}\right)\left(\exp\left(\frac{\Delta G_1^{S-L}}{RT}\right)\right) \tag{6.37}$$

Usually the adsorption data available in terms of q_e and b_e from such data z_1 can be calculated from the following

$$z_1 = \frac{q_e/\text{mol kg}^{-1}}{1000/12 + (q_e/\text{mol kg}^{-1})} \qquad (6.38)$$

where q_e is moles of solute adsorbed $\cdot$ kg of adsorbent^{-1}

Similarly x_1 is the mole fraction of the solute in the liquid phase which can be calculated from the experimental data on solute concentration (b_e). If b_e is in the units of $\text{mol} \cdot \text{kg}^{-1}$ then x_1 is calculated by the following expression

$$x_1 = \frac{b_e/\text{mol kg}^{-1}}{1000/18 + (b_e/\text{mol kg}^{-1})} \qquad (6.39)$$

Gibbs energy change required in Eq. (6.37) is obtained from equation. (2.13).

6.2. Correlations for the new models

6.2.1. Correlations for new model – 1

The equilibrium data obtained for the malachite green oxalate and safranin O dyes in this study was used to correlate the model– 1 equation (6.15). The parameters A', B',C' and l_{ij} were estimated by minimizing the absolute value of average relative deviation (AARD %) between experimental and predicted x_i .The optimization procedure [6.8] reduces the averaged absolute relative deviation percentage, AARD (%). It is defined as $(100/N_i)\left|x_i^{cal} - x_i^{\exp}\right| / x_i^{\exp}$ where N_i is the number of data points, x_i^{cal}

and $X_i^{\exp}$ are the mole fraction of the adsorbate (solute) in liquid that is in equilibrium with adsorbent (solid). Table 6.1shows the basic physiochemical properties of the dyes considered in this study.

Table 6.1 Physical and chemical properties of dye compounds investigated in this study.

Name of the dye (Formula)	Molecular weight / $g \cdot mol^{-1}$	Boiling point / K	Molar density of pure solid / $mol \cdot m^{-3}$	Melting point / K	Molar volume of pure liquid / $m^3 \cdot mol^{-1}$	Enthalpy of vaporization (ΔH_{vi}) / $J \cdot mol^{-1}$
Safranine O ($C_{20}H_{19}ClN_4$)	350.84	990.84[a]	3755.64[b]	573.15[e]	2.7159×10^{-4}[c]	964344 [d]
Malachite green oxalate ($C_{52}H_{54}N_4O_{12}$)	927.01	2483.76[a]	1379.43[b]	433.15[e]	7.3944×10^{-4}[c]	252337 [d]

[a] Estimated by the Joback method [6.9]

[b] Estimated by the additivity method of immirizi and pirini [6.6]

[c] Estimated by the method suggested by D.H. Diger et al [Hu,1982] [6.3] (i.e., Molar volume of the liquid = (1/molar density of the pure solid) $\times 1.02$) [6.3]

[d] Estimated by the rule suggested by Kistiakowsky [6.9]

[e] Observed using BUCHI melting point apparatus model M-560

The value of the parameters of equation (6.15) and equation (2.12) were reported in table 6.2 and table 6.3 respectively. The AARD values from the new model equation (6.15) are below 6.84 for safranine O and 4.08 for malachite green oxalate with activated carbon system.. On the other hand, the AARD values determined using the model proposed by Khan (equation 2.12) were 11.28 for safranine O and 14.24 for malachite green oxalate. The result shows that the new model correlates the isotherm better than the existing

model. This is also seen, in figure 6.1 and 6.2 It is clearly evident that the solid line, which represents correlation of the new model, indicates that this model is able to correlate better than the Khan et al., model reported in the literature. The equation (6.15) is based on the concept of regular solution theory and thus imposes constraints on l_{ij}, which is a constant, small compared to unity, characteristic of solute-solvent interaction [6.3]. Further, this model requires the melting temperature of the sorbate hence it cannot be applied to substances whose melting point is not known.

TABLE 6.2 Correlation parameters for adsorption of dye compounds onto activated carbon obtained using new model equation (6.15).

Name of the dye	T / K	Correlation parameters				AARD (%)
		l_{ij}	A'	B'	C'	
Safranine O	303	$2.0065 \cdot 10^{-2}$	36.262	- 339.31	301830	5.12
	313	$2.5797 \cdot 10^{-4}$	34.130	-102.22	237420	6.61
	323	$1.6646 \cdot 10^{-6}$	32.343	121.68	180670	6.84
Malachite green oxalate	303	$5.699 \cdot 10^{-3}$	134.43	- 5760.4	3428600	3.58
	313	$1.5463 \cdot 10^{-2}$	132.49	-4000.5	2658900	3.27
	323	$6.5239 \cdot 10^{-3}$	123.71	-3546.9	2413900	4.08

Table 6.3 Correlation Parameters for adsorption of dye compound onto activated carbon obtained using A.R. Khan et al., Model equation 2.12.

Name of the dye	*T*/K	Correlation parameters			AARD (%)
		A	*B*	*C*	
Orange G	303	-1.3528	4484.5	-324.96	6.06
	313	-1.9812	3899.8	-288.99	6.72
	323	-1.6244	3907.9	-302.29	5.66
Safranine O	303	-3.5807	4495.4	-332.15	10.51
	313	-5.1029	3836.2	-276.02	10.42
	323	-6.2223	3220.5	-222.02	11.28
Malachite green Oxalate	303	3.3697	17249	-1004.1	14.24
	313	-0.043889	14133	-799.53	8.96
	323	-0.98229	13104	-738.52	10..53

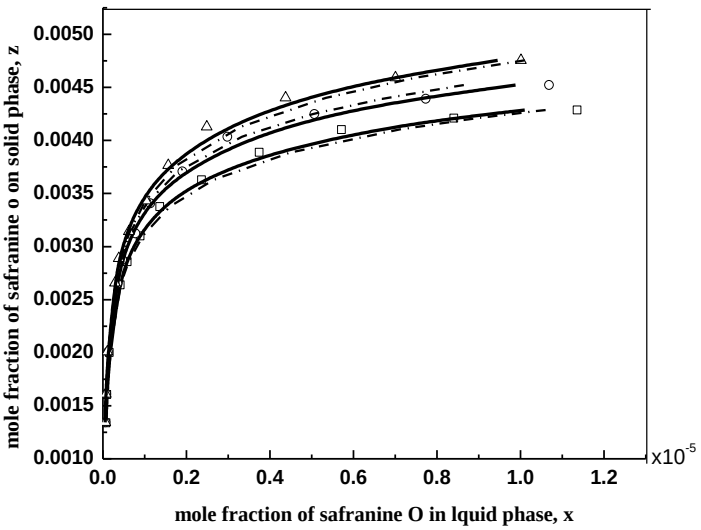

Figure 6.1 Mole fraction of safranine O on solid phase (z) against mole fraction of safranin O in liquid phase (x) at several temperatures. The solid lines are models predictions based on proposed new model in this study. The dash dot lines are the predictions based on Khan et al.[6.1]. Experimental values □, T = 303 K, ○, T = 313 K and Δ, T = 323 K.

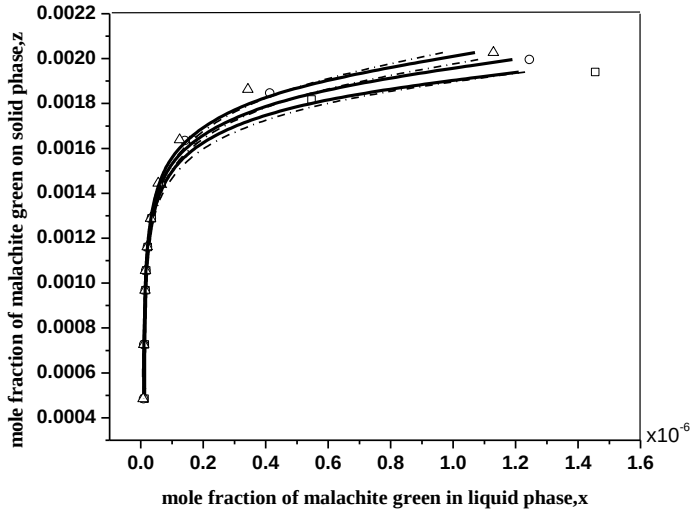

Figure 6.2 Mole fraction of malachite green oxalate on solid phase (z) against mole fraction of malachite green oxalate in liquid phase (x) at several temperatures. The solid lines are models predictions based on proposed new model in this study. The dash dot lines are the predictions based on Khan et al.[6.1] model. Experimental values □, T = 303 K, ○, T = 313 K and Δ, T = 323 K.

6.2.2 Correlations for new model - 2

The adsorption data of orange G obtained in this study were correlated with the new model and with the model proposed by A.R. Khan et al. The advantage of the new model over the existing model is its flexibility in terms of number of adjustable parameters. The new model is capable of giving the infinite dilution activity coefficient and melting point of the solute from the equilibrium adsorption data. The deviation of experimental data from the model was quantified in terms of AARD % (average absolute relative deviation percentage) and given by,

$$AARD\% = \left(100 / N_i\right) \left| x_i^{cal} - x_i^{\exp} \right| / x_i^{\exp} \qquad (6.40)$$

In equation(6.40) N_i is the number of data points, x_i represents the mole fraction of the adsorbate (solute) in liquid that is in equilibrium with adsorbent (solid) and the superscripts *cal*and *exp*denotes the calculated and experimental values, respectively. The optimization procedure directly gives these parameters. The Nelder-Mead simplex algorithm, implemented in Matlab 6.1, was used to determine the interaction parameters [6.8]. In Table 6.4 the values of $\gamma^{\infty L}$, A', B', C', α and β are reported. In table 6.3 the values of Khan et al. model parameters along with AARDs were reported. From table 6.4 and 6.3 it is clearly evident that the new model present in this study is better than the existing khan et al. model. To indicate this visually, the adsorption of orange G on activated carbon correlated by the model equations were represented in the figure 6.3. The solid line, which represents correlation of the new model, indicates that this model is able to correlate better than the khan et al. model. The parameter, $\gamma^{\infty L}$ in new model

indicates the solution behavior either positively deviating or negatively deviating from Raoult's law. If $\gamma^{\infty L}$ value is more than one, we can say that the solution is positively deviating from Raoult's law for other case (i.e., $\gamma^{\infty L}$ <1) we say that solution is negatively deviating. The value of $\gamma^{\infty L}$ varies with temperature. Conceptually, the ratio of parameters β and α gives the melting point of the solute. From Table 6.4 we can say that the orange G solution is positively deviating from Raoult's law, $\gamma^{\infty L}$ value is decreasing with increase in temperature and predicted melting point (ratio of β and α) for the orange G is 400 - 416 K.

Table 6.4 Correlation parameters for adsorption of orange G onto activated carbon obtained using new model equation (6.24).

Name of the dye	*T*/K	Correlation parameters						AARD (%)
		$\gamma^{\infty L}$	A'	B'	C'	α	β	
Orange G	303	2.8021	405.58	-423.30	506460	1275.6	511050	5.11
	313	2.4737	345.06	-402.69	424310	1117.9	459690	5.68
	323	2.3115	367.87	-472.58	415700	1286.2	536100	3.91

The new model derived in this study was used to correlate the equilibrium adsorption data of phenol – activated carbon system taken from the literature [6.10]. The correlations coefficients of phenol – activated carbon system were found to be $\gamma^{\infty L}$ =

23.24, A' = 45.86, B' = 145.17, C' = 1793.6, α = 815.77 and β = 255300.0 with AARD of 3.3%. Figure 6.4 shows the plot for new model. This indicates the applicability of the new model to the data other than investigated in this study.

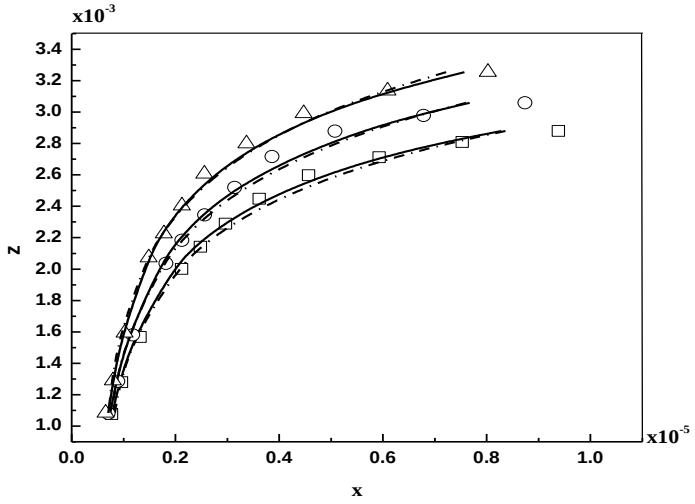

Figure 6.3 Mole fraction of orange G on solid phase (z) against mole fraction of orange G in liquid phase(x). Experimental values: □, T = 303 K; ○, T = 313 K; Δ, T = 323 K. The solid lines are models predictions based on new model in this study. The dash dot lines are the predictions based on Khan et al.[6.1] model.

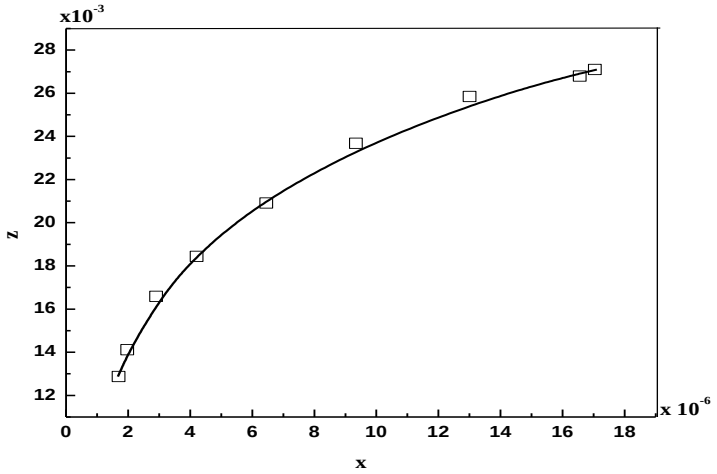

Figure 6.4 Mole fraction of phenol on solid phase (z) against mole fraction of phenol in liquid phase(x). Experimental values: □, T = 294 K. The solid lines are models predictions based on new model in this study [5.10].

6.2.3 Correlations for new model – 3

The experimental data obtained in this study for eosin Y and indigo carmine – chitosan system are used to correlate the new model (equation 6.37). The new model requires knowledge of Gibbs energy change. This parameter was estimated by Langmuir isotherm model as discussed in the chapter 2 (equation 2.4). In table 5.13 and table 5.14 the parameters values of Langmuir isotherm model are reported. In table 5.7 the thermodynamic parameters values are reported. The model parameters γ, D, E, F were estimated by minimizing the absolute value of average relative deviation between experimental and predicted x_1.These parameters are obtained by correlating the experimental adsorption data with the model equation 6.37 and are shown in table 6.5 along with AARD%. The AARD values are below9.002 (for eosin Y) and 1.95 (for indigo carmine). The experimental and model prediction are shown in figure 6.5 and figure 6.6 for eosin y and indigo carmine respectively.

Table 6.5 Correlation parameters for adsorption of dye compounds onto chitosan obtained using new model equation 6.37.

Name of the dye	T / K	Correlation parameters				AARD (%)
		γ	D	E	F	
Eosin Y	303	1.2713	3.6836	$7.3066 \cdot 10^3$	$6.9949 \cdot 10^6$	8.5221
	313	1.1984	3.3882	$9.1874 \cdot 10^3$	$1.8692 \cdot 10^6$	9.002
	323	1.0501	3.3285	$8.3297 \cdot 10^3$	$3.3307 \cdot 10^6$	8.4736
Indigo carmine	303	1.3870	5.5657	$-4.2567 \cdot 10^3$	$1.3013 \cdot 10^7$	1.0124
	313	1.3413	4.9958	$-2.8902 \cdot 10^3$	$9.9278 \cdot 10^6$	2.1
	323	1.2064	4.9432	$-3.2483 \cdot 10^3$	$1.0047 \cdot 10^7$	1.9504

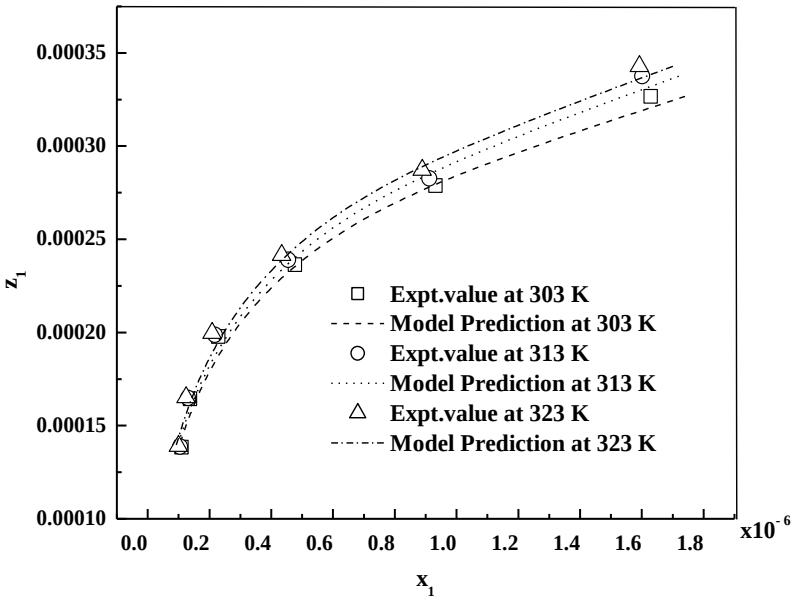

Figure 6.5 Mole fraction of eosin Y on solid phase z_1 against mole fraction of eosin Y in liquid phase x_1

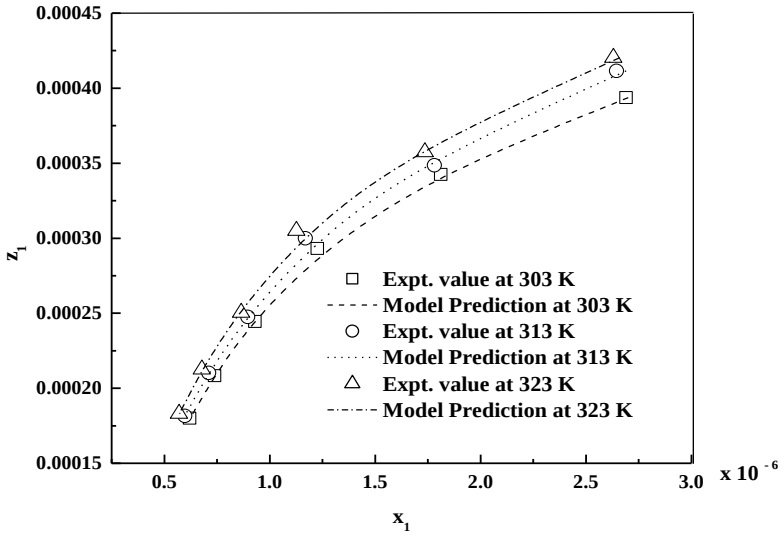

Figure 6.6 Mole fraction of indigo carmine on solid phase z_1 against mole fraction of indigo carmine in liquid phase x_1

6.3. Conclusions

The major outcome of this study is the development of three new mathematical models which are based on phase equilibrium criteria. The batch experimental results obtained in this work are successfully used to correlate the new models developed in this study. The success of the models are evaluated in terms of arithmetic average relative deviation (AARD) percent. The lowest AARD indicates the good agreement between the theoretical prediction and the experimental data. The developed new models 1 and 2 are predicting better than the Khan et al. model.

Reference

[6.1] A.R. Khan, M.R. Riazi, Y.A. Al-Roomi, A thermodynamic model for liquid adsorption isotherms. Sepr. Purif. Technol. 18 (2000) 237-250.

[6.2] M.R. Riazi, A.R. Khan, A thermodynamic model for gas adsorption isotherms. J. Colloid Interface Sci. 210 (1999) 309-319.

[6.3] J.M. Prausnitz, R.N. Lichtenthaler, E.G. de Azevedo, Molecular thermodynamics of fluid phase equilibria. Prentice Hall PTR, NJ, 1999.

[6.4] B. Wang, Q. Li, Z. Zhang, J. Yang, Y. Liu, A new model for predicting solute solubility in supercritical fluids based on the Wilson equation. Korean. J. Chem. Eng. 23(2006) 131-137.

[6.5] Q. Li, C. Zhong, Z. Zhang, Q. Zhou, Modeling of the solubility of solid solutes in supercritical CO_2 with and without cosolvent using solution theory. Korean. J. Chem. Eng. 21 (2004) 1173-1177.

[6.6] W.J. Lyman, W.F. Reehl, D.H. Rosenblatt, Handbook of chemical property estimation methods. 3rd ed., McGraw –Hill, New York (1982).

[6.7] R.H. Perry, D.W. Green, Perry's Chemical Engineers hand book, seventh ed., McGraw – Hill. New York (1997)

[6.8] C. Garlapati, G. Madras, Solubilities of palmitic and steric fatty acids in super critical carbon dioxide. J. Chem. Thermodyn. 42 (2010) 193 – 197.

[6.9] R.C. Reid, J.M. Prausnitz, B.E. Poling The properties of gases and liquid. Mc. Graw Hill Inc. New York. 4^{th} ed., (1986).

[6.10] O. Hamdaoui, E. Naffrechoux, Modeling of adsorption isotherms of phenol and chlorophenols onto granular activated carbon part I. Two parameter models and equations allowing determination of thermodynamic parameters. J. Hazard. Mater. 147 (2007) 381- 394.

CHAPTER 7

FIXED BED STUDIES

Fixed bed adsorption is a commonly adopted method to remove solute from the solution. In the fixed bed, the fluid to be treated is admitted at constant flow rate either from top or from the bottom of the column. The overall dynamics of the system determines the efficiency of the process, rather than just the equilibrium considerations. In this chapter, the breakthrough characteristics of fixed bed of the newly prepared adsorbent with different dye compounds are presented.

7.1Experimental setup

The materials utilized in the fixed bed studies (chitosan and palmyra male inflorescence carbon) are discussed in the chapter 4. The experiments were conducted with fixed quantity of adsorbent at varying feed concentration. The breakthrough analysis is carried out in a fixed bed glass column of diameter 5 cm. The liquid is pumped to the fixed bed with the help of a peristaltic pump. The photograph of the fixed bed set up is shown in figure7.1.

Figure 7.1 The photograph of the fixed bed set up

7.2 Results and discussion

The successful design of a fixed bed requires prediction of breakthrough curve for the adsorbate-adsorbent system. The plot of the breakthrough curve, which is the ratio of effluent concentration to the inlet concentration (C_t/C_o) vs time (t) were analyzed by three models proposed by Thomas, Yoon – Nelson and Adam – Bohart. These models provide information on the influence of parameters such as kinetic coefficients and saturation concentration on the solid phase.

7.2.1 Effect of initial concentration

The inlet concentration was varied from 10 mg L^{-1} to 50 mg L^{-1}. At higher concentrations, the outlet concentration is seen to increase drastically at initial stage of operation. The effect of the inlet concentration on the shape of the breakthrough curve is shown in the figure 7.2 to figure 7.5 for different adsorbate-adsorbent system (palmyra male inflorescence carbon – safranine O dye and chitosan with eosin y and indigo carmine dyes). It is clearly seen that as the inlet adsorbate concentration increases the corresponding breakthrough curve shifts towards the left [7.1- 7.2]. This indicates that the mass transfer zone increase at higher feed concentration. This effect can be readily seen in the quantification of break through characteristics times. Similar trends are obtained for bio sorption of methylene blue – rice husk system [7.3] and removal of acid dye using pristine and acid activated clay [7.4]. The adsorption capacity increases with increasing inlet concentration because a high concentration difference provides a higher driving force [7.5].

7.2.2 Breakthrough curves correlation

7.2.2 (a) Thomas model

The ln($C_o/C_t - 1$) vs t data were fitted to determine the Thomas rate constant and maximum solid phase concentration [7.6]. The square of correlation coefficient, R^2 is found to be more than 0.93. The Thomas kinetic coefficient (K_{Th}) and maximum solid phase concentration (mg g^{-1}) obtained from equation 2.21 is shown in table 7.1 and table 7.2 for chitosan and palmyra male inflorescence carbon dye system respectively. The fixed bed study with chitosan the increase in feed concentration of dye solution from 10 mg L^{-1} to 50 mg L^{-1} , the value of the Thomas kinetic coefficient varied between 0.487 (ml $min^{-1}mg^{-1}$) and 0.317 (ml $min.^{-1}mg^{-1}$) and the q_{max} value shows the increased trend between 0.372 (mg g^{-1}) and 1.210 (mg g^{-1}). For eosin Y chitosan system the value of the Thomas kinetic coefficient varied between 0.0.558 (ml $min.^{-1}mg^{-1}$) and 0.0.270 (ml $min.^{-1}mg^{-1}$), the q_{max} value shows the increased trend between 0.884 (mg g^{-1}) and 2.93 (mg g^{-1}) For palmyra male inflorescence carbon safranine o system treated with KOH, the Thomas kinetic coefficient values varied between 0.656 and 0.443 (ml $min.^{-1}mg^{-1}$), the q_{max} value shows the increased trend between 0.495 and 0.861 (mg g^{-1}).Similar trends were obtained for KOH and $ZnCl_2$ treated carbon. From these tables it is clear that as the inlet concentration increased from 10 ppm to 50 ppm. The value of q_{max} increased but the value of K_{Th} decreased for most of the cases in the concentration range that has been examined. This may be attributed to the change in concentration difference (i.e., driving force). The comparison of the experimental values and the correlated values according to the Thomas model are shown in figure 7.2 (a), 7.2 (b), 7.3 (a), 7.3 (b) and 7.3 (c).

Table 7.1 Parameters predicted by the Thomas model for chitosan – dye system

Compound name	$C_o\,(mg/l)$	$Q(ml/\min)$	$k_{Th}(ml/\min mg)$	$q_{\max}(mg/g)$	R^2
Indigo carmine	10	15	0.487	0.372	0.969
	20	15	0.374	0.522	0.930
	30	15	0.402	0.751	0.950
	40	15	0.360	0.979	0.968
	50	15	0.317	1.210	0.993
Eosin Y	10	15	0.558	0.884	0.965
	20	15	0.411	1.138	0.957
	30	15	0.268	1.530	0.984
	40	15	0.313	1.860	0.980
	50	15	0.270	2.930	0.982

Table 7.2 Parameters predicted by the Thomas model for Palmyra male inflorescence carbon – dye system

Compound name	$C_o\,(mg/l)$	$Q(ml/\min)$	$k_{Th}(ml/\min mg)$	$q_{\max}(mg/g)$	R^2
Safranine O (H_3PO_4)	10	15	0.6566	0.495	0.969
	20	15	0.6322	0.5448	0.968
	30	15	0.5285	0.6494	0.994
	40	15	0.454	0.7616	0.996
	50	15	0.443	0.861	0.982
KOH	10	15	0.7111	0.5007	0.996
	20	15	0.6732	0.5743	0.982
	30	15	0.7002	0.6198	0.966
	40	15	0..6004	0.6131	0.994
	50	15	0.565	0.6754	0.983
$ZnCl_2$	10	15	0.5515	0.6381	0.991
	20	15	0.5079	0.6560	0.994
	30	15	0.498	0.762	0.989
	40	15	0.4459	0.7582	0.992
	50	15	0.431	0.8352	0.985

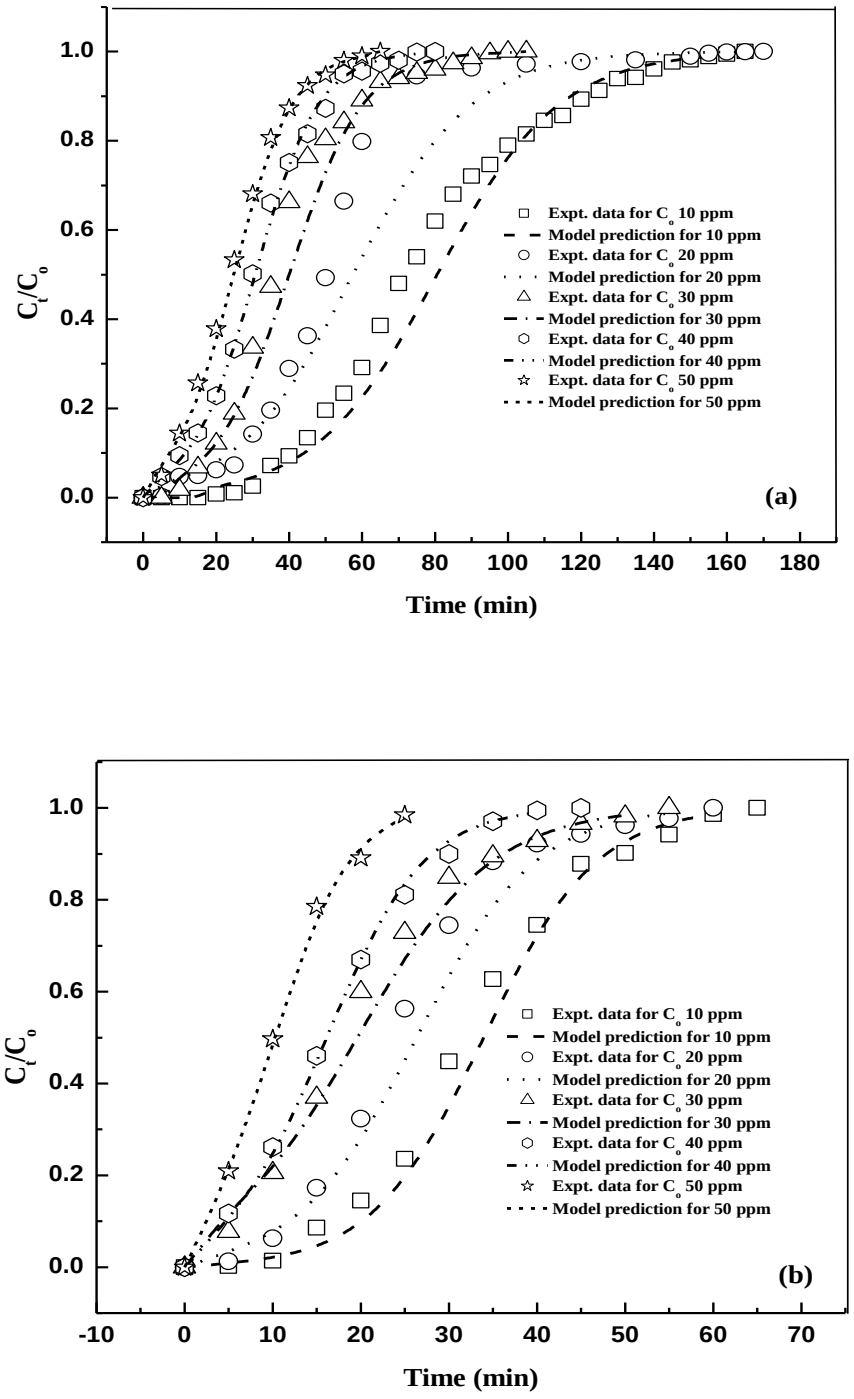

Figure 7.2 Breakthrough curves for adsorption of (a) Indigo carmine dye (b) Eosin Y dye onto chitosan for different initial concentration at temperature 303.15 K. The dash dotted lines indicate Thomas model predictions. (Flow rate 15 ml/min, adsorbent dose 5 gm.)

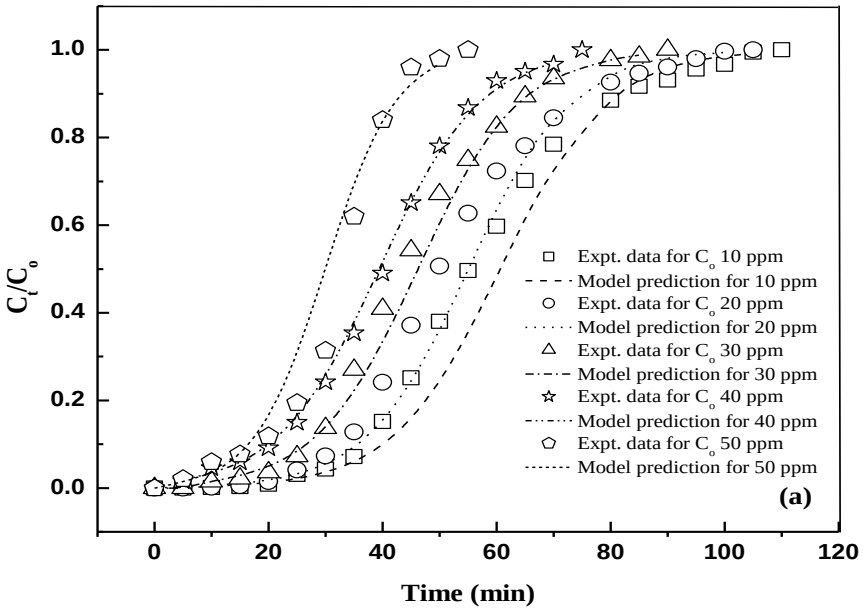
1.0
0.8
0.6
0.4
0.2
0.0
C_t/C_o
0
20
40
60
80
100
120
Time (min)
Expt. data for C_o 10 ppm
Model prediction for 10 ppm
Expt. data for C_o 20 ppm
Model prediction for 20 ppm
Expt. data for C_o 30 ppm
Model prediction for 30 ppm
Expt. data for C_o 40 ppm
Model prediction for 40 ppm
Expt. data for C_o 50 ppm
Model prediction for 50 ppm
(a)

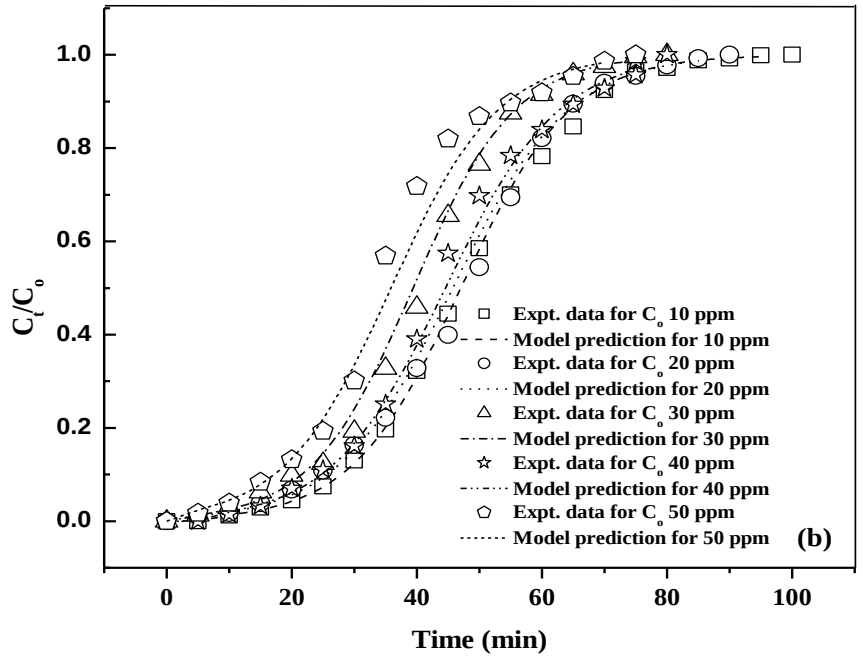
1.0
0.8
0.6
0.4
0.2
0.0
C_t/C_o
0
20
40
60
80
100
Time (min)
Expt. data for C_o 10 ppm
Model prediction for 10 ppm
Expt. data for C_o 20 ppm
Model prediction for 20 ppm
Expt. data for C_o 30 ppm
Model prediction for 30 ppm
Expt. data for C_o 40 ppm
Model prediction for 40 ppm
Expt. data for C_o 50 ppm
Model prediction for 50 ppm
(b)

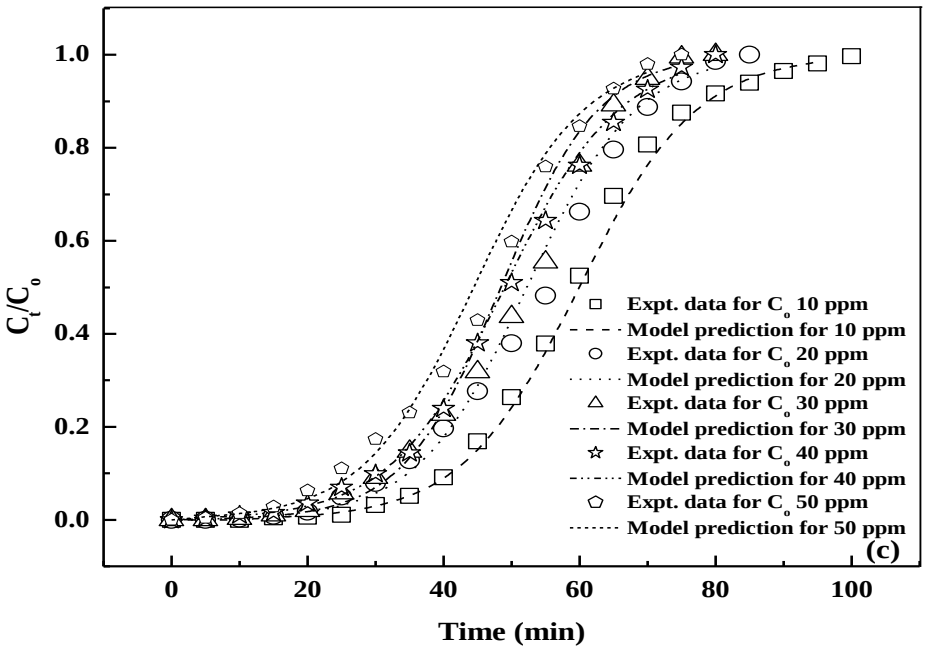

Figure 7.3 Breakthrough curves for adsorption of safranine O onto palmyra male inflorescence carbon for different initial concentration at temperature 303.15 K. The dash dotted lines indicate Thomas model predictions. (a) H_3PO_4 treated, (b) $ZnCl_2$ treated and (c) KOH treated. (Flow rate 15 ml/min, adsorbent dose 5 gm.)

7.2.2 (b) Yoon – Nelson model

The $\ln\left(\frac{C_o}{C_t}-1\right)$ vs*t* data were fitted to determine the Yoon – Nelson model constants [7.7], K_{YN} and τ from equation 2.22. The correlation results are shown in Table 7.3 and Table 7.4 for chitosan and palmyra male inflorescence carbon dye system. It is seen that the rate constant K_{YN} increased and τ decreased with the increasing in inlet concentration of the adsorbate from 10 ppm to 50 ppm for most of the cases. The comparison of the experimental values and the correlated values according to the Yoon – Nelson model are shown in Figure.7.4(a), 7.4 (b) and Fig.7.5(a), 7.5(b) and 7.5 (c).

Table 7.3 Parameters predicted by the Yoon – Nelson model for chitosan dye system

Compound name	$C_o\,(mg/l)$	$Q(ml/\min)$	$k_{YN}(\min^{-1})$	$\tau(\min)$	R^2
Indigo carmine	10	15	0.0604	80.58	0.968
	20	15	0.0652	57.44	0.930
	30	15	0.1006	39.97	0.948
	40	15	0.1176	30.65	0.968
	50	15	0.1277	24.79	0.993
Eosin Y	10	15	0.1645	33.95	0.965
	20	15	0.1599	26.35	0.957
	30	15	0.1365	19.60	0.984
	40	15	0.1939	16.12	0.980
	50	15	0.2629	10.25	0.980

Table 7.4 Parameters predicted by the Yoon – Nelson model for Palmyra male inflorescence carbon – dye system

Compound name	$C_o\,(mg/l)$	$Q(ml/\min)$	$k_{YN}(\min^{-1})$	$\tau(\min)$	R^2
SafranineO (H_3PO_4)	10	15	0.1083	60.628	0.968
	20	15	0.1148	55.07	0.967
	30	15	0.1144	46.198	0.994
	40	15	0.1152	39.39	0.996
	50	15	0.1272	34.795	0.982
KOH	10	15	0.1187	59.915	0.995
	20	15	0.1289	52.23	0.982
	30	15	0.1447	48.38	0.996
	40	15	0.1266	48.97	0.994
	50	15	0.1272	44.42	1.00
$ZnCl_2$	10	15	0.1173	47.02	0.991
	20	15	0.1081	46.16	0.996
	30	15	0.1264	39.359	0.989
	40	15	0.1127	39.562	0.992
	50	15	0.1215	35.162	0.972

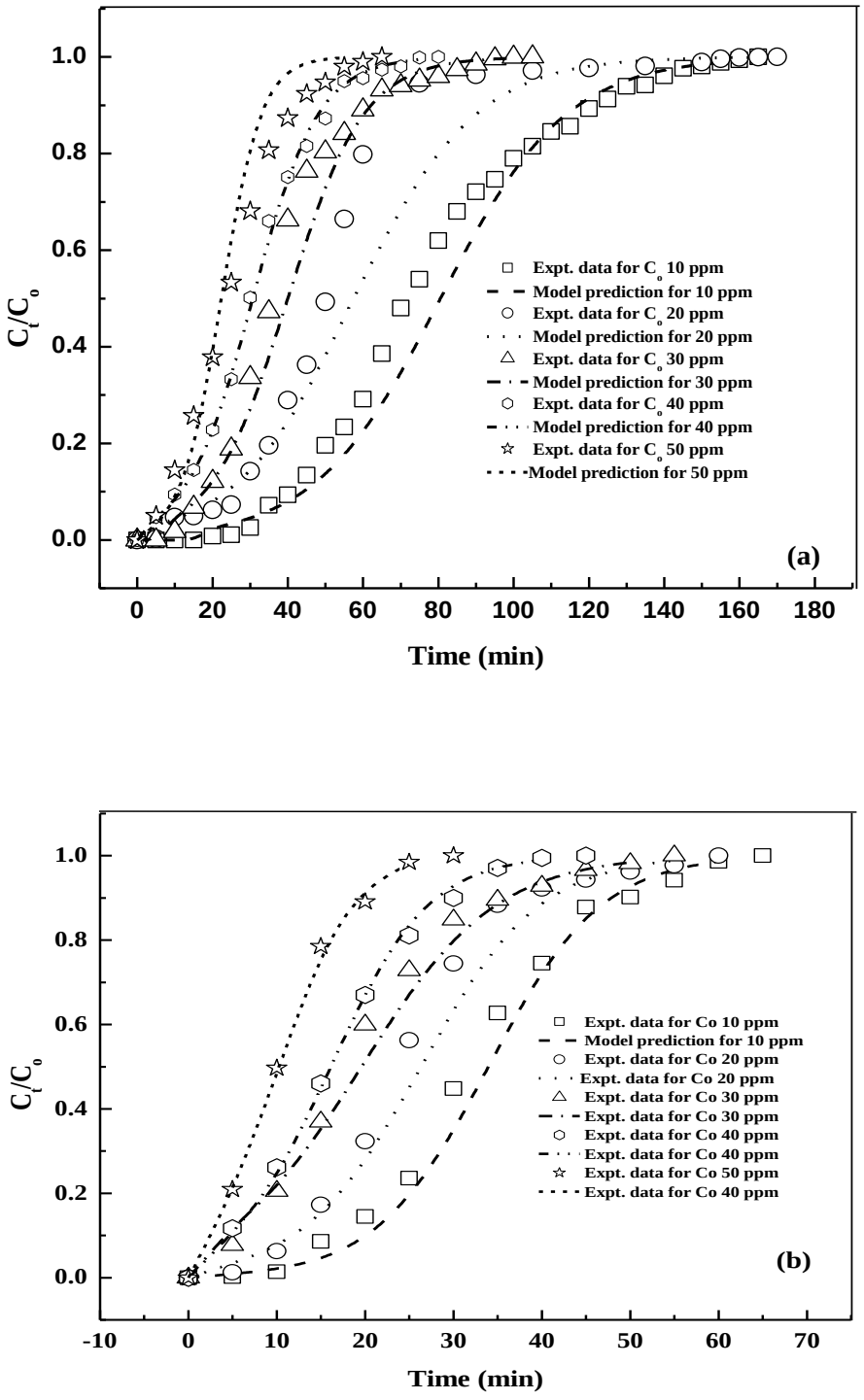

Figure 7.4 Breakthrough curves for adsorption of (a) Indigo carmine dye (b) Eosin Y dye onto chitosan for different initial concentration at temperature 303.15 K. The dash dotted lines indicate Yoon Nelson model predictions. (Flow rate 15 ml/min, adsorbent dose 5 gm.)

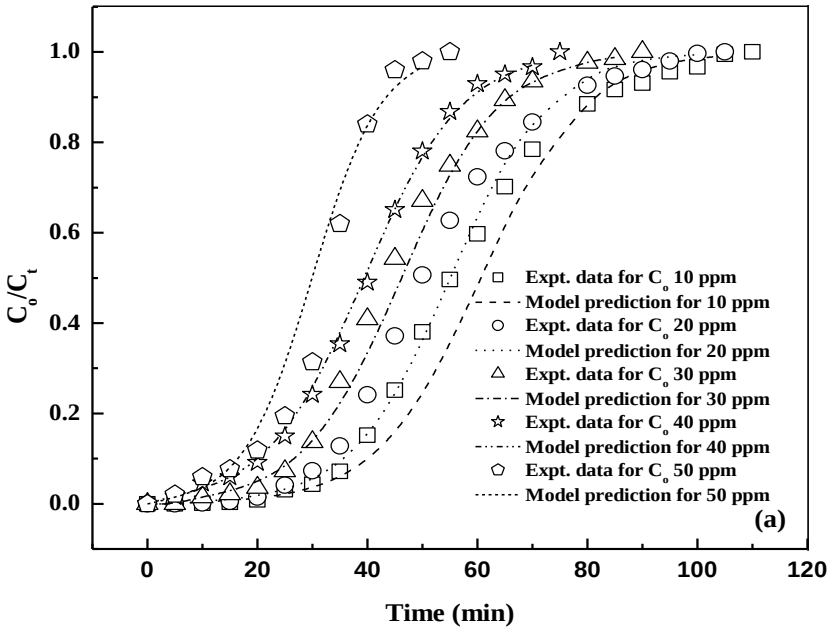
1.0
0.8
0.6
0.4
0.2
0.0
C_o/C_t
0
20
40
60
80
100
120
Time (min)
Expt. data for C_o 10 ppm
Model prediction for 10 ppm
Expt. data for C_o 20 ppm
Model prediction for 20 ppm
Expt. data for C_o 30 ppm
Model prediction for 30 ppm
Expt. data for C_o 40 ppm
Model prediction for 40 ppm
Expt. data for C_o 50 ppm
Model prediction for 50 ppm
(a)

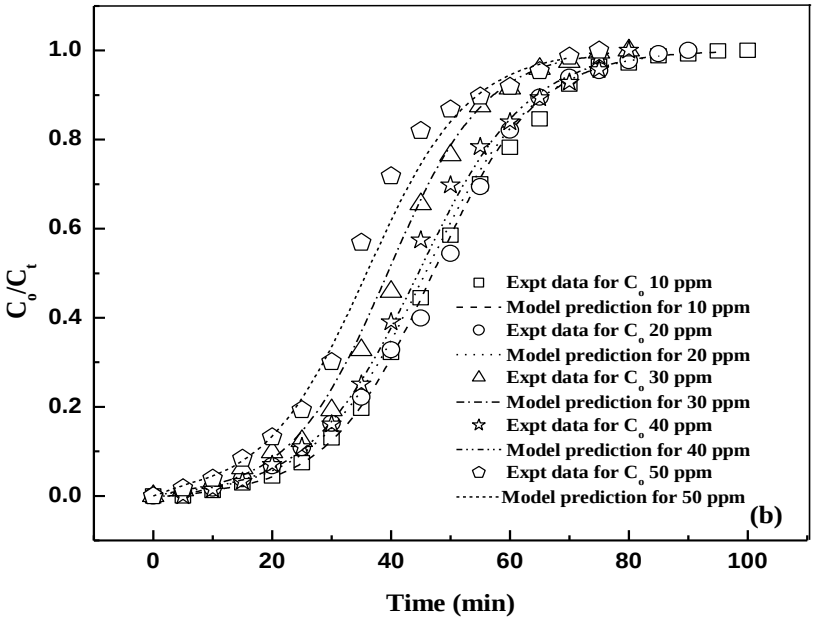
1.0
0.8
0.6
0.4
0.2
0.0
C_o/C_t
0
20
40
60
80
100
Time (min)
Expt data for C_o 10 ppm
Model prediction for 10 ppm
Expt data for C_o 20 ppm
Model prediction for 20 ppm
Expt data for C_o 30 ppm
Model prediction for 30 ppm
Expt data for C_o 40 ppm
Model prediction for 40 ppm
Expt data for C_o 50 ppm
Model prediction for 50 ppm
(b)

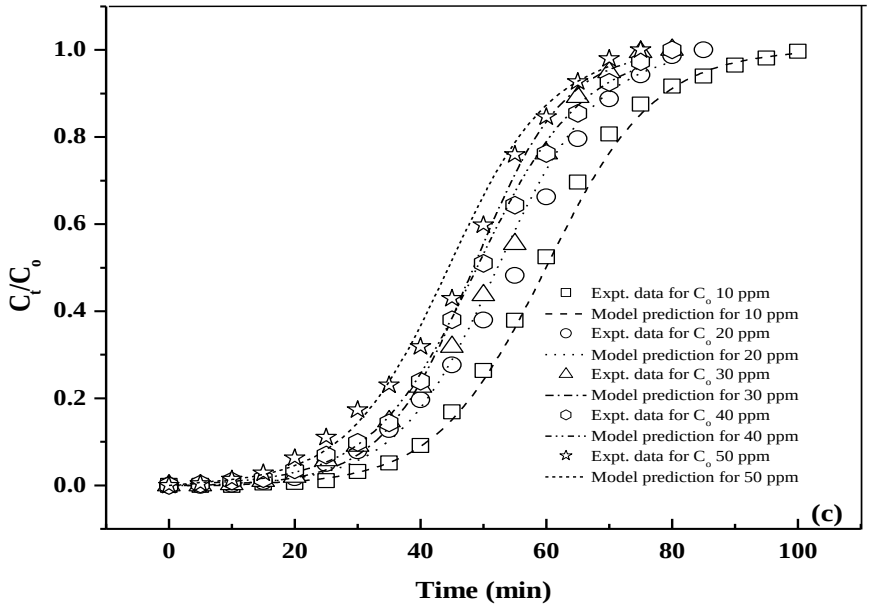

Figure 7.5 Breakthrough curves for adsorption of safranine O onto palmyra male inflorescence carbon for different initial concentration at temperature 303.15 K. The dash dotted lines indicate Yoon - Nelson model predictions. (a) H_3PO_4 treated, (b) ZnCl2 treated and (c) KOH treated. (Flow rate 15 ml/min, adsorbent dose 5 gm.)

7.2.2 (c) Adam – Bohart model

The $\ln(C_t/C_o)$ vs*t* data were fitted to determine the Adam-Bohart model [7.] constants from equation 2.23. The values of N_o and k_{AB} are presented in Table 7.5 and Table7.6 together with the correlation coefficients for chitosan and palmyra male inflorescence carbon dye system. The model is seen to poorly predict the breakthrough curve. The magnitude of N_o and k_{AB} shows mixed trend. The comparison of the experimental values and the correlated values according to the Adam-Bohart model are not shown here due to its poor correlation.

Table7.5. Parameters predicted by the Adam – Bohart model for chitosan – dye system

Compound name	$C_o\,(mg/l)$	$Q(ml/\min)$	$k_{AB}(L/mg\min)$	$N_o\,(mg/L)$	R^2
Indigo Carmine	10	15	0.00272	934.56	0.709
	20	15	0.001095	1871.69	0.576
	30	15	0.00108	1707.31	0.647
	40	15	0.00098	1762.14	0.802
	50	15	0.00091	1782.28	0.769
Eosin Y	10	15	0.00929	357.05	0.770
	20	15	0.00733	322.78	0.730
	30	15	0.00481	299.38	0.744
	40	15	0.00564	247.27	0.822
	50	15	0.007368	162.73	0.837

Table.7.6 Parameters predicted by the Adam – Bohart model for Palmyra male inflorescence carbon – dye system

Compound name	$C_o\,(mg/l)$	$Q(ml/\min)$	$k_{AB}(L/mg\min)$	$N_o\,(mg/L)$	R^2
Safranine O	10	15	0.00479	961.65	0.8219
H_3PO_4	20	15	0.003049	1170.712	0.7544
	30	15	0.001937	1510.637	0.8283
	40	15	0.001528	1737.741	0.9034
	50	15	0.001738	1642.093	0.958
ZnCl2	10	15	0.00479	963.3194	0.8219
	20	15	0.00277	1028.881	0.8822
	30	15	0.00199	1364.573	0.883
	40	15	0.001458	1926.381	0.868
	50	15	0.001172	2285.836	0.84
KOH	10	15	0.006489	1484.05	0.8586
	20	15	0.003985	1557.942	0.884
	30	15	0.002613	3644.349	0.8738
	40	15	0.001848	3434.912	0.90
	50	15	0.001452	4280.647	0.8754

7.3 Characteristics of break through curve

Important characteristics of fixed bed such as break through time (t_b), stoichiometric wave front time(t_s) and exhaust time(t_u) were estimated using standard procedure described in the literature [7.9-7.10]. In this work, a new integration approach was applied for calculating the stoichiometric wave front time. In the proposed new approach, the breakthrough curve is fitted with higher order polynomial and the same is evaluated for obtaining stoichiometric wave front time with the usual equal area criterion (i.e., area below the break through curve between t_b and t_s is equal to the area above the curve between t_s and t_u) [7.10]. The expression used in the calculation of stoichiometric wave front time is

$$t_s = t_u - \int_{t_b}^{t_u} f(t)\,dt \qquad (7.1)$$

where $f(t)$is higher order polynomial. Eighth order polynomial was found to be suitable for all the systems considered in this work. The evaluated characteristics parameters are reported in Table 7.7 for chitosan and Table 7.8 for palmyra male inflorescence carbon. The stoichiometric wave front time obtained by this method is same with the methods described in the literature [7.9. 7.10]. The results show that there is decrease of all characteristic time quantities when the concentration increased from 10 mg/L to 50 mg/L. For example, for the system indigo carmine – chitosan breakthrough varied from 31.9 min to 4 min for this range of change in concentration. This may be attributed to sharp increase in the slope of break through curves when adsorbate concentration was increased from 10 mg/L to 50 mg/L.

Table 7.7 Characteristic parameters of fixed bed for chitosan dye system at flow rate, Q = 15 ml/min

Compound Name	$C_o\,(mg/l)$	Break through time, t_b (min)	Stoichiometric wave front Time, t_s (min)	Exhaust time, t_u (min)
Indigo Carmine	10	31.92	71.83	165
	20	10.67	50.17	160
	30	13.19	37.98	105
	40	5.34	30.95	75
	50	4.00	24.68	65
Eosin Y	10	12.5	32.44	65
	20	8.50	24.67	60
	30	3.30	19.50	55
	40	2.45	16.57	40
	50	1.19	10.66	30

Table 7.8 Characteristic parameters of fixed bed at fixed flow rate for palmyra male inflorescence carbon at flow rate $Q = 15\,\mathrm{ml/min}$

Compound Name	$C_o\,(mg/l)$	Break through time, t_b (min)	Stoichiometric wave front Time, t_s (min)	Exhaust time, t_u (min)
Safranine O	10	31.15	57.46	110
(H_3PO_4 treated)	20	25.76	52.21	105
	30	21.71	45.04	90
	40	10.85	39.53	75
	50	8.72	33.86	50
KOH treated	10	34.53	58.93	100
	20	20.70	53.03	85
	30	23.76	50.21	80
	40	21.25	49.20	80
	50	18.68	45.094	75
$ZnCl_2$ treated	10	20.22	47.47	100
	20	16.76	46.63	90
	30	14.13	40.29	80
	40	12.25	39.04	80
	50	10.94	35.01	75

7.4 Establishing adsorption isotherm data in fixed bed

Frontal study is quite useful for single solute adsorption isotherm development. In industrial practice of effluent treatment, fixed – bed adsorbers are often utilized therefore, the isotherms developed in a fixed – bed are more appropriate for predicting the

performance of the absorber.The analysis of packed bed adsorption is generally based on the exit stream concentration (C_t) vstime (t) data, which is a functions of column geometry, operating conditions and equilibrium adsorption data. A typical breakthrough curve is given in the figure 7.6. From the shaded area behind the breakthrough curve between initial (t_o) and exhaust time (t_u) we can calculate the uptake of adsorbate by the adsorbent, which give the value of adsorbate per unit amount of adsorbent and is known as q and it is calculated with equation 7.2 [7.11] The corresponding equilibrium concentration in liquid (C_e) in liquid phase can be calculated using equation 7.3.

Thus, estimated q and C_e gives a point on adsorption isotherm. By performing breakthrough test for various inlet concentrations at constant temperature and the adsorbent dosage, we get several q values. Thus an isotherm can be drawn [7.12-7.13].

$$q = \frac{(\text{shaded area})F}{m} \tag{7.2}$$

Where F is the flow rate and m is the mass of adsorbent.

$$q = \frac{(C_o - C_e)V}{m} \tag{7.3}$$

Where C_o Initial concentration, C_e equilibrium concentration, V is the cumulative volume and m is the mass of adsorbent.

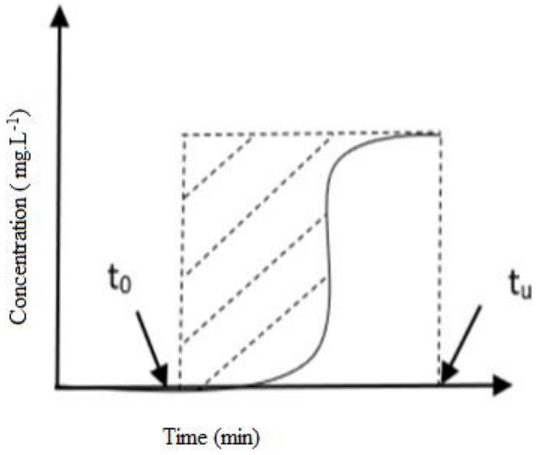

Figure 7.6 A typical breakthrough curve

7.4.1 Adsorption isotherm models

The *q* and *Ce* data obtained from the breakthrough curves were used to fit the Freundlich [7.14] and Langmuir models [7.15]. Both the models were found to correlate q vs C_e data. The square of correlation coefficients is observed to be more than 0.99 for chitosan system and more than 0.88 for palmyra male inflorescence carbon system. The model constants were reported in table 7.9 and table 7.10 for chitosan and palmyra male inflorescence carbon. The experimental and the model predictions curves were shown in figure 7.7 (a), 7.7(b) for chitosan, and for palmyra male inflorescence carbon in figure7.8(a), 7.8(b) and 7.8(c) respectively.

It is seen from table 7.9 that for chitosan- indigo carmine system the value of Langmuir constant q_m and k_L obtained by frontal technique is 4.407 mg g^{-1} and 0.1823 Lmg^{-1} respectively. The value of these parameters determined from batch equilibrium data is 23.364 mg g^{-1} and 0.02815 L mg^{-1} respectively. For chitosan- eosin Y system the value of the Langmuir parameters are 2.679 mg g^{-1} and 0.1126 L mg^{-1} respectively using frontal method. These values from batch data are 20.57 mg g^{-1} and 0.1337 L mg^{-1}

respectively. It is seen that there is significant difference in the values of the constants. The difference could be due to non-ideal flow within the fixed bed.

Table 7.9 Isotherm parameters for fixed bed adsorption of dye on to chitosan at T = 303.15 K

Compound Name	Freundlich constants		R^2	Langmuir constants		R^2
	$K_F\left((mg/g)/(L)\frac{1}{n}\right)$	$1/n$		$q_m(mg/g)$	$K_L(L/mg)$	
Indigo Carmine	1.4035	0.2612	0.98	4.407	0.1823	0.994
Eosin Y	0.544	0.2612	0.998	2.679	0.1126	0.990

Table 7.10 Isotherm parameters for fixed bed adsorption of dye on to palmyra male inflorescence carbon at T= 303.15 K

Compound Name	Freundlich constants		R^2	Langmuir constants		R^2
	$K_F\left((mg/g)/(mg/l)^{\frac{1}{n}}\right)$	$1/n$		$q_m(mg/g)$	$K_L(L/mg)$	
SafranineO (H_3PO_4 treated)	0.659	0.649	0.949	8.065	0.0615	0.880
KOH treated	0.542	0.863	0.993	25.974	0.0184	0.917
$ZnCl_2$ treated	0.373	0.826	0.992	16.502	0.0183	0.936

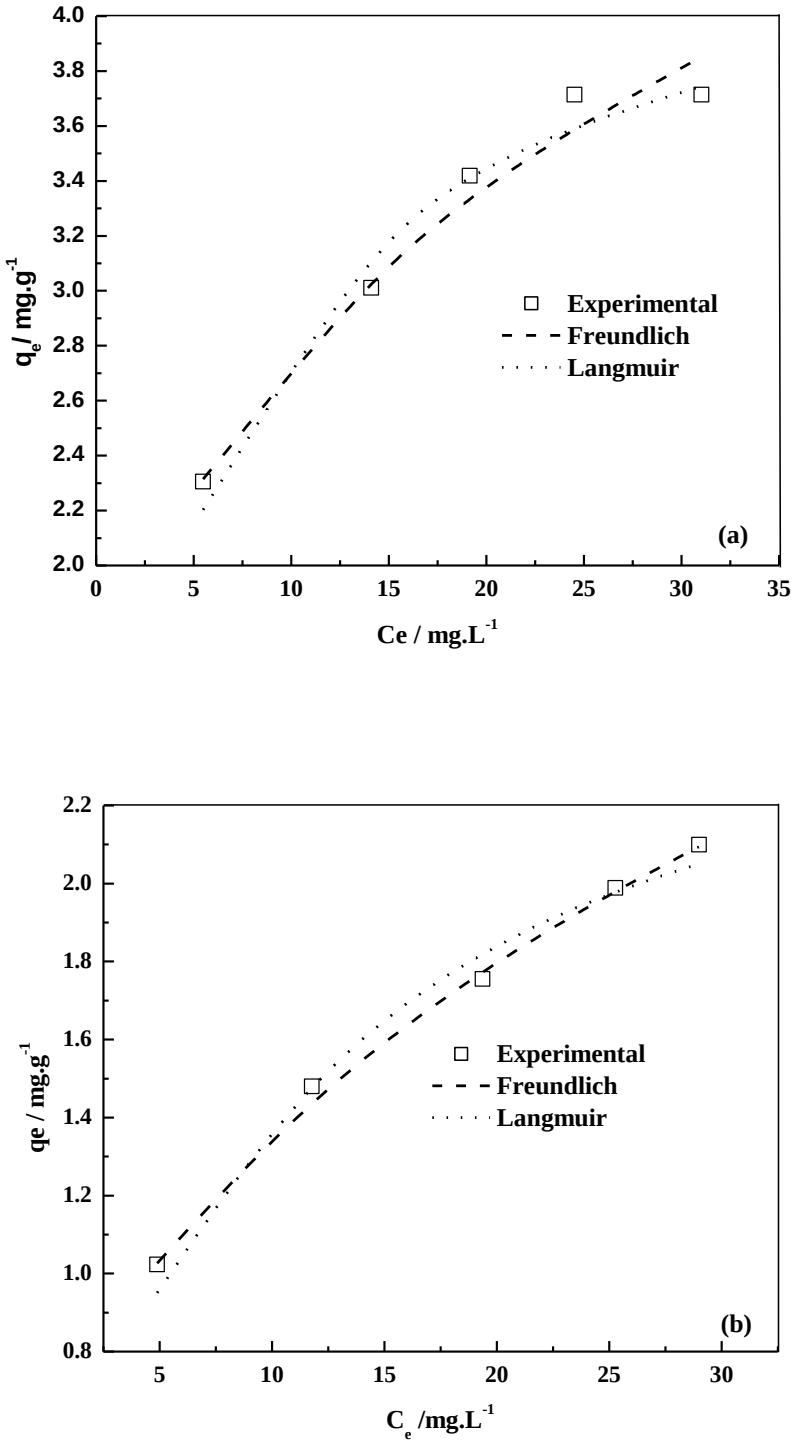

Figure 7.7 Comparison of experimental values with Freundlich and Langmuir isotherm models for adsorption of (a) Indigo carmine dye and (b) Eosin Y dye onto chitosan.

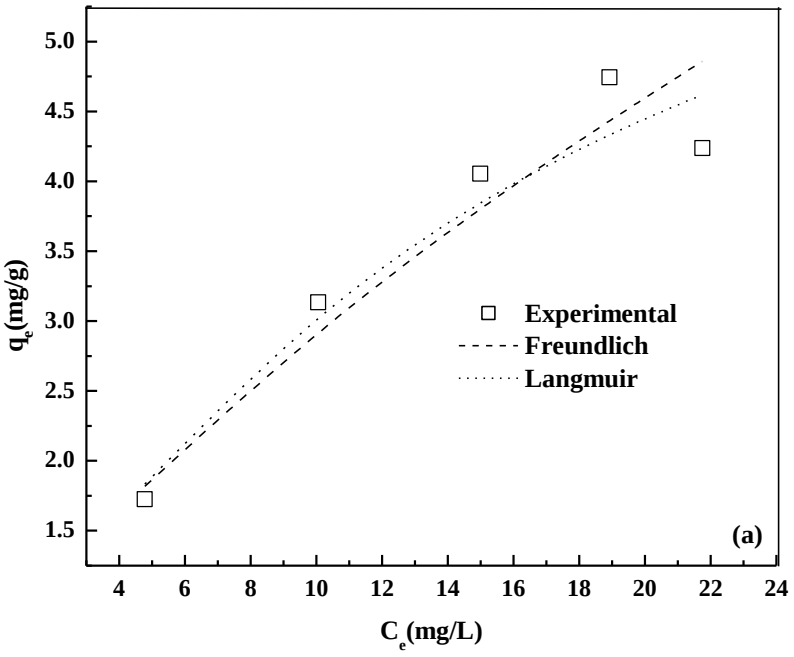
5.0
4.5
4.0
3.5
3.0
2.5
2.0
1.5
q_e(mg/g)
4
6
8
10
12
14
16
18
20
22
24
C_e(mg/L)
Experimental
Freundlich
Langmuir
(a)

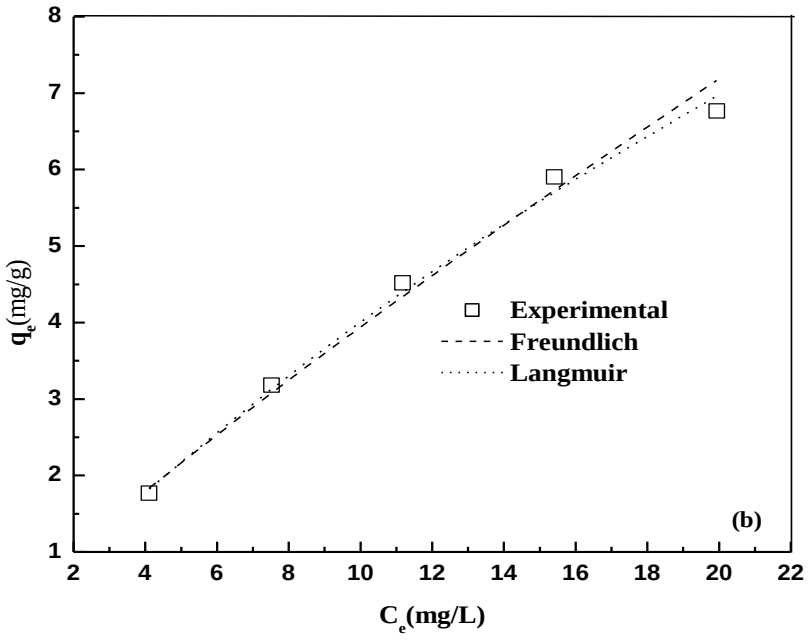
8
7
6
5
4
3
2
1
q_e(mg/g)
2
4
6
8
10
12
14
16
18
20
22
C_e(mg/L)
Experimental
Freundlich
Langmuir
(b)

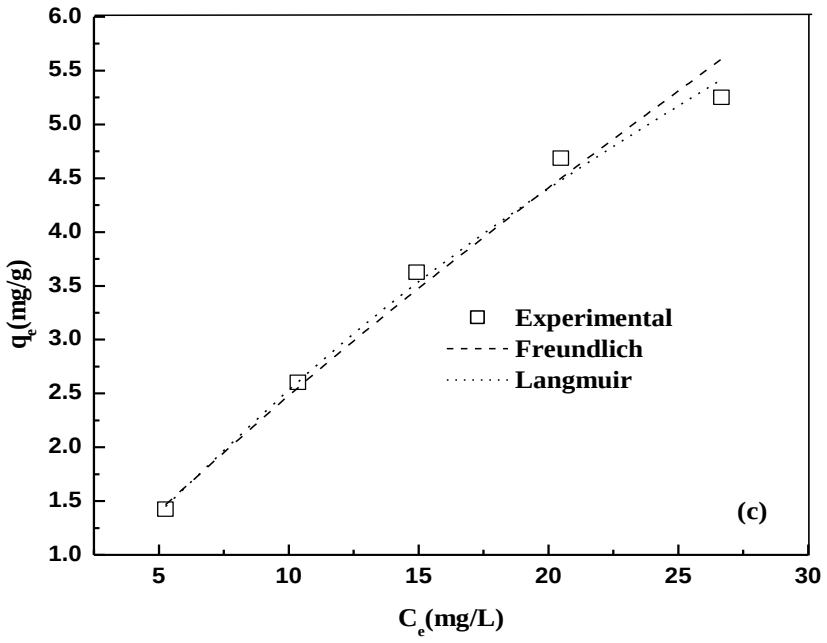

Figure 7.8 Comparison of experimental values with Freundlich and Langmuir isotherm models for adsorption of safranine O onto palmyramale inflorescence carbon. (a)H_3PO_4 treated (b)KOH treated and (c) $ZnCl_2$ treated.

7.5 Conclusion

In this work, experiments are carried out in a fixed bed to determine the breakthrough profiles for the removal of dyes (i.e., eosin Y- chitosan, indigo carmine – chitosan and safranine O – palmyra male inflorescence carbon) from the aqueous solution. The effect of initial concentration on fixed bed is reported. The important characteristics parameters such as breakthrough time, stoichiometric wave front time and exhaust time of the fixed bed were estimated. The effect of initial concentration on the characteristics parameters of the fixed bed could be used in the scale up studies. The break through models would be useful in predicting the performance of the fixed bed. Adsorption isotherms established are appropriate for the design of fixed bed adsorbers.

References

[7.1] N. Gopal, M. Asaithambi, P. Sivakumar, V.Sivakumar, Continuous fixed bed studies of Rhodamine – B dye using polymer bound adsorbent. I. J. Che. Technol. 23(2016) 53 – 58.

[7.2] A.A. Ahmad, B.H. Hameed, Fixed – bed adsorption of reactive azo dye onto granular activated carbon prepared from waste. J. Hazard. Mater.175 (2010) 298 – 303.

[7.3] R. Han, Y. Wang, W. Yu, W. Zo, J. Shi, H. Liu, Biosorption of methylene blue from aqueous solution by rice husk in a fixed – bed column. J. Hazard. Mater.141 (2007) 713 – 718.

[7.4] S.H. Lina, R.S. Juangb, Y.H. Wang, Adsorption of acid dye from water onto pristine and acid activated clays in fixed beds. J. Hazard. Mater. B 113 (2014) 195 – 200.

[7.5] A.P. Lim, A.Z. Continuous fixed – bed column study and adsorption modeling : Removal of cadmium (II) and lead (II) ions in aqueous solution by dead calcareous skeletons. Biochemical Eng. J. 87 (2014)50 -61.

[7.6] H.C. Thomas, Heterogeneous ion exchange in a flow system. J. Am. Chem. Soc. 66 (1944) 1664 – 1666.

[7.7] Y. H. Yoon, J.H. Nelson, Application of gas adsorption kinetics, Part 1 A theoretical model for respirator cartridge service time. Am. Ind. Hyg. Assoc. J. 45 (1984) 509 – 516.

[7.8] G. Bohart, E.Q. Adams, Some aspects of the behavior of charcoal with respect to chlorine. J. Am. Chem. Soc. 42 (1920) 523 – 544.

[7.9] C.J. Geankoplis, transport processes and separation process principles. PHI Ltd., New Delhi, 2012.

[7.10] A.L. Hines, R.N. Maddox, Mass transfer fundamentals and applications. Prentice Hall Inc. New Jersey, 1985.

[7.11] A. Shahbazi, H. Younesi, A. Badiei, Batch and fixed bed column adsorption of Cu (II), PB (II), and CD(II) from aqueous solution onto functionalized SBA – 15 mesoporous silica. Can. J. Chem. Eng. 9 (2012) 1- 12.

[7.12] D.L.A. Fernandes, M.R.B. Xavier, A.D. Silva, C.M. Silva, Dynamic and equilibrium adsorption experiments. J. Chem. Edu. 82(6) (2005) 919 – 923.

[7.13] O. Lisec, P. Hugo, A.S. Morgenstern. Frontal analysis method to determine competitive adsorption isotherms. J. Chromatogr. A 908 (2001) 19-34

[7.14] H.M.F. Freundlich, Over the adsorption in solution. J. Phys. Chem. 57 (1906) 385 – 471.

[7.15] I. Langmuir, the constitution and fundamental properties of solids and liquids. J. Am. Chem. Soc. 38 (11) (1916) 2221 – 2295.

CHAPTER 8
OVERALL CONCLUSION
AND
FUTURE SCOPE

The discharge of the dye effluents into water bodes affect aquatic life as colour reduces sunlight penetration. Many of these dyes are toxic and can be carcinogenic and affect the human health. Various techniques such as coagulation, flocculation, ultra-filtration, oxidation, precipitation, electro chemical methodology, photo decomposition and biological treatment are available in the literature to remove the dyes from the effluent. Among all of these removal methods, adsorption has been found to be attractive due to the simplicity of design, low cost, rapid and high removal efficiency and ease of operation.

One of the objectives was to study the feasibility of replacing costly activated carbon generally used in industry with adsorbents from agricultural and sea food waste. Two new adsorbents namely palmyra male inflorescence carbon and chitosan are prepared. The dyes studied were safranin O, malachite green oxalate, orange G, indigo carmine and eosin Y. It was noted that pH had a significant effect on uptake. The favourable pH for adsorption onto activated carbon with safranin O and malachite green oxalate is 6.0, orange G is 4.0, indigo carmine and eosin Y is 2.0. The maximum Langmuir adsorption capacity of the new adsorbent palmyra male inflorescence carbon is found to be 259.93 mg g^{-1}, and 343.50 mg $g^{-1}$for safranin O and malachite green oxalate respectively. For activated carbon system maximum Langmuir adsorption capacity is found to be 141.42mg g^{-1} and 159.14 mg $g^{-1}$for safranin O and malachite green oxalate respectively. The results indicate that the newly prepared adsorbent palmyra male inflorescence carbon is effective in removing the dyes. The Langmuir adsorption capacity of chitosan with eosin Y and indigo carmine is 21.57 mg $g^{-1}$and 24.88 mg g^{-1}respectively. These values are comparable with the literature reported values.

The thermodynamic parameters were evaluated and it reveals that the process is spontaneous and exothermic. The results of kinetic studies revealed that the pseudo second order kinetic model provides good correlation for all the adsorbent dye systems studied. The value of correlation coefficient, R^2 was greater than 0.99.

Another objective was the development of new mathematical models which are based on phase equilibrium criteria to overcome the limitations of Langmuir, Freundlich etc. Three models were proposed. Model-1 requires knowledge of the melting temperature of the sorbate and heat of formation of the solute and solvents. Model-2 does not require this information. Model-3 requires only the Gibbs energy change of the adsorption process. The success of the models is evaluated in terms of arithmetic average relative deviation (AARD) percent. The AARD between the experimental and the predicted values was less than 6.84 for Model-1. The AARD was less than 5.68 for Model-2 and less than 9.0 for Model-3. In comparison, the AARD value for similar model available in the literature is 14.24 for the different systems. Thus all the three models developed in this work are able to correlate the adsorption data's successfully.

Fixed bed studies are carried out to determine the breakthrough profiles for the removal of dyes from the aqueous solution. The result suggested that the breakthrough curve is affected by initial concentration. The important characteristics parameters such as breakthrough time, stoichiometric wave front time and exhaust time of the fixed bed estimated would be helpful for design of fixed bed for this system. The adsorption isotherms data obtained from the breakthrough profiles using frontal technique would be useful in more accurate modelling of fixed bed adsorption.

Future scope

This work has investigated both batch and continuous mode of removal of dye by adsorption. These studies have been performed in lab scale with single dye solutions. However, effluent may contain a mixture of dyes. Therefore, the study needs to be extended to multi-component adsorption systems.

Pilot plant studies needs to be carried out as the effluent to be handled in real time would be in large scale.

There is a scope to study the surface modification of the adsorbents studied in this work for the effective removal of dyes from the effluents.

Further studies are needed to understand the regeneration of the adsorbents developed in this study.

The prepared adsorbent may also be tested for the removal of contaminants other than dyes.